POLITECNICO DI MILANO

Facoltà di Ingegneria Industriale

Corso di Laurea in
Ingegneria Aeronautica

Linear stability of plane Poiseuille flow over a steady Stokes layer

Relatore: Prof. Maurizio Quadrio
Co-relatore: Dr. Fulvio Martinelli

Tesi di laurea di:
Carlo SOVARDI Matr. 750615

Anno Accademico 2010 - 2011

Contents

List of Figures

List of Tables

Abstract

Linear stability of plane Poiseuille flow subject to spanwise velocity forcing applied at the wall is studied. The forcing is stationary and sinusoidally distributed along the streamwise direction. The long-term aim of the study is to explore a possible relationship between the modification induced by the wall forcing to the stability characteristic of the unforced Poiseuille flow and the significant capabilities demonstrated by the same forcing in reducing turbulent friction drag. This work presents the statement of the mathematical problem, which is quite more complex than the classic Orr-Sommerfeld-Squire approach. Complexities are due to the forcing velocity at the wall that makes streamwise direction non-homogeneous. We aim at exploring the main physical parameters that influence the stability of a plane Poiseuille flow subject to the varying boundary condition comparing it with the reference unforced problem. We present some preliminary results, although not yet conclusive, which describe the main effects of wall forcing on modal and nonmodal stability of the flow at different flow conditions.

Key Words: Linear Stability, Poiseuille flow, sinusoidal waves, wall forcing, steady Stokes layer, transient growth.

Sommario

Viene studiata la stabilità lineare di un flusso piano di Poiseuille soggetto a una forzante di velocità trasversale applicata a parete. La forzante è stazionaria è distribuita sinusoidalmente lungo la direzione del flusso. L'obiettivo a lungo termine di questo studio è ricercare una possibile relazione tra la modifica indotta dalla forzante a parete sulla stabilità di un flusso di Poiseuille non forzato e le significative capacità dimostrate dalla medesima forzante nella riduzione della resistenza di attrito turbolento. Questo lavoro presenta la formulazione del problema matematico, che è particolarmente più complesso del classico approcio di Orr-Sommerfeld-Squire. Le difficoltà sono dovute alla forzante di velocità a parete che rende la direzione del flusso non omogenea. Intendiamo analizzare i principali parametri fisici che influenzano la stabilità del flusso piano di Poiseuille soggetto a condizioni al contorno varianti paragonandoli al caso di riferimento non forzato. Si presentano alcuni risultati preliminari dello studio, non ancora completi, che descrivono i principali effetti della forzante a parete sulla stabilità modale e non-modale del flusso, per condizioni di flusso differenti.

Parole chiave: Stabilità lineare, flusso di Poiseuille, onde sinusoidali, forzante di parete, strato limite di Stokes stazionario, crescita transitoria.

Introduction

The present work is a linear stability analysis of plane Poiseuille flow enforced by a wavelike velocity field at the boundary. The basic idea consists in creating at the wall of a channel flow a distribution of spanwise (azimuthal) velocity which varies along the streamwise coordinate, to produce a wavelike wall forcing and to analyse the effect of the latter on the stability characteristics of the plane Poiseuille flow.

The concept of a wavelike forcing comes from recent results [19],[3], [18] [17] about turbulent drag reduction using travelling waves. Waves designed to reduce drag have been shown to decrease friction by more than 50%. These waves create a spanwise, unsteady and streamwise-modulated transversal boundary layer that has been named the generalized Stokes layer or GSL [18]. It is interesting to notice that near-optimal performances are guaranteed by stationary waves, where the spanwise wall forcing does not depend upon time and the GSL becomes stationary (SSL, or steady Stokes layer, as described by [29]).

The present work has thus turbulent skin-friction drag reduction as its background objective, but deals with a significantly different matter. We aim at exploring how the stability characteristics of the indefinite plane channel flow (Poiseuille flow) are modified by the presence of an additional component to the base flow given by the spanwise velocity distribution at the wall. It is our hope that understanding how the SSL interacts with the Poiseuille flow in terms of linear stability properties will help understanding how the SSL affects the turbulent drag.

This is essentially a preliminary study, with the aim to understand how the parameters introduced by the spanwise wavelike forcing influence the stability of plane Poiseuille base flow. We limit ourselves to the simpler case of standing waves (SSL) describing the problem formulation that is required in this case where homogeneity in streamwise direction is lost. The problem analysed is global in streamwise direction and spectral in spanwise, therefore the simple spectral decomposition used for the unforced plane Poiseuille flow, that leads to the well known Orr-Sommerfeld-Squire equations, can not be employed. Hence the new formulation in Fourier space needs a Fourier discrete transform of variables in streamwise direction that involves an appropriate set of wavenumbers.

Linear stability is studied through both modal and nonmodal approaches [24], [27], [26] analysing the least stable eigenvalue and computing the transient energy growth function.

We also report some preliminary results that concern both modal and nonmodal stability properties with respect to an unforced plane Poiseuille flow. We aim at exploring

if a steady Stokes layer may influence the stability characteristics of the channel flow considering both the asymptotic behaviour of an infinitesimal perturbation and its transient energy growth.

The work is structured as follows:

- **Introduction**
- **Chapter 1: Governing equations**: A description of linear stability analysis, focusing on the process of linearization of Navier-Stokes equations, their wall-normal velocity and wall-normal vorticity formulation and its linearization. Introduction of the Orr-Sommerfeld-Squire problem and a description of modal and nonmodal stability theory.
- **Chapter 2: Plane Poiseuille flow over SSL**: An exposition of the main equations of the problem analysed: the linearization of Navier-Stokes equations in presence of wavelike forcing at the wall, their wall-normal velocity and vorticity formulation and its relative Fourier transform focusing on differences with Orr-Sommerfeld-Squire case. A description of the modification of general equations in case of spanwise invariance of the infinitesimal perturbation and their numerical implementation. Finally, we describe the main implementation details of the equations.
- **Chapter 3: Results**: A description of the main discretization parameters considered to obtain reliable results. Linear code validations and results concerning modal and nonmodal stability analysis. The least stable eigenvalue and the maximum of the transient growth as functions of main physical parameters are reported with respect to the plane Poiseuille flow.
- **Conclusions**
- **Appendix A: Further Results**: Further results computed through linear analysis. Results of modal and nonmodal stability analysis as function of spanwise wavenumber. Spatial frameworks of an optimal initial condition and an optimal output condition. Optimal output conditions on modal expansion.

CHAPTER 1

Governing Equations

1.1. Nonlinear Disturbance Equations and Linearization

Navier-Stokes equations govern the general evolution of incompressible viscous fluid flows. These equations are a mathematical statement of the conservation law of mass and of the balance law for the momentum of a fluid. Written in non-dimensional formulation [20], [16], [25], the equations read

$$\begin{cases} \nabla \cdot \mathbf{V} = 0 \\ \\ \dfrac{\partial \mathbf{V}}{\partial t} + (\mathbf{V} \cdot \nabla)\mathbf{V} = -\nabla p + \dfrac{1}{Re}\nabla^2 \mathbf{V} \end{cases} \tag{1.1}$$

where $\mathbf{V}(\mathbf{x})$ is the non-dimensional velocity field and $\mathbf{x} \in \Omega$, $p(\mathbf{x}) = P/\overline{\rho}U^2$ is the non-dimensional pressure field and $Re = LU/\nu$ is the Reynolds number. U is an appropriate velocity scale, i.e. the centerline velocity for the channel flow, L is a length scale, for example half-height of the channel flow. The incompressible nature of the fluid involves that the energy equation is decoupled from (1.1) and pressure does not satisfy a state equation but it acts as a *Lagrange multiplier* to enforce the incompressibility constraint. Moreover mass conservation is expressed by an equation which is not evolutive. These equations have to be supplemented with boundary and initial conditions of the form

$$\mathbf{V}(\mathbf{x}, 0) = \mathbf{V_0}((\mathbf{x})), \quad \mathbf{x} \in \Omega, \quad \nabla \cdot \mathbf{V_0} = 0 \tag{1.2}$$

$$\mathbf{V}(\mathbf{x}, t) = \mathbf{b}(\mathbf{x}, t), \quad \mathbf{x} \in \partial\Omega, \quad t \geq 0. \tag{1.3}$$

Boundary values must satisfy an important compatibility condition due to the divergence theorem

$$\int_{\Omega} \nabla \cdot \mathbf{V} d\Omega = \int_{\partial\Omega} \mathbf{V} \cdot \mathbf{n} d\Omega = \int_{\partial\Omega} \mathbf{b} \cdot \mathbf{n} d\Omega = 0, \quad t \geq 0. \tag{1.4}$$

Since only the pressure gradient appears in the governing equations, pressure is defined up to an arbitrary function of time $\overline{P}(t)$ which may be assigned [20], [21] as

$$\overline{P}(t) = \frac{1}{\Omega} \int_{\Omega} P(\mathbf{x}, t) d\Omega \tag{1.5}$$

Navier Stokes equations are nonlinear partial derivative equations, and can be solved analytically for a few simple cases, and also numerical solutions involve a huge amount of numerical resources (DNS).

Stability analysis involves the study of the evolution of an infinitesimal perturbation of a fluid flow.

Assuming to know a stationary solution $\overline{\mathbf{V}}(\mathbf{x})$, $\overline{P}(\mathbf{x})$ of Navier Stokes equations, we want to study the evolution of a small velocity-pressure field perturbation in the fluid. The evolutive equations for an infinitesimal disturbance can be derived by considering a basic state $(\overline{\mathbf{V}}(\mathbf{x}), \overline{P}(\mathbf{x})$ and a perturbed state $(\overline{\mathbf{V}}(\mathbf{x}) + \mathbf{v}(\mathbf{x}, t), \overline{P}(\mathbf{x}) + p(\mathbf{x}, t)$, both satisfying the Navier-Stokes equations. By substituting these variables in the momentum equation and taking into account that the base flow satisfy the equations of the stationary problem, one obtains the following equation

$$\frac{\partial \mathbf{v}}{\partial t} + (\overline{\mathbf{V}} \cdot \nabla)\mathbf{v} + (\mathbf{v} \cdot \nabla)\overline{\mathbf{V}} + (\mathbf{v} \cdot \nabla)\mathbf{v} + \nabla p = \frac{1}{Re} \nabla^2 \mathbf{v} \tag{1.6}$$

This equation still remains nonlinear because of the term $(\mathbf{v} \cdot \nabla)\mathbf{v}$ which is quadratic for the perturbation velocity. However if the initial perturbation is small enough (possibly infinitesimal), one could think to study its evolution not considering this nonlinear term. This approximation is the basis of the nonlinear stability analysis and it represents the basis of the present work. The solutions analysed are linear solutions obtained through the linearization of fluid equations, for a proper established, stationary base flow which is a known stationary solution of Navier-Stokes equations.

With a linearized formulation the equations state:

$$\begin{cases} \nabla \cdot \mathbf{v} = 0 \\ \\ \dfrac{\partial \mathbf{v}}{\partial t} + (\overline{\mathbf{V}} \cdot \nabla)\mathbf{v} + (\mathbf{v} \cdot \nabla)\overline{\mathbf{V}} = -\nabla p + \dfrac{1}{Re} \nabla^2 \mathbf{v} \\ \\ \mathbf{v}(\mathbf{x}, 0) = \mathbf{v_0} \quad \mathbf{x} \in \Omega \\ \\ \mathbf{v}(\mathbf{x}, t) = \mathbf{b}(\mathbf{x}, \mathbf{t}) \quad \mathbf{v} \in \partial\Omega \end{cases} \tag{1.7}$$

where $\mathbf{b}(\mathbf{x}, t)$ can be an appropriate base flow imposed at the boundary. These representation is characterized by a simpler solution in terms of computational resources even if it is useful to introduce a more compact formulation of the problem through the use of the well-known *wall-normal velocity-vorticity formulation.*

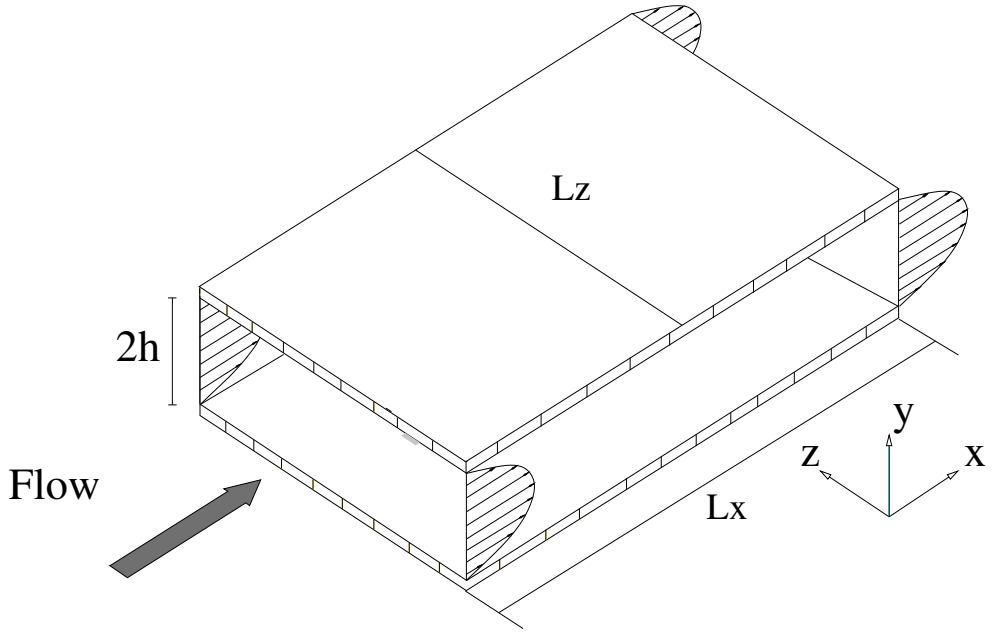

Figure 1.1.: *Flow Physical domain geometry*

1.2. Wall-normal velocity and vorticity formulation

Wall-normal velocity and vorticity formulation of Navier-Stokes equations is now displayed.

Introducing a spatial discretization of Eq. (1.1) and Eq. (1.7) one obtains an algebraic-differential problem in time.

Mass equation is not evolutive equation in time, whereas momentum equation is an evolutive (differential) equation in time. It would be useful to introduce a particular formulation that has only evolutive equations. It is useful to introduce a model problem which consists in an incompressible flow between two plane parallel infinite walls, also known as channel flow represented in Fig. (1.1). No-slip and no-penetration boundary conditions are imposed at the walls. In cartesian coordinates $\mathbf{x} = (x, y, x)$ one may define three Velocity components in streamwise (x), wall-normal (y) and spanwise (z) directions U, V, W respectively

$$\mathbf{V} = (U, V, W) \tag{1.8}$$

After substitution of the velocity components into Navier-Stokes equations (1.1), one obtains:

$$\begin{cases} \dfrac{\partial U}{\partial x} + \dfrac{\partial V}{\partial y} + \dfrac{\partial W}{\partial z} \\ \dfrac{\partial U}{\partial t} + U\dfrac{\partial U}{\partial x} + V\dfrac{\partial U}{\partial y} + W\dfrac{\partial U}{\partial z} = -\dfrac{\partial p}{\partial x} + \dfrac{1}{Re}\nabla^2 U \\ \dfrac{\partial V}{\partial t} + U\dfrac{\partial V}{\partial x} + V\dfrac{\partial V}{\partial y} + W\dfrac{\partial V}{\partial z} = -\dfrac{\partial p}{\partial y} + \dfrac{1}{Re}\nabla^2 V \\ \dfrac{\partial W}{\partial t} + U\dfrac{\partial W}{\partial x} + V\dfrac{\partial W}{\partial y} + W\dfrac{\partial W}{\partial z} = -\dfrac{\partial p}{\partial z} + \dfrac{1}{Re}\nabla^2 W. \end{cases} \tag{1.9}$$

Considering the geometry of the domain of the problem analysed, Reynolds number Re can be defined as

$$Re = \frac{U_C h}{\nu} \tag{1.10}$$

where U_C is the centerline velocity of the Poiseuille flow and h is the half-width of the channel flow. Projecting the equations (1.9) on a divergence-free manifold, where continuity equation is implicitly satisfied and pressure no longer appears, in cartesian coordinates, one obtains only evolutive equations in time, also known as $V - \eta\, formulation$ of Navier-Stokes equations. This formulation is a system of two scalar differential equations for the wall-normal velocity V and for the wall normal vorticity η defined as

$$\eta = \frac{\partial U}{\partial z} - \frac{\partial W}{\partial x} \tag{1.11}$$

The equation for the wall-normal velocity can be obtained by taking the laplacian of the y-component of the momentum equation.

$$\frac{\partial \nabla^2 V}{\partial t} + \nabla^2\left(U\frac{\partial V}{\partial x}\right) + \nabla^2\left(V\frac{\partial V}{\partial y}\right) + \nabla^2\left(W\frac{\partial V}{\partial z}\right) = -\frac{\partial \nabla^2 p}{\partial y} + \frac{1}{Re}\nabla^2\left(\nabla^2 V\right) \tag{1.12}$$

Considering (1.1) and taking the divergence of the momentum equation and using continuity equation leads to a Poisson equation for the pressure field

$$\nabla^2 p = -\nabla \cdot \left[\left(\mathbf{V}\cdot\nabla\right)\mathbf{V}\right] \tag{1.13}$$

Expanding term by term (1.13) one obtains

$$\begin{aligned}\nabla^2 p = &\frac{\partial}{\partial x}\left(U\frac{\partial U}{\partial x} + V\frac{\partial U}{\partial y} + W\frac{\partial U}{\partial z}\right)\\ &+ \frac{\partial}{\partial y}\left(U\frac{\partial V}{\partial x} + V\frac{\partial V}{\partial y} + W\frac{\partial V}{\partial z}\right)\\ &+ \frac{\partial}{\partial z}\left(U\frac{\partial W}{\partial x} + V\frac{\partial W}{\partial y} + W\frac{\partial W}{\partial z}\right)\end{aligned} \tag{1.14}$$

Substituting the laplacian of pressure p in Eq. (1.12) and remembering that

$$\nabla^2 = \left[\frac{\partial^2}{\partial x^2}, \frac{\partial^2}{\partial y^2}, \frac{\partial^2}{\partial z^2}\right], \tag{1.15}$$

after some algebra one obtains:

$$\frac{\partial \nabla^2 V}{\partial t} = f_V + \frac{1}{Re}\nabla^2(\nabla^2 V) \tag{1.16}$$

where f_V reads:

$$\begin{aligned}f_V = &\frac{\partial}{\partial y}\left[\frac{\partial}{\partial x}\left(U\frac{\partial U}{\partial x} + V\frac{\partial U}{\partial y} + W\frac{\partial U}{\partial z}\right) + \frac{\partial}{\partial z}\left(U\frac{\partial W}{\partial x} + V\frac{\partial W}{\partial y} + W\frac{\partial W}{\partial z}\right)\right]\\ &- \left(\frac{\partial^2}{\partial x^2} + \frac{\partial^2}{\partial z^2}\right)\left(U\frac{\partial V}{\partial x} + V\frac{\partial V}{\partial y} + W\frac{\partial V}{\partial z}\right).\end{aligned} \tag{1.17}$$

The equation for the wall-normal vorticity can be easily obtained by taking the $y-component$ of the curl of the momentum equation for $\overline{V}$, or by subtracting the x derivative of the z momentum equation to the z derivative of the x momentum equation:

$$\frac{\partial \eta}{\partial t} = f_\eta + \frac{1}{Re}\nabla^2 \eta \tag{1.18}$$

where f_η reads:

$$f_\eta = \frac{\partial}{\partial x}\left(U\frac{\partial W}{\partial x} + V\frac{\partial W}{\partial y} + W\frac{\partial W}{\partial z}\right) - \frac{\partial}{\partial z}\left(U\frac{\partial U}{\partial x} + V\frac{\partial U}{\partial y} + W\frac{\partial U}{\partial z}\right) \tag{1.19}$$

The $V-\eta\, formulation$ is therefore composed by two evolutive equations for the wall-normal velocity component V and for the wall-normal vorticity component η:

$$\begin{cases}\frac{\partial \nabla^2 V}{\partial t} = f_V + \frac{1}{Re}\nabla^2(\nabla^2 V)\\ \\ \frac{\partial \eta}{\partial t} = f_\eta + \frac{1}{Re}\nabla^2 \eta\end{cases} \tag{1.20}$$

These equations have to be supplemented with boundary, typically of the form

$$V(x, \pm h, z, t) = 0 \tag{1.21}$$

$$\frac{\partial V}{\partial y}(x, \pm h, z, t) = 0 \tag{1.22}$$

$$\eta(x, \pm h, z, t) = 0 \tag{1.23}$$

where Eq. (1.21) is due to no-slip condition at the boundary of the velocity field, whereas Eq. (1.22) results from the continuity equation at the boundary, hence $\nabla \cdot \mathbf{V}\,|_{y=\pm h} = 0$, where $U\,|_{y\pm h} = 0$ and $W\,|_{y\pm h} = 0$.

The boundary condition Eq. (1.23) is homogeneous because of the no-slip condition at the boundary. Indeed the $y-component$ of the curl at the boundary depends only on the variation at the walls of (u, w) which are tangent at the surface and equal to zero. It is useful to remember that these boundary conditions depend on the choice to use a domain delimited by two parallels infinite walls. One could think to define different boundary conditions for example imposing a proper velocity flow $W(x, y = \pm h) \neq 0$, then the problem solved would be completely different because $\eta(x, \pm h, z, t) = -\frac{\partial W}{\partial x}|_{y=\pm h}$.
A complete description of the fluid dynamic in both space and time needs also initial conditions:

$$V(x, y, z, t = 0) = V_0(x, y, z) \tag{1.24}$$

$$\eta(x, y, z, t = 0) = \eta_0(x, y, z) \tag{1.25}$$

The spanwise and streamwise velocity components may be recovered from th definition of η and the continuity equations:

$$\begin{cases} \frac{\partial U}{\partial x} + \frac{\partial W}{\partial z} = -\frac{\partial V}{\partial y} \\ \frac{\partial U}{\partial z} - \frac{\partial W}{\partial x} = \eta \end{cases} \tag{1.26}$$

Once the full velocity field is known, p is recovered from the relative Poisson equation.

1.3. Poiseuille flow: Orr-Sommerfeld-Squire equations

The wall-normal velocity-vorticity formulation of Navier-Stokes equations has been derived for a global flow field $\mathbf{V} = (U, V, W)$. The study of linear stability of a plane Poiseuille flow is based on linearized equations, so considering a reference steady solution, the linearization process is now exposed.

1.3.1. Linear disturbance equations

Let us consider the indefinite channel flow as before, characterized by two plane parallel infinite walls, and a channel half-gap $h = 1$. The wall boundary conditions are homogeneous for the U, V and W velocity components.

The streamwise steady base flow solution $\overline{U}(y)$ of the governing equations (1.1) generated by the longitudinal pressure gradient $\overline{P}_x$, is also known as Poiseuille flow:

$$\overline{U} = 1 - y^2 \tag{1.27}$$

The velocity field $\mathbf{V}$, considering a three-dimensional small perturbation is decomposed as:

$$U = \overline{U} + u \tag{1.28}$$
$$V = v \tag{1.29}$$
$$W = w \tag{1.30}$$

Assuming this, it may be noticed that flow is spatially invariant in x and z direction, or the problem is characterized by two homogeneous directions x, z, and one non-homogeneous direction y. Expanding the equations (1.7) for the velocity field considered, one obtains:

$$\begin{cases} \dfrac{\partial u}{\partial x} + \dfrac{\partial v}{\partial y} + \dfrac{\partial w}{\partial z} = 0 \\ \dfrac{\partial u}{\partial t} + \overline{U}\dfrac{\partial u}{\partial x} + v\overline{U}' = -\dfrac{\partial p}{\partial x} + \dfrac{1}{Re}\nabla^2 u \\ \dfrac{\partial v}{\partial t} + \overline{U}\dfrac{\partial v}{\partial x} = -\dfrac{\partial p}{\partial y} + \dfrac{1}{Re}\nabla^2 v \\ \dfrac{\partial w}{\partial t} + \overline{U}\dfrac{\partial w}{\partial x} = -\dfrac{\partial p}{\partial z} + \dfrac{1}{Re}\nabla^2 w \end{cases} \tag{1.31}$$

This is a system of linearized partial differential equations and it can be noticed that the homogeneity of x and z directions is verified because the coefficients of the equations of the system depend only on y coordinate. The equations could be translated either in x and z directions but they do not change, mathematically speaking this is also called an *autonomous system* of differential equations in x and z directions [22].

Upon linearization of the equations in $v - \eta$ (1.20), one obtains:

$$\begin{cases} \dfrac{\partial \nabla^2 V}{\partial t} = \left[-\overline{U}\nabla^2\dfrac{\partial}{\partial x} + \overline{U}''\dfrac{\partial}{\partial x} + \dfrac{1}{Re}\nabla^2\nabla^2\right] v \\ \dfrac{\partial \eta}{\partial t} = \left[-\overline{U}'\dfrac{\partial}{\partial z}\right] v + \left[-\overline{U}\dfrac{\partial}{\partial x} + \dfrac{1}{Re}\nabla^2\right] \eta \end{cases} \tag{1.32}$$

It can be noticed that the equations are characterized by one-way coupling of the η equation with the v equation. Moreover also this system is an autonomous system of differential evolutive equations in x and z directions.

This pair of equations with the boundary conditions

$$v\left(x,\pm 1,z,t\right)=0 \tag{1.33}$$

$$\frac{\partial v}{\partial y}\left(x,\pm 1,z,t\right)=0 \tag{1.34}$$

$$\eta\left(x,\pm 1,z,t\right)=0 \tag{1.35}$$

and the initial conditions

$$v\left(x,y,z,t=0\right)=v_0\left(x,y,z\right) \tag{1.36}$$

$$\eta\left(x,y,z,t=0\right)=\eta_0\left(x,y,z\right) \tag{1.37}$$

provides a complete description of the evolution of an arbitrary disturbance in both space and time.

1.3.2. Projection in Fourier Space

The assumption of spatial invariance in x and z allows using a Fourier series expansion [4] [8] of the unknowns v, η [27]:

$$v(x,y,z,t)=\sum_{\alpha=-\infty}^{\infty}\sum_{\beta=-\infty}^{\infty}=\hat{v}\left(\alpha,y,\beta,t\right)e^{j(\alpha x+\beta z)} \tag{1.38}$$

$$\eta(x,y,z,t)=\sum_{\alpha=-\infty}^{\infty}\sum_{\beta=-\infty}^{\infty}=\hat{\eta}\left(\alpha,y,\beta,t\right)e^{j(\alpha x+\beta z)} \tag{1.39}$$

where α and β denote the streamwise and spanwise wavenumbers. We are looking for wavelike solutions of period 2π, and wave-length respectivelyL_x for α and L_z for β wavenumbers. Hence one obtains $\alpha=\frac{2\pi}{L_x}$ and $\beta=\frac{2\pi}{L_z}$.

It is not possible to solve the equations (1.32) for each wavenumber so the expansions are truncated. N_x and N_z define the degree of the spectral expansion respectively for streamwise wavenumbers and for spanwise wavenumbers:

$$v(x,y,z,t)=\sum_{\alpha=-N_x}^{N_x}\sum_{\beta=-N_z}^{N_z}=\hat{v}\left(\alpha,y,\beta,t\right)e^{j(\alpha x+\beta z)} \tag{1.40}$$

$$\eta(x,y,z,t)=\sum_{\alpha=-N_x}^{N_x}\sum_{\beta=-N_z}^{N_z}=\hat{\eta}\left(\alpha,y,\beta,t\right)e^{j(\alpha x+\beta z)} \tag{1.41}$$

Introducing these expansions into (1.32), considering that the linearized equations are characterized by constant coefficient in x and z, is equivalent in taking the Fourier transform in x and z directions, hence it results

$$\begin{cases} \dfrac{\partial \hat{\Delta}\hat{v}}{\partial t} = \left[-j\alpha\overline{U}\hat{\Delta} + j\alpha\overline{U}''\dfrac{1}{Re}\hat{\Delta}\hat{\Delta} \right] v \\ \dfrac{\partial \hat{\eta}}{\partial t} = \left[-j\beta\overline{U}' \right] \hat{v} + \left[-j\alpha\overline{U} + \dfrac{1}{Re}\hat{\Delta} \right] \hat{\eta} \end{cases} \tag{1.42}$$

where $\hat{\Delta} = \frac{\partial^2}{\partial y^2} - \kappa^2 = \mathcal{D}^2 - \kappa^2$ and $\kappa^2 = \alpha^2 + \beta^2$.
This is a parametric family of partial differential equations in y, t whose parameters are α and β.
Linear dynamics decouples in wavenumber space because Fourier modes are orthogonal. This is an important simplification because one can consider one wavenumber at a time and solve (1.42) for each couple of wavenumbers (α, β).

In physical space this leads to solve the linearized equation for a small disturbance in a spatial domain whose dimensions are $(L_x = 2\pi/\alpha, 2, L_z = 2\pi/\beta)$ for each couple of wavenumbers (α, β) because each solution is periodic in x and z directions.

The equations (1.42) can be rewritten in the form

$$\frac{\partial}{\partial t} \begin{pmatrix} \hat{v} \\ \hat{\eta} \end{pmatrix} = \begin{pmatrix} \mathcal{L}_{OS} & 0 \\ \mathcal{L}_C & \mathcal{L}_{SQ} \end{pmatrix} \begin{pmatrix} \hat{v} \\ \hat{\eta} \end{pmatrix}, \tag{1.43}$$

where:

- $\mathcal{L}_{OS} = \hat{\Delta}^{-1} \left[-j\alpha\overline{U}\hat{\Delta} + j\alpha\overline{U}''\frac{1}{Re}\hat{\Delta}\hat{\Delta} \right]$ is the Orr-Sommerfeld operator
- $\mathcal{L}_{SQ} = \left[-j\alpha\overline{U} + \frac{1}{Re}\hat{\Delta} \right]$ is the Squire operator
- $\mathcal{L}_C = \left[-j\beta\overline{U}' \right]$ is the coupling operator

To recover the other components of the perturbation u and w one has to consider an expansion like (1.38) and (1.39); using the continuity equation and the definition of η in Fourier space:

$$j\alpha\hat{u} + j\beta\hat{w} = -\frac{d\hat{v}}{dy} \tag{1.44}$$

$$j\beta\hat{u} - j\alpha\hat{w} = \hat{\eta} \tag{1.45}$$

If one wants to study the amplitude growth or decay of a disturbance, assuming a temporal dependence of the form

$$\begin{pmatrix} \hat{v}(y,t) \\ \hat{\eta}(y,t) \end{pmatrix} = \begin{pmatrix} \tilde{v}(y) \\ \tilde{\eta}(y) \end{pmatrix} e^{-j\omega t}, \tag{1.46}$$

obtains:

$$\begin{cases} \left[\left(-j\omega + j\alpha\overline{U}\right)\left(\mathcal{D}^2 - \kappa^2\right) - j\alpha\overline{U}'' - \dfrac{1}{Re}\left(D^2 - \kappa^2\right)^2\right]\tilde{v} = 0 \\ \left[\left(-j\omega + j\alpha\overline{U}\right) - \dfrac{1}{Re}\left(\mathcal{D}^2 - \kappa^2\right)\right]\tilde{\eta} = -j\beta\overline{U}'\tilde{v} \end{cases} \tag{1.47}$$

which is known as the Orr-Sommerfeld-Squire form of equations. The first equation of (1.47) is the classical Orr-Sommerfeld equation and the second equation for the normal vorticity is also known as the Squire equation.

The frequency ω appears as the eigenvalue of the Orr-Sommerfeld equation, and together with the associated eigenfuncion $\tilde{v}$ are generally complex. The same conclusions can be done for Squire equation with the only difference that is coupled with Orr-Sommerfeld equation.

The Orr-Sommerfeld-Squire equations have two classes of eigensolutions:

- Orr-Sommerfeld modes $\left\{\tilde{v}, \tilde{\eta}^f, w\right\}$ if $\tilde{\eta}^f$ is given by forcing the η equation with $\tilde{v}$ modes
- Squire modes $\{\tilde{v} = 0, \tilde{\eta}, w\}$ when the Orr-Sommerfeld equation has homogeneous solutions.

The study of modes leads to (linear) modal stability analysis of the disturbance in order to find the minimum parameter values above which a specific initial condition of infinitesimal amplitude grows exponentially, or is asymptotic stable.

1.4. Hydrodynamic Stability Theory

The hydrodynamic stability theory concerns the description of the behaviour of a flow subject to an infinitesimal disturbance superimposed. This assumption is based on the linearization of Navier-Stokes equation exposed in Sec. (1.1) in which, considering infinitesimal perturbation of a steady solution of steady Navier-Stokes equations, leads to consider the nonlinear terms negligible. Therefore the principal aim of hydrodynamic stability is to describe the evolution of an initial perturbation in time and to define the critical parameters above which a baseflow solution of Navier-Stokes becomes unstable.

In this section we introduce the general concepts of stability analysis referring to the simple case of Orr-Sommerfeld-Squire equations. The analysis for the Poiseuille flow over a steady Stokes layer, which is the aim of the present work, will be discussed in Chap. (2), for a better comprehension of the operators used in this work.

1.4.1. Stability: definitions

The description of the development of an initial infinitesimal perturbation can be done introducing a function that measures its size. The natural choice usually is the disturbance kinetic energy. Considering a reference volume $\mathcal{V}$ the kinetic energy of a perturbation $\mathbf{v}$ is defined as :

$$E_{\mathcal{V}}(t) = \frac{1}{2}\int_{\mathcal{V}} \mathbf{v}\cdot\mathbf{v}dV. \tag{1.48}$$

In cartesian coordinate (x, y, z) for a parallel channel flow whose dimensions are L_x, L_y, L_z obviously

$$E_{\mathcal{V}}(t) = \frac{1}{2}\int_{L_x}\int_{L_y}\int_{L_z}\left(u^2+v^2+w^2\right)dxdydz. \tag{1.49}$$

The choice of V depends on the flow geometry; for a plane Poiseuille channel flow a correct choice could be a box containing one space-period of the disturbance in x and z direction and the height of the channel in y direction.

Considering $E_{\mathcal{V}}(t)$ as an indicator of the stability characteristics of a base flow, we introduce four definitions of stability.

Definition 1 (Stability)**.** *A solution $\overline{\mathbf{V}}, \overline{P}$ solution to the Navier-Stokes equations is stable to a perturbation if the perturbation energy goes to 0 as time tends to infinity:*

$$\lim_{t\to\infty} E_V(t) = 0 \tag{1.50}$$

Definition 2 (Conditional Stability)**.** *A solution $\overline{\mathbf{V}}, \overline{P}$ is conditionally stable if exists a threshold $\overline{E} > 0$ and it is stable for $E(0) < \overline{E}$.*

Definition 3 (Global Stability)**.** *A solution $\overline{\mathbf{V}}, \overline{P}$ is globally stable if it is conditionally stable and the threshold energy is infinite $\overline{E} \to \infty$*

Definition 4. *A solution $\overline{\mathbf{V}}, \overline{P}$ is monotonically stable if it is globally stable and:*

$$\frac{dE}{dt} < 0 \qquad \forall t > 0 \tag{1.51}$$

1.4.2. Critical Reynolds Number

Considering the definitions of stability, it is possible to introduce the following critical Reynolds number:

- (Re_E) For $Re < Re_E$ the flow is monotonically stable
- (Re_G) For $Re < Re_G$ the flow is globally stable
- (Re_L) For $Re < Re_L$ the flow is linearly stable

It can be observed that frequently for different base flows the following relation is verified:

$$Re_E < Re_G < Re_L. \tag{1.52}$$

1.4.3. Classical Stability analysis: Modal stability

The stability of a viscous channel flow perturbed with an infinitesimal perturbation has been studied in two different ways: linear stability analysis and energy methods. These approaches consist in:

- Linear stability: deals with defining the minimum critical parameters above which a specific initial condition of infinitesimal amplitude grows exponentially;

- Energy stability: deals with defining the maximum critical parameters below which a general initial condition of finite amplitude decays monotonically.

The linear stability analysis involves two steps: linearization of Navier-Stokes equations and diagonalization by determining the eigenvalues of the linearized problem. A common simplification in many stability calculations is the assumption of an exponential time dependence of the evolution of the perturbation: this leads to Orr-Sommerfeld-Squire equation form Eq. (1.47) which can be considered as an eigenvalue problem. This analysis is also known as normal-mode approach. The computed eigenvalues are investigated and the basic flow is considered unstable if an eigenvalue is found in the unstable complex-half plane, because there is an exponentially growing mode of the eigenvalue problem.

Energy methods are based on variational approach and yield conditions for no energy growth for perturbation of arbitrary amplitude.

The results of these analysis show that Poiseuille flow is linearly stable if the Reynolds number $Re < Re_c = 5772.22$ [15] and there could be possible energy amplifications for $Re > Re_E = 49.6$, whereas experiments show that Poiseuille flow undergoes transition at $Re \approx 1000$. These discrepancies between analytical and experimental results allow us to infer that both energy and linear stability methods do not give informations when $Re_E < Re < Re_c$. In this intermediate case the energy of small perturbations decays to zero as $\lim t \to \infty$, but there could be a transient growth before the decay. Indeed, the eigenvalues of an eigenvalue problem give us informations about the asymptotic behaviour of the solutions, as $t \to \infty$ but we do not have informations about short-time dynamics as $t \to 0^+$. This growth occurs with absence of nonlinear effects and can be explained by the non-orthogonality of the Orr-Sommerfeld eigenfunctions. This non orthogonality is caused by Orr-Sommerfeld operator, associated to Orr-Sommerfeld equation, which is non-normal. A complete analysis of stability must take account this non-orthogonality, and analyse only the eigenvalues for a non-normal operator, is not sufficient to understand completely the dynamic of an initial perturbation. Indeed we have to take into account a possible linear instability without unstable eigenvalues.

1.4.4. Nonmodal Stability

We present a new formulation of linear stability which takes into account the evolution of a perturbation for $t \to 0^+$ also called nonmodal stability.

Problem Statement

We start, without any lack of generality by considering the linearized Navier-Stokes equations Eq. (1.7) for an infinitesimal perturbation of a plane Poiseuille flow, characterized by one non-homogeneous direction y and two homogeneous directions x and z. The same procedure will be presented in Chap. (2) for the plane Poiseuille flow over steady Stokes Layer.

Rewriting Eq. (1.43)

$$\frac{\partial}{\partial t}\begin{pmatrix} \hat{v} \\ \hat{\eta} \end{pmatrix} = \begin{pmatrix} \mathcal{L}_{OS} & 0 \\ \mathcal{L}_C & \mathcal{L}_{SQ} \end{pmatrix}\begin{pmatrix} \hat{v} \\ \hat{\eta} \end{pmatrix}, \tag{1.53}$$

where $\mathcal{L}_{OS}$ and $\mathcal{L}_{SQ}$ are respectively Orr-Sommerfeld and Squire operators and $\mathcal{L}_C$ is the coupling operator, one may consider the following Cauchy problem:

$$\begin{cases} \dot{\hat{\mathbf{q}}} = A\hat{\mathbf{q}} \\ \hat{\mathbf{q}}(0) = \hat{\mathbf{q}}_0 \end{cases} \tag{1.54}$$

where $\hat{\mathbf{q}}_0$ is the initial condition and with

$$\hat{\mathbf{q}} = \begin{pmatrix} \hat{v} \\ \hat{\eta} \end{pmatrix} \tag{1.55}$$

The solution of Eq. (1.54) may be expressed as

$$\hat{\mathbf{q}}(t) = \mathrm{e}^{At}\hat{\mathbf{q}}_0 \tag{1.56}$$

This expresses the evolution of an initial perturbation.

The development of a perturbation is measured by kinetic energy so we have to define the kinetic energy density in Fourier space for the wall-normal velocity-vorticity formulation.

Kinetic energy density

The kinetic energy density is

$$e_V(t) = \frac{1}{2L_xL_yL_z}\int_{L_x}\int_{L_y}\int_{L_z}\left(u^2+v^2+w^2\right)dxdydz. \tag{1.57}$$

In $\hat{v}-\hat{\eta}$ formulation we have to Fourier transform; considering Eqs. (1.44)(1.45) the wall-tangent velocities $\hat{u}$ and $\hat{w}$ can be written as

$$\hat{u} = \frac{1}{k^2}\left(\alpha\frac{\partial\hat{v}}{\partial y} - \beta\hat{\eta}\right) \tag{1.58}$$

$$\hat{\eta} = \frac{1}{k^2}\left(\beta\frac{\partial\hat{v}}{\partial y} + \alpha\hat{\eta}\right). \tag{1.59}$$

The kinetic energy density can be easily written in Fourier-space as:

$$e(\alpha,\beta,t)=\frac{1}{2}\left(\frac{1}{2\kappa^2}\int_{-1}^{+1}\left(|\mathcal{D}\hat{v}|^2+k^2|\hat{v}|^2+|\hat{\eta}|^2\right)\right)dy \tag{1.60}$$

This is an integral operator and considering the inner product formulation [24] may be expressed as:

$$e(\alpha,\beta,t)=\frac{1}{2}\left(\frac{1}{2\kappa^2}\int_{-1}^{+1}(\hat{\mathbf{q}})^H\begin{pmatrix}k^2+\mathcal{D}^2 & 0\\ 0 & 1\end{pmatrix}(\hat{\mathbf{q}})\right)dy \tag{1.61}$$

We define the *energy norm* [24][27] as

$$\|\hat{\mathbf{q}}\|_E^2=\int_{-1}^{+1}\left(|\mathcal{D}\hat{v}|^2+\kappa^2|\hat{v}|^2+|\hat{\eta}|^2\right)dy \tag{1.62}$$

Therefore introducing an appropriate weighting operators in Eq. (1.62) one obtains

$$\|\hat{\mathbf{q}}\|_E^2=\hat{\mathbf{q}}^H Q\hat{\mathbf{q}} \tag{1.63}$$

where $Q=Q^H>0$

Transient energy growth

The energy growth function is defined as [24]

$$G(t)=\max_{\hat{\mathbf{q}}_0\neq 0}\frac{\|\hat{\mathbf{q}}(t)\|_E^2}{\|\hat{\mathbf{q}}_0\|_E^2}=\left\|\mathrm{e}^{At}\right\|_E^2 \tag{1.64}$$

and its maximum is

$$G_{max}=\max_{t\geq 0}G(t)=G(t_{max}) \tag{1.65}$$

Let $Q=C^HC$ be the Cholesky decomposition of Q defined in Eq. (1.62), then

$$\|\hat{\mathbf{q}}\|_E^2=\hat{\mathbf{q}}^HC^HC\hat{\mathbf{q}}=\|\hat{\mathbf{q}}\|_2^2 \tag{1.66}$$

and for any matrix

$$\|A\|_E^2=\left\|CAC^{-1}\right\|_2^2 \tag{1.67}$$

Rewriting the initial value problem Eq. (1.54)

$$\begin{cases}\dot{\hat{\mathbf{q}}}=A\hat{\mathbf{q}}\\ \hat{\mathbf{q}}(0)=\hat{\mathbf{q}}_0\end{cases} \tag{1.68}$$

and applying the spectral decomposition $A=T\Lambda T^-1$ one obtains

$$G(t)=\max_{\hat{\mathbf{q}}_0\neq 0}\frac{\left\|CT\mathrm{e}^{\Lambda t}T^{-1}C^{-1}C\hat{\mathbf{q}}_0\right\|_E^2}{\|C\hat{\mathbf{q}}_0\|_2^2}=\left\|CT\mathrm{e}^{\Lambda t}T^{-1}C^{-1}\right\|_2^2 \tag{1.69}$$

Optimal input - Optimal output

The energy growth function $G(t)$ is the envelope of many individual growth curve of different initial condition $\hat{\mathbf{q}}_0$. For each t on $G(t)$, a specific initial condition reaches its maximum energy amplification at that time. We are interested in defining the initial condition that results in the maximum energy amplification.

Consider a fixed time $\bar{t}$ and an initial condition $\hat{\mathbf{q}}_0$, the solution of the Cauchy problem Eq. (1.54) at time $\bar{t}$ is

$$\hat{\mathbf{q}}(\bar{t}) = \mathrm{e}^{A\bar{t}}\hat{\mathbf{q}}_0 \tag{1.70}$$

where we can call:

- $\hat{\mathbf{q}}_0$ input (or initial condition)
- $\hat{\mathbf{q}}(\bar{t})$ output (or final condition)

Assuming that $\|\hat{\mathbf{q}}_0\|_E = 1$ and the output is normalized such that $\left\|\hat{\mathbf{q}}(\bar{t})\right\|_E = 1$ one obtains

$$\mathrm{e}^{A\bar{t}}\hat{\mathbf{q}}_0 = \left\|\mathrm{e}^{A\bar{t}}\right\|_E \hat{\mathbf{q}}(\bar{t}) \tag{1.71}$$

or considering the assumptions of Sec. (1.4.4)

$$\mathrm{e}^{A\bar{t}}\hat{\mathbf{q}}_0 = CT\mathrm{e}^{\Lambda\bar{t}}T^{-1}C^{-1}C\hat{\mathbf{q}}_0 = \left\|CT\mathrm{e}^{\Lambda\bar{t}}T^{-1}C^{-1}\right\|_2 C\hat{\mathbf{q}}(\bar{t}) \tag{1.72}$$

where $\left\|CT\mathrm{e}^{\Lambda\bar{t}}T^{-1}C^{-1}\right\|_2$ can be considered the amplification factor of the normalized output condition.

In order to define the optimal initial perturbation we have to introduce two important theorems

Theorem 1. *Let $\sigma_1(A)$ be the highest singular value of A then*

$$\|A\|_2 = \sigma_1(A) \tag{1.73}$$

If A is hermitian then

$$\|A\|_2 = \rho(A) \tag{1.74}$$

where $\rho(A)$ is the spectral radius of A. If A is unitary $\|A\|_2 = 1$

Theorem 2. *Given $A \in \mathbb{C}^{m\times n}$, with $m \geq n$, there exist two unitary matrices $U \in \mathbb{C}^{m\times m}$ and $V \in \mathbb{C}^{n\times n}$ and a diagonal matrix $\Sigma \in \mathbb{C}^{m\times n}$ having non negative diagonal entries such that*

$$U^H MV = \Sigma = \mathsf{diag}(\sigma_1, \sigma_2, ...\sigma_n) \tag{1.75}$$

with $\sigma_{max} = \sigma_1 \geq \sigma_2 \geq ... \geq \sigma_n = \sigma_{min}$
Entries of the matrix Σ *are called singular values of A.*
Columns of the matrix U are called left singular vectors of A.
Columns of the matrix V are called right singular vectors of A.

Taking SVD of $CT\mathrm{e}^{\Lambda\bar{t}}T^{-1}C^{-1}$ one can write

$$\left[CT\mathrm{e}^{\Lambda\bar{t}}T^{-1}C^{-1}\right]\left[\begin{array}{c|c|c|c} & & \cdots & \\ \mathbf{v}_1 & \mathbf{v}_2 & \cdots & \mathbf{v}_n \\ & & \cdots & \\ & & \cdots & \end{array}\right] = \left[\begin{array}{cccc} \sigma_1 & & & \\ & \sigma_2 & & \\ & & \ddots & \\ & & & \sigma_n \end{array}\right]\left[\begin{array}{c|c|c|c} & & \cdots & \\ \mathbf{u}_1 & \mathbf{u}_2 & \cdots & \mathbf{u}_n \\ & & \cdots & \\ & & \cdots & \end{array}\right] \tag{1.76}$$

Eq. (1.72) can be written as follows:

$$\left[CT\mathrm{e}^{\Lambda\bar{t}}T^{-1}C^{-1}\right]\mathbf{v_1} = \sigma_1\mathbf{u_1} \tag{1.77}$$

where $\hat{\mathbf{q}}_0 = C^{-1}\mathbf{v_1}$ is the initial condition for an output at time t, $q(\bar{t}) = C^{-}1\mathbf{u_1}$. Since

$$G_{max} = \max_{\hat{\mathbf{q}}_0 \neq 0} \frac{\left\|CT\mathrm{e}^{\Lambda t_{G_{max}}}T^{-1}C^{-1}C\hat{\mathbf{q}}_0\right\|_E^2}{\|C\hat{\mathbf{q}}_0\|_2^2} = \left\|CT\mathrm{e}^{\Lambda t}T^{-1}C^{-1}\right\|_2^2 \tag{1.78}$$

Let $\mathbf{v_1}$ the first right singular vector $\mathbf{u_1}$ the first left singular vector and σ_1 the largest singular value of matrix $CT\mathrm{e}^{\Lambda t_{G_{max}}}T^{-1}C^{-1}$ then:

- the optimal initial condition is $\hat{\mathbf{q}}_{0,opt} = C^{-}1v_1$
- the optimal output is $\hat{\mathbf{q}}(t_{G_{max}})_{opt} = C^{-}1u_1$
- $Gmax = \sigma_1^2$

CHAPTER 2

Plane Poiseuille flow over SSL

The linearized Navier-Stokes disturbance equations for a plane Poiseuille flow lead, in $v - \eta\, formulation$ to Orr-Sommerfeld-Squire equations.

We aim at exploring how the stability characteristics of the indefinite plane channel flow, or Poiseuille flow, are modified by the presence of an additional component to the base flow given by the spanwise velocity distribution at the wall. In order to achieve this goal we present the usual procedure of converting the disturbance evolution equations into the $v - \eta$ formulation.

It is our hope that understanding how the GSL interacts with the Poiseuille flow in terms of linear stability properties, will help understanding how the GSL affects the turbulent drag.

2.1. Problem statement

We consider the non-dimensional incompressible Navier-Stoke equations in cartesian coordinates for the geometry of an indefinite plane channel flow as in Fig. (2.1). We limit ourselves to the simpler case of standing waves, Steady Stokes Layer (SSL).

The wall boundary conditions are homogeneous for the U and V components, whereas the spanwise non-dimensional component is given by

$$W = A\cos(\kappa x) \tag{2.1}$$

on both channel walls, where A is the wave amplitude of spanwise velocity forcing and κ is its relative wavenumber.

The reference length and velocity scales are the channel half-gap $h = 1$ and the centerline velocity U_C of the reference Poiseuille flow. The reference Reynolds number can be written as follow:

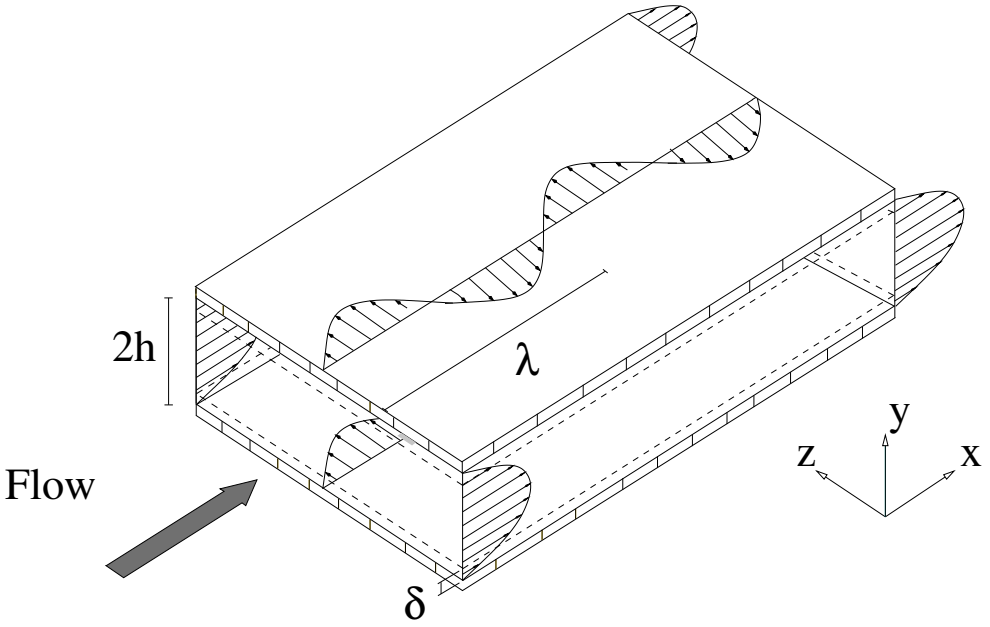

Figure 2.1.: *Flow Physical domain geometry with a steady Stokes layer imposed*

$$Re = \frac{U_C h}{\nu}, \tag{2.2}$$

where ν is the fluid viscosity.

The base flow solution of steady Navier-Stokes equations for an indefinite plane channel flow characterized by a pressure gradient $\overline{P}_x$ and a spanwise velocity (2.1) at the walls, can be considered, if the streamwise flow is laminar, as the overlap of two independent base flows:

- The streamwise baseflow $\overline{U}(y)$;
- The spanwise baseflow $\overline{W}(x, y)$.

Indeed it has been shown by [18] that, when the streamwise flow is laminar its parabolic profile does not interact with the spanwise boundary layer, also called steady Stokes Layer created by the waves at the walls.

The streamwise non-dimensional parabolic profile for $y \in [-1, 1]$ is the Poiseuille solution:

$$\overline{U}(y) = 1 - y^2. \tag{2.3}$$

The spanwise profile is given an analytic expression under the hypotheses that its thickness is small compared to the channel half-height [18], and the streamwise viscous diffusion term is negligible w.r.t. the wall-normal diffusion term. If the streamwise profile is linear within the SSL, with $u_{y,0}$ its slope at the wall, then the analytical solution is:

$$\overline{W}(x,y) = \frac{1}{\mathrm{Ai}(0)} \Re \left\{ \mathrm{e}^{j\kappa x} \mathrm{Ai}\left(-\frac{jy}{\delta_x} \mathrm{e}^{-j4/3\pi} \right) \right\} \tag{2.4}$$

with Ai indicating the Airy special function, and $\delta_x = (\nu/\kappa u_{y,0})$ expressing a representative wall-normal length scale of the transversal boundary layer, defined in terms of the fluid viscosity ν, the wave length $2\pi/\kappa$ of the wall forcing and the longitudinal wall shear $u_{y,0}$.

The spanwise base flow can also be computed considering the third component W of momentum equation of (1.9). In the laminar case where $\overline{U}$ is analytically known, for a stationary problem one obtains for W velocity component

$$\left(1-y^2\right) \frac{\partial W}{\partial x} = \frac{1}{Re} \left(\frac{\partial^2 W}{\partial x^2} + \frac{\partial^2 W}{\partial y^2} \right) \tag{2.5}$$

The non-dimensional boundary condition is:

$$W(x,\pm 1,z,t) = \frac{A}{2} \left(\mathrm{e}^{j\kappa x} + \mathrm{e}^{-j\kappa x} \right) \tag{2.6}$$

where A is made non-dimensional against the centerline velocity U_C of the reference Poiseuille flow. The equation (2.5) is linear and has constant coefficient in x direction. Considering periodic boundary condition one uses the separation of variables by assuming that:

$$W(x,y) = \frac{1}{2} \left(f(y) \mathrm{e}^{j\kappa x} + f^*(y) \mathrm{e}^{-j\kappa x} \right) \tag{2.7}$$

with $*$ denoting complex conjugate. By substitution in (2.5) one obtains:

$$\begin{aligned} jk\left(1-y^2\right)\left(f(y)\mathrm{e}^{j\kappa x} - f^*(y)\mathrm{e}^{-j\kappa x}\right) = &-\frac{k^2}{Re}\left(f(y)\mathrm{e}^{j\kappa x} + f^*(y)\mathrm{e}^{-j\kappa x}\right) \\ &+ \frac{1}{Re}\left(f''(y)\mathrm{e}^{j\kappa x} + f^{*\prime\prime}(y)\mathrm{e}^{-j\kappa x}\right) \end{aligned} \tag{2.8}$$

one obtains

$$\begin{cases} f''(y) - \kappa\left[\kappa + jRe\left(1-y^2\right)\right] f(y) = 0 \\ f^{*\prime\prime}(y) - \kappa\left[\kappa - jRe\left(1-y^2\right)\right] f^*(y) = 0 \end{cases} \tag{2.9}$$

with $f(\pm 1) = A$. This equation can be solved numerically using Chebyshev polynomials (or an equivalent polynomials expansion) or analytically using parabolic cylinder functions [1] [11].

2.1.1. Equations for linear stability

The procedure to obtain Linearized Navier Stokes equations is now exposed.

The linear stability involves the evolution of a perturbation of an established base flow.

We want to show how the presence of a spanwise flow modifies the linearized equations. The problem is not homogeneous in streamwise direction. Indeed the usual procedure of converting the evolutive equations of the disturbance into the well-known v-η formulation [27] leads to coefficients that are functions of streamwise direction. Our aim is thus to work around this problem, by first arriving to an extended form of the v-η formulation of the equations that accounts for the new base flow, and by then showing how they can still be Fourier-transformed in the streamwise direction, notwithstanding their variable coefficients.

Considering a velocity field, superimposition of two dimensional base flow $\overline{U}(y)$ and $\overline{W}(x,y)$, and three-dimensional small perturbations as

$$U = \overline{U} + u \tag{2.10}$$
$$V = v \tag{2.11}$$
$$W = \overline{W} + w \tag{2.12}$$

After substitution into the Navier-Stokes equations, and after linearization via dropping the quadratic terms in the perturbation field, considering now on the notation $\frac{\partial(*)}{\partial x} = (*)_x$ one obtains:

$$\begin{cases} u_x + v_y + w_z = 0 \\ u_t + \overline{U}u_x + v\overline{U}' + \overline{W}u_z = -\left(\overline{P}_x + p_x\right) + \dfrac{1}{Re}\overline{U}'' + \dfrac{1}{Re}\nabla^2 u \\ v_t + \overline{U}v_x + \overline{W}v_z = -p_y + \dfrac{1}{Re}\nabla^2 v \\ w_t + \overline{U}\ \overline{W}_x + \overline{U}w_x + u\overline{W}_x + v\overline{W}_y + \overline{W}w_z = -p_z + \dfrac{1}{Re}\left(\overline{W}_{xx} + \overline{W}_{yy}\right) + \dfrac{1}{Re}\nabla^2 w \end{cases} \tag{2.13}$$

In [18] as presented in 2.1 it is shown that the base flow components obey to the following equations

$$\begin{cases} 0 = -\overline{P}_x + \dfrac{1}{Re}\overline{U}'' \\ \overline{U}\ \overline{W}_x = \dfrac{1}{Re}\left(\overline{W}_{xx} + \overline{W}_{yy}\right) \end{cases} \tag{2.14}$$

and thus the corresponding terms can be subtracted from the above perturbation equations. The final form in cartesian coordinates is then:

$$\begin{cases} u_x + v_y + w_z = 0 \\ u_t + \overline{U}u_x + v\overline{U}' + \overline{W}u_z = -p_x + \dfrac{1}{Re}\nabla^2 u \\ v_t + \overline{U}v_x + \overline{W}v_z = -p_y + \dfrac{1}{Re}\nabla^2 v \\ w_t + \overline{U}w_x + u\overline{W}_x + v\overline{W}_y + \overline{W}w_z = -p_z + \dfrac{1}{Re}\nabla^2 w \end{cases} \tag{2.15}$$

Considering Eq. (1.31) there are two major differences: several additional terms arise due to the presence of $\overline{W}$, and the resulting two equations, which are now fully coupled, will not have constant coefficients, thus preventing the simple Fourier transform procedure leading to one-dimensional eigenvalue problem parametrized by the disturbance wavenumber.

2.2. Wall-normal velocity-vorticity formulation

The usual procedure applied for Poiseuille flow of converting the disturbance evolution equations into wall-normal velocity-vorticity formulation is now shown.

2.2.1. Wall-normal vorticity equation

Remembering that the wall-normal component of the vorticity vector can be written as

$$\eta = u_z - w_x \tag{2.16}$$

the governing equation for η can be obtained by taking the x derivative of the z momentum equation

$$\frac{\partial w_x}{\partial t} + \overline{U} w_{xx} + u_x \overline{W}_x + u\overline{W}_{xx} + v_x \overline{W}_y + v\overline{W}_{yx} + \overline{W}_x w_z + \overline{W} w_{zx} = -p_{zx} + \frac{1}{Re}\frac{\partial}{\partial x}\nabla^2 w, \tag{2.17}$$

and subtracting it from the z derivative of the x momentum equation

$$\frac{\partial u_z}{\partial t} + \overline{U} u_{xz} + v_z \overline{U}' + \overline{W} u_{zz} = -p_{xz} + \frac{1}{Re}\frac{\partial}{\partial z}\nabla^2 u. \tag{2.18}$$

After some simple algebraic operations, one obtains:

$$\eta_t + \left(\overline{U}\frac{\partial}{\partial x} + \overline{W}\frac{\partial}{\partial z}\right)\eta + \left(\overline{W}_x \frac{\partial}{\partial y} + \overline{U}'\frac{\partial}{\partial z} - \overline{W}_{xy} - \overline{W}_y \frac{\partial}{\partial x}\right) v - u\overline{W}_{xx} = \frac{1}{Re}\nabla^2 \eta \tag{2.19}$$

By comparing Eq. (2.19) with its counterpart in the Orr–Sommerfeld case Eq. (1.32), one notices, besides the additional terms containing the base flow $\overline{W}$, the appearance of one term containing the u velocity component. At this stage of the procedure, the system that relates u and w to v and η is still a differential system, and cannot be conveniently used to get rid of this term via algebraic substitution.

2.2.2. Wall-normal velocity equation

The evolutive equation for v can be obtained with the same procedure used for the Orr-Sommerfeld case, which involves taking the laplacian of the v-component of the

momentum equation and taking advantage of the continuity equation. The laplacian of y-momentum equation is

$$\frac{\partial}{\partial t}\nabla^2 v + \nabla^2\left(\overline{U}v_x\right) + \nabla^2\left(\overline{W}v_z\right) = -\frac{\partial}{\partial y}\nabla^2 p + \frac{1}{Re}\nabla^2\nabla^2 v \tag{2.20}$$

Expanding term by term and considering Eq. (1.13) one obtains

$$\nabla^2\left(\overline{U}v_x\right) = \overline{U}''v_x + \overline{U}\frac{\partial}{\partial x}\nabla^2 u + 2\overline{U}'v_{xy} \tag{2.21}$$

$$\nabla^2\left(\overline{W}v_z\right) = \left(\overline{W}_{xx} + \overline{W}_{yy}\right)v_z + \overline{W}\frac{\partial}{\partial z}\nabla^2 v + 2\overline{W}_x v_{zx} + 2\overline{W}_y v_{zy} \tag{2.22}$$

$$\begin{aligned} -\nabla^2 p = {} & \overline{U}u_{xx} + v_x\overline{U}' + \overline{W}_x u_z + \overline{W}u_{zx} \\ & + \overline{U}'v_x + \overline{U}v_{xy} + \overline{W}_y v_z + \overline{W}v_{zy} \\ & + \overline{U}w_{xz} + u_z\overline{W}_x + u\overline{W}_{xz} + v_z\overline{W}_y + v\overline{W}_{yz} + \overline{W}_z w_z + \overline{W}w_{zz} \\ = {} & 2\overline{U}'v_x + 2\overline{W}_x u_z + 2\overline{W}_y v_z \end{aligned} \tag{2.23}$$

$$-\frac{\partial}{\partial y}\nabla^2 p = 2\overline{U}''v_x + 2\overline{U}'v_{xy} + 2\overline{W}_{xy}u_z + 2\overline{W}_x u_{zy} + 2\overline{W}_{yy}v_z + 2\overline{W}_y v_z y \tag{2.24}$$

and after some algebra, results in:

$$\begin{aligned} & \frac{\partial}{\partial t}\nabla^2 v + \left(\overline{U}\frac{\partial}{\partial x} + \overline{W}\frac{\partial}{\partial z}\right)\nabla^2 v - \left(\overline{U}''\frac{\partial}{\partial x} + \overline{W}_{yy}\frac{\partial}{\partial z}\right)v \\ & - 2\overline{W}_{xy}u_z - 2\overline{W}_x\frac{\partial}{\partial z}\left(u_y - v_x\right) + \overline{W}_{xx}v_z = \frac{1}{Re}\nabla^2\nabla^2 v \end{aligned} \tag{2.25}$$

Analogously to what has been just observed for Eq. (2.19), the equation for v presents several additional terms compared to its Orr–Sommerfeld counterpart, among which there are the spanwise baseflow $\overline{W}$ and the velocity components u which, up to this stage, cannot be easily substituted.

2.2.3. Fourier transform in spanwise direction

The governing equations present x-varying coefficients. A straightforward preliminary step is to apply a Fourier transform in the z direction, along which the coefficients are constants. It could be noticed that the system of differential equations is autonomous in z direction and so taking the Fourier transform is equal to consider wavelike solutions in z as:

$$v\left(x,y,z,t\right)=\sum_{\beta=-\infty}^{\infty}\overline{v}(x,y,t;\beta)\mathrm{e}^{j\beta z} \tag{2.26}$$

$$v\left(x,y,z,t\right)=\sum_{\beta=-\infty}^{\infty}\overline{v}(x,y,t;\beta)\mathrm{e}^{j\beta z} \tag{2.27}$$

In order to have a lighter notation we omit using different symbols for discriminating quantities which depend on z or on the spanwise wavenumber β.

and the dynamic of the problem is described by system of equations:

$$\eta_t+\left(\overline{U}\frac{\partial}{\partial x}+j\beta\overline{W}\right)\eta+\left(\overline{W}_x\frac{\partial}{\partial y}+j\beta\overline{U}'-\overline{W}_{xy}-\overline{W}_y\frac{\partial}{\partial x}\right)v-u\overline{W}_{xx}=\frac{1}{Re}\Delta\eta \tag{2.28}$$

$$\begin{gathered}\frac{\partial}{\partial t}\Delta v+\left(\overline{U}\frac{\partial}{\partial x}+j\beta\overline{W}\right)\Delta v-\left(\overline{U}''\frac{\partial}{\partial x}+j\beta\overline{W}_{yy}\right)v \\ -2j\beta\overline{W}_{xy}u-2j\beta\overline{W}_x\left(u_y-v_x\right)+j\beta\overline{W}_{xx}v=\frac{1}{Re}\Delta\Delta v\end{gathered} \tag{2.29}$$

where Δ is defined as:

$$\Delta=\frac{\partial}{\partial x^2}+\frac{\partial}{\partial y^2}-\beta^2 \tag{2.30}$$

2.3. Fourier transform in the streamwise direction

The (spanwise) base flow $\overline{W}$ has a sinusoidal dependence on x, and not just a generic one. This feature is what is exploited to transform the perturbation equations in Fourier space, notwithstanding its variable coefficients. Therefore we consider a proper Fourier expansion of the unknown v and η.

In doing this we first express the spanwise base flow as:

$$\overline{W}(x,y)=\Re\left[f(y)\mathrm{e}^{j\kappa x}\right]=\frac{1}{2}\left[f(y)\mathrm{e}^{j\kappa x}+f^*(y)\mathrm{e}^{-j\kappa x}\right] \tag{2.31}$$

so that the various derivatives of $\overline{W}$ become:

$$\overline{W}_x=\frac{j\kappa}{2}\left[f(y)\mathrm{e}^{j\kappa x}-f^*(y)\mathrm{e}^{-j\kappa x}\right] \tag{2.32}$$

$$\overline{W}_{xx}=-\kappa^2\overline{W} \tag{2.33}$$

$$\overline{W}_y=\frac{1}{2}\left[f'(y)\mathrm{e}^{j\kappa x}+f^{*\prime}(y)\mathrm{e}^{-j\kappa x}\right] \tag{2.34}$$

$$\overline{W}_{yy} = \frac{1}{2}\left[f''(y)\mathrm{e}^{j\kappa x} + f^{*''}(y)\mathrm{e}^{-j\kappa x}\right] \tag{2.35}$$

$$\overline{W}_{xy} = \frac{j\kappa}{2}\left[f'(y)\mathrm{e}^{j\kappa x} - f^{*'}(y)\mathrm{e}^{-j\kappa x}\right] \tag{2.36}$$

Now the above assumptions are inserted into Eqs. (2.28) and (2.29), and the unknowns are expanded with a Fourier series with κ as base wavenumber as follows:

$$\eta(x,y,t;\beta) = \sum_{i=-M}^{+M} \hat{\eta}(y,t;\beta)\mathrm{e}^{ji\kappa x} \tag{2.37}$$

$$v(x,y,t;\beta) = \sum_{i=-M}^{+M} \hat{v}(y,t;\beta)\mathrm{e}^{ji\kappa x} \tag{2.38}$$

where, i a positive integer that spans from $-M$ to M, with the truncation defined by M expressing the degree of the spectral expansion of the flow variables; $m \in [0,1)$ is a real number defining the actual expansion wavenumber:

$$\alpha = (m+i)\kappa. \tag{2.39}$$

m parameter is needed for this study because x direction is not homogeneous and the problem is global in that direction. This parameter is also called detuning-parameter because it is used to detune the perturbation against the spanwise base flow, in order to consider perturbations that could have different lower wavenumbers and different spatial periodicities than the base flow fundamental wavenumber. Therefore $m \neq 0$, we allow for a detuning of the perturbation against the base flow, and in particular $m = 1/2$ describes the case of subharmonic flow, while $m = 0$ implies that the perturbation is locked into the fundamental wavenumber. The detuning wavenumber $m\kappa$ is a fraction of the base flow wavenumber κ, and the higher harmonics of the perturbations are spaced by κ.

The continuity equation and the definition of wall-normal vorticity are a differential system that relates v and η to u and w:

$$\begin{cases} u_x + v_y + w_z = 0 \\ u_z - w_x = \eta \end{cases} \tag{2.40}$$

This system can now be made algebraic if the above assumption is accounted for, so considering a Fourier series expansion also for the variable u and w

$$u(x,y,t;\beta) = \sum_{i=-M}^{+M} \hat{u}(y,t;\beta)\mathrm{e}^{ji\kappa x} \tag{2.41}$$

$$w(x,y,t;\beta) = \sum_{i=-M}^{+M} \hat{w}(y,t;\beta)\mathrm{e}^{ji\kappa x} \tag{2.42}$$

and substituting into continuity equation and in the definition of wall- normal vorticity one obtains:

$$\hat{u} = \frac{j}{\alpha^2+\beta^2}\left(\alpha\frac{\partial\hat{v}}{\partial y} - \beta\hat{\eta}\right) \tag{2.43}$$

$$\hat{w} = \frac{j}{\alpha^2+\beta^2}\left(\alpha\hat{\eta} + \beta\frac{\partial\hat{v}}{\partial y}\right) \tag{2.44}$$

and this paves the way for arriving at the final form of the equations for v and η.

2.3.1. Wall-normal vorticity equation

By introducing the operator $\hat{\Delta} = \partial^2/\partial y^2 - \alpha^2 - \beta^2$ and by substituting variables $\hat{u}$ and $\hat{w}$ Eq.(2.28) becomes:

$$\begin{aligned}
&\sum_{i=-M}^{+M}\left\{\frac{\partial\hat{\eta}}{\partial t} + j\alpha\overline{U}\hat{\eta} + j\beta\overline{U}'\hat{v} - \frac{1}{Re}\hat{\Delta}\eta\right\}\mathrm{e}^{j\alpha x} = \\
&\quad\sum_{i=-M}^{+M}\left\{-\frac{j\beta}{2}\left[f(y)\mathrm{e}^{j\kappa x} + f^*(y)\mathrm{e}^{-j\kappa x}\right]\hat{\eta} - \frac{j\kappa}{2}\left[f(y)\mathrm{e}^{j\kappa x} - f^*(y)\mathrm{e}^{-j\kappa x}\right]\frac{\partial\hat{v}}{\partial y}\right. \\
&\quad+\frac{j\kappa}{2}\left[f'(y)\mathrm{e}^{j\kappa x} - f^{*\prime}(y)\mathrm{e}^{-j\kappa x}\right]\hat{v} + \frac{1}{2}\left[f'(y)\mathrm{e}^{j\kappa x} + f^{*\prime}(y)\mathrm{e}^{-j\kappa x}\right]j\alpha\hat{v} \\
&\quad\left.-\frac{\kappa^2}{2}\left[f(y)\mathrm{e}^{j\kappa x} + f^*(y)\mathrm{e}^{-j\kappa x}\right]\frac{j}{\alpha^2+\beta^2}\left(\alpha\frac{\partial\hat{v}}{\partial y} - \beta\hat{\eta}\right)\right\}\mathrm{e}^{j\alpha x}
\end{aligned} \tag{2.45}$$

Since the hatted variables depend on y and t (besides wall-parallel wavenumbers), and $f = f(y)$, in the above equation the dependence on the streamwise coordinate x is uniquely contained in the complex exponentials $\mathrm{e}^{j\alpha x}$ and $\mathrm{e}^{\pm j\kappa x}\mathrm{e}^{j\alpha x}$; as such, every term $q(x)$ of the equation can be Fourier-transformed according to the general formula

$$\hat{q}(\tilde{\alpha}) = \frac{\kappa}{2\pi}\int_0^{2\pi/\kappa} q(x)\mathrm{e}^{-j\tilde{\alpha}x}dx \tag{2.46}$$

When evaluating integrals of the kind

$$\int_0^{2\pi/\kappa} \mathrm{e}^{\pm j\kappa x}\mathrm{e}^{j\alpha x}\mathrm{e}^{-j\tilde{\alpha}x}dx \tag{2.47}$$

one exploits the orthogonality of the trigonometric functions to state that they are equal to $\delta_{\tilde{\alpha},\pm\kappa+\alpha}$ (Kronecker symbol), i.e. they are always zero unless $\alpha = \tilde{\alpha} - \kappa$. By introducing the further notation $\tilde{\Delta} = \partial^2/\partial y^2 - \tilde{\alpha}^2 - \beta^2$, Eq. (2.45) for a given $\tilde{\alpha}$ becomes:

$$
\begin{aligned}
\frac{\partial}{\partial t}\hat{\eta}_{\tilde{\alpha}} = & -j\tilde{\alpha}\overline{U}\hat{\eta}_{\tilde{\alpha}} - j\beta\overline{U}'\hat{v}_{\tilde{\alpha}} + \frac{1}{Re}\tilde{\Delta}\hat{\eta}_{\tilde{\alpha}} \\
& - \frac{j\beta}{2} f \left(1 - \frac{\kappa^2}{(\tilde{\alpha}-\kappa)^2+\beta^2}\right)\hat{\eta}_{\tilde{\alpha}-\kappa} \\
& - \frac{j\beta}{2} f^* \left[1 - \frac{\kappa^2}{(\tilde{\alpha}+\kappa)^2+\beta^2}\right]\hat{\eta}_{\tilde{\alpha}+\kappa} \\
& - \frac{j}{2}\left[\kappa f \left(1 + \frac{\kappa(\tilde{\alpha}-\kappa)}{(\tilde{\alpha}-\kappa)^2+\beta^2}\right)\frac{\partial}{\partial y} - f'\tilde{\alpha}\right]\hat{v}_{\tilde{\alpha}-\kappa} \\
& + \frac{j}{2}\left[\kappa f^* \left(1 - \frac{\kappa(\tilde{\alpha}+\kappa)}{(\tilde{\alpha}+\kappa)^2+\beta^2}\right)\frac{\partial}{\partial y} + f^{*\prime}\tilde{\alpha}\right]\hat{v}_{\tilde{\alpha}+\kappa}
\end{aligned}
\tag{2.48}
$$

The Eq. (2.48) it is quite different with its counterpart in the Orr-Sommerfeld case; one can notice the presence of the spanwise base flow in the terms containing the functions $f(y)$ and $f^*(y)$. The evolution of each $\hat{\eta}_{\tilde{\alpha}}$ depends on $\hat{v}$ $\hat{\eta}$ valued at the same wavenumber $\tilde{\alpha}$ and at the previous and following wavenumbers $\tilde{\alpha}-k$ and $\tilde{\alpha}+k$.

The equations can be considered as a generalization of Orr-Sommerfeld case in presence of a spanwise flow; indeed terms containing variables $\hat{v}$ and $\hat{\eta}$ valued in $\tilde{\alpha}$ are the same as Orr-Sommerfeld counterpart η equation whereas the additional terms can be considered as the influence of the next and previous wavenumber perturbation to the wall-normal vorticity $\hat{\eta}_{\tilde{\alpha}}$

2.3.2. Wall-normal velocity equation

An analogous derivation leads to the following form for the wall-normal velocity component:

$$
\begin{aligned}
\sum_{i=-M}^{+M} & \left\{\frac{\partial}{\partial t}\hat{\Delta}\hat{v} + j\alpha\overline{U}\hat{\Delta}\hat{v} - j\alpha\overline{U}''\hat{v} - \frac{1}{Re}\hat{\Delta}\hat{\Delta}\hat{v}\right\}\mathrm{e}^{j\alpha x} = \\
& \sum_{i=-M}^{+M}\left\{-\frac{j\beta}{2}\left[f\mathrm{e}^{j\kappa x} + f^*\mathrm{e}^{-j\kappa x}\right]\hat{\Delta}\hat{v} + \frac{j\beta}{2}\left[f''\mathrm{e}^{j\kappa x} + f^{*\prime\prime}\mathrm{e}^{-j\kappa x}\right]\hat{v}\right. \\
& -\beta\kappa\left[f'\mathrm{e}^{j\kappa x} - f^{*\prime}\mathrm{e}^{-j\kappa x}\right]\frac{j}{\alpha^2+\beta^2}\left(\alpha\frac{\partial\hat{v}}{\partial y} - \beta\hat{\eta}\right) \\
& -\beta\kappa\left[f\mathrm{e}^{j\kappa x} - f^*\mathrm{e}^{-j\kappa x}\right]\left(\frac{j}{\alpha^2+\beta^2}\left(\alpha\frac{\partial^2\hat{v}}{\partial y^2} - \beta\frac{\partial\hat{\eta}}{\partial y}\right) - j\alpha\hat{v}\right) \\
& \left.+\frac{j\beta}{2}\kappa^2\left[f\mathrm{e}^{j\kappa x} + f^*\mathrm{e}^{-j\kappa x}\right]\hat{v}\right\}\mathrm{e}^{j\alpha x}
\end{aligned}
\tag{2.49}
$$

After rearranging, and introducing the notation $\tilde{\Delta}_{\pm} = \partial^2/\partial y^2 - (\tilde{\alpha}\pm\kappa)^2 - \beta^2$ Eq. (2.49) can be rewritten as:

$$\begin{aligned}\frac{\partial}{\partial t}\tilde{\Delta}\hat{v}_{\tilde{\alpha}} = &-j\tilde{\alpha}\overline{U}\tilde{\Delta}\hat{v}_{\tilde{\alpha}} + j\tilde{\alpha}\overline{U}''\hat{v}_{\tilde{\alpha}} + \frac{1}{Re}\tilde{\Delta}\tilde{\Delta}\hat{v}_{\tilde{\alpha}} \\ &+ \frac{j\beta^2\kappa}{(\tilde{\alpha}-\kappa)^2+\beta^2}\left(f' + f\frac{\partial}{\partial y}\right)\hat{\eta}_{\tilde{\alpha}-\kappa} \\ &- \frac{j\beta^2\kappa}{(\tilde{\alpha}+\kappa)^2+\beta^2}\left(f^{*'} + f^*\frac{\partial}{\partial y}\right)\hat{\eta}_{\tilde{\alpha}+\kappa} \\ &- \frac{j\beta}{2}\left[f\tilde{\Delta}_- - f'' - \kappa f\left(2\tilde{\alpha}-\kappa\right) + 2\frac{\kappa(\tilde{\alpha}-\kappa)}{(\tilde{\alpha}-\kappa)^2+\beta^2}\left(f'\frac{\partial}{\partial y} + f\frac{\partial^2}{\partial y^2}\right)\right]\hat{v}_{\tilde{\alpha}-\kappa} \\ &- \frac{j\beta}{2}\left[f^*\tilde{\Delta}_+ - f^{*''} + \kappa f^*\left(2\tilde{\alpha}+\kappa\right) - 2\frac{\kappa(\tilde{\alpha}+\kappa)}{(\tilde{\alpha}+\kappa)^2+\beta^2}\left(f^{*'}\frac{\partial}{\partial y} + f^*\frac{\partial^2}{\partial y^2}\right)\right]\hat{v}_{\tilde{\alpha}+\kappa}\end{aligned} \tag{2.50}$$

The same conclusions of η equation can be done. The equation for each $\hat{v}_{\tilde{\alpha}}$ can be considered as the equation of v for the Orr-Sommerfeld case at the same wavenumber $\tilde{\alpha}$ in x forced by the spanwise flow through the previous wavenumber perturbation $\tilde{\alpha}-k$ and the subsequent wavenumber perturbation $\tilde{\alpha}+k$.

2.4. Numerical discretization of the equations

We present the numerical resolution of the stability analysis of the Poiseuille flow over a steady Stokes layer. We intend to present in details the numerical implementation of the $\hat{v}-\hat{\eta}$ equations, their discretization through Chebyshev polynomials and the nonmodal stability analysis.

2.4.1. Discretization of x coordinate

In Sec. (2.3) we have introduced the $\hat{v}-\hat{\eta}$ formulation of linearized Navier-Stokes equations for a plane Poiseuille flow over a steady Stokes layer.

In order to define an easiest formulation we consider a slightly different notation.

The non-homogeneous x direction leads to consider a perturbation which is global in x and that can be expressed through the Fourier expansions:

$$\eta(x,y,t;\beta) = \sum_{i=-M}^{+M}\hat{\eta}(y,t;\beta)\mathrm{e}^{j(i+m)kx} \tag{2.51}$$

$$v(x,y,t;\beta) = \sum_{i=-M}^{+M}\hat{v}(y,t;\beta)\mathrm{e}^{j(i+m)kx} \tag{2.52}$$

Substituting into $v-\eta$ equations the expansions above and Fourier transforming against a testing function of the form $\exp j(p+m)\kappa$, where $p\in[-M,+M]$ is an integer such that $\tilde{\alpha}=(p+m)\kappa$

$$\begin{aligned}\frac{\partial}{\partial t}\hat{\eta}_p = &-j(p+m)\kappa\overline{U}\hat{\eta}_p - j\beta\overline{U}'\hat{v}_p + \frac{1}{Re}\tilde{\Delta}\hat{\eta}_p \\ &- \frac{j\beta}{2}f\left(1-\frac{\kappa^2}{((p+m-1)\kappa)^2+\beta^2}\right)\hat{\eta}_{p-1} \\ &- \frac{j\beta}{2}f^*\left[1-\frac{\kappa^2}{((p+m+1)\kappa)^2+\beta^2}\right]\hat{\eta}_{p+1} \\ &- \frac{j}{2}\left[\kappa f\left(1+\frac{\kappa((p+m-1)\kappa)}{((p+m-1)\kappa)^2+\beta^2}\right)\frac{\partial}{\partial y} - f'(p+m)\kappa\right]\hat{v}_{p-1} \\ &+ \frac{j}{2}\left[\kappa f^*\left(1-\frac{\kappa((p+m+1)\kappa)}{((p+m+1)\kappa)^2+\beta^2}\right)\frac{\partial}{\partial y} + f^{*'}(p+m)\kappa\right]\hat{v}_{p+1}\end{aligned} \tag{2.53}$$

$$\begin{aligned}\frac{\partial}{\partial t}\tilde{\Delta}\hat{v}_p = &-j(p+m)\kappa\overline{U}\tilde{\Delta}\hat{v}_p + j(p+m)\kappa\overline{U}''\hat{v}_p + \frac{1}{Re}\tilde{\Delta}\tilde{\Delta}\hat{v}_p \\ &+ \frac{j\beta^2\kappa}{((p+m-1)\kappa)^2+\beta^2}\left(f' + f\frac{\partial}{\partial y}\right)\hat{\eta}_{p-1} \\ &- \frac{j\beta^2\kappa}{((p+m+1)\kappa)^2+\beta^2}\left(f^{*'} + f^*\frac{\partial}{\partial y}\right)\hat{\eta}_{p+1} \\ &- \frac{j\beta}{2}\left[f\tilde{\Delta}_- - f'' - \kappa f\left((2(p+m)-1)\kappa\right)\right. \\ &\qquad\left. + 2\frac{\kappa((p+m-1)\kappa)}{((p+m-1)\kappa)^2+\beta^2}\left(f'\frac{\partial}{\partial y} + f\frac{\partial^2}{\partial y^2}\right)\right]\hat{v}_{p-1} \\ &- \frac{j\beta}{2}\left[f^*\tilde{\Delta}_+ - f^{*''} + \kappa f^*\left((2(p+m)+1)\kappa\right)\right. \\ &\qquad\left. - 2\frac{\kappa((p+m+1)\kappa)}{((p+m+1)\kappa)^2+\beta^2}\left(f^{*'}\frac{\partial}{\partial y} + f^*\frac{\partial^2}{\partial y^2}\right)\right]\hat{v}_{p+1}\end{aligned} \tag{2.54}$$

we must now set an appropriate numerical implementation to solve them for each $p \in [-M, M]$ with M high enough.

2.4.2. Discretization of y coordinate

The variables dependent on y direction have been numerically implemented through the use of Chebyshev polynomials on a grid of Gauss-Lobatto nodes. The choice of using Chebyshev polynomials instead of finite differences depends on the accuracy of the two methods. Although Chebyshev polynomials, and in general spectral methods have higher computational costs, they are characterized by infinite convergence order.

Using Gauss-Lobatto nodes y coordinate can be discretized as follows:

$$y_i = \cos\left(\frac{i\pi}{N}\right), \qquad for\, i = 1 \dots N \tag{2.55}$$

where $N+1$ is the number of Gauss-Lobatto nodes.

The Chebyshev polynomials are defined as

$$T_n(y) = \cos(n\theta), \qquad with\, \theta = \arccos(y) \tag{2.56}$$

Eq. (2.56) is also known as trigonometric formulation of Chebyshev polynomials, but they can be implemented using recursive formula:

$$T_0 = 1 \tag{2.57}$$
$$T_1 = x \tag{2.58}$$
$$T_{n+1} = 2xT_n - T_{n-1} \tag{2.59}$$

For a given coordinate y we may express the perturbation for a given p, $\hat{\eta}_p$ and $\hat{v}_p$ as

$$\begin{aligned} \hat{v}_p(y_i) &= \sum_{n=0}^{N} v_{p,n} T_n(y_i) \\ \hat{\eta}_p(y_i) &= \sum_{n=0}^{N} \eta_{p,n} T_n(y_i) \end{aligned} \tag{2.60}$$

The discretization of $\hat{v}_p(y)$ in y direction as for $\hat{u}_p, \hat{w}_p, \hat{\eta}_p$, leads to define the following linear system

$$\underbrace{\begin{Bmatrix} \hat{v}_p(y_0) \\ \vdots \\ \hat{v}_p(y_i) \\ \vdots \\ \hat{v}_p(y_N) \end{Bmatrix}}_{N+1\times 1} = \underbrace{\begin{bmatrix} T_0(y_0) & \dots & T_n(y_0) & \dots & T_N(y_0) \\ \vdots & & \vdots & & \vdots \\ T_0(y_i) & \dots & T_n(y_i) & \dots & T_N(y_i) \\ \vdots & & \vdots & & \vdots \\ T_0(y_N) & \dots & T_n(y_N) & \dots & T_N(y_N) \end{bmatrix}}_{N+1\times N+1} \underbrace{\begin{Bmatrix} v_{p,0} \\ \vdots \\ v_{p,n} \\ \vdots \\ v_{p,n} \end{Bmatrix}}_{N+1\times 1}. \tag{2.61}$$

or with a more readable notation

$$\{\hat{v}_p\} = [\mathcal{D}_0]\,\{v_p\}$$

The unknowns of $v - \eta$ formulation can be now expressed as

$$\hat{\mathbf{q}}_p = \begin{Bmatrix} \{\hat{v}_p\} \\ \{\hat{\eta}_p\} \end{Bmatrix} = \begin{bmatrix} [\mathcal{D}_0] & [0] \\ [0] & [\mathcal{D}_0] \end{bmatrix} \begin{Bmatrix} \{v_p\} \\ \{\eta_p\} \end{Bmatrix} = \begin{bmatrix} [\mathcal{D}_0] & [0] \\ [0] & [\mathcal{D}_0] \end{bmatrix} \mathbf{q}_p \tag{2.62}$$

Chebyshev polynomials can also be used to compute derivatives easily. Indeed taking derivatives in y direction of Eq. (2.60) one obtains:

$$
\begin{aligned}
\hat{v}_p'(y_i) &= \sum_{n=0}^{N} v_{p,n} T_n'(y_i) \qquad \rightarrow \quad \{\hat{v}_p\} = [\mathcal{D}_1]\{v_p\} \\
\hat{\eta}_p'(y_i) &= \sum_{n=0}^{N} \eta_{p,n} T_n'(y_i) \qquad \rightarrow \quad \{\hat{\eta}_p\} = [\mathcal{D}_1]\{\eta_p\} \\
\hat{v}_p''(y_i) &= \sum_{n=0}^{N} v_{p,n} T_n''(y_i) \qquad \rightarrow \quad \{\hat{v}_p\} = [\mathcal{D}_2]\{v_p\} \\
\hat{\eta}_p''(y_i) &= \sum_{n=0}^{N} \eta_{p,n} T_n''(y_i) \qquad \rightarrow \quad \{\hat{\eta}_p\} = [\mathcal{D}_2]\{\eta_p\} \\
\hat{v}_p''''(y_i) &= \sum_{n=0}^{N} v_{p,n} T_n''''(y_i) \qquad \rightarrow \quad \{\hat{v}_p\} = [\mathcal{D}_4]\{v_p\}
\end{aligned}
\tag{2.63}
$$

Operators $\mathcal{D}_0, \mathcal{D}_1, \mathcal{D}_2, \mathcal{D}_4$ contain respectively zero order derivatives, first order derivatives, second order derivatives and fourth order derivatives, of Chebyshev polynomials discretized on Gauss-Lobatto nodes. We aim to introduce these Chebyshev operators to express the computational implementation of $\hat{v} - \hat{\eta}$ equations.

In order to consider an easier computational formulation we introduce also the following operators:

$$\tilde{\Delta} = \mathcal{D}_2 - \left(((p+m)k)^2 + \beta^2\right)\mathcal{D}_0 \tag{2.64}$$

$$\tilde{\Delta}_+ = \mathcal{D}_2 - \left(((p+m+1)\kappa)^2 + \beta^2\right)\mathcal{D}_0 \tag{2.65}$$

$$\tilde{\Delta}_- = \mathcal{D}_2 - \left(((p+m-1)\kappa)^2 + \beta^2\right)\mathcal{D}_0 \tag{2.66}$$

$$\tilde{\Delta}\tilde{\Delta} = \mathcal{D}_4 - 2\left(((p+m)\kappa)^2 + \beta^2\right)\mathcal{D}_2 + \mathcal{D}_0\left(((p+m)\kappa)^2 + \beta^2\right)^2 \tag{2.67}$$

2.4.3. Base flow

The streamwise base flow, once one has implemented the Gauss-Lobatto nodes in y direction can be simply computed with

$$\overline{U}(y_i) = 1 - y_i^2$$

The spanwise baseflow can be implemented in two ways

- using Airy special function
- solving Eq .(2.5) on Gauss Lobatto nodes

The spanwise base flow computed with Airy special function on $\mathbf{y} = \{y_i\} \quad for\, y_i \in [-1, 1]$ is

$$\Delta_x = \left(\frac{1}{2Re\kappa}\right)^{\frac{1}{3}} \tag{2.68}$$

$$f(y_i > 0) = \frac{A}{\mathsf{Airy}(0)} * \mathsf{Airy}\left(-j\,(y_i + 1)\,\Delta_x \mathrm{e}^{-j\frac{4\pi}{3}}\right) \tag{2.69}$$

$$f(y_i < 0) = \frac{A}{\mathsf{Airy}(0)} * \mathsf{Airy}\left(+j\,(y_i - 1)\,\Delta_x \mathrm{e}^{-j\frac{4\pi}{3}}\right) \tag{2.70}$$

$$\tag{2.71}$$

$$f(\mathbf{y}) = f\left(\{y_i\}\right) = f\left(\{y_i < 0\}\right) \cup f\left(\{y_i > 0\}\right) \tag{2.72}$$

$$f'(\mathbf{y}) = \mathcal{D}_1\left(\mathcal{D}_0^{-1} f(\mathbf{y})\right) \tag{2.73}$$

$$f''(\mathbf{y}) = \mathcal{D}_2\left(\mathcal{D}_0^{-1} f(\mathbf{y})\right) \tag{2.74}$$

where A is the wave amplitude spanwise velocity. The spanwise base flow computed with a discretization of Eq. (2.9) on Gauss-Lobatto nodes and using Chebyshev operators, this leads to a linear system of equations, that has been implemented defining the following matrix

$$[M] = \mathcal{D}_2 - \kappa \left[\begin{bmatrix} \diagdown & & \\ & \kappa + jRe(1 - y_i^2) & \\ & & \diagup \end{bmatrix}\right] \mathcal{D}_0 \tag{2.75}$$

$$\{rhs(\mathbf{y})\} = \{0\} \tag{2.76}$$

with the boundary conditions

$$\begin{array}{lll} [M(0,i)] = \mathcal{D}_0(0,i) & \forall i \in (0,N) & \{rhs(0)\} = A \\ [M(N,i)] = \mathcal{D}_0(N,i) & \forall i \in (0,N) & \{rhs(0)\} = A. \end{array} \tag{2.77}$$

The linear system has been simply solved inverting matrix $[M]$ so one can recover the values of function $f(\mathbf{y})$ and its derivatives used in Eq. (2.53) discretized on Gauss-Lobatto nodes. The solution of the linear system is

$$f(\mathbf{y}) = f\left(\{y_i\}\right) = \mathcal{D}_0\left[M\right]^{-1} * \{rhs(\mathbf{y})\} \tag{2.78}$$

$$f'(\mathbf{y}) = \mathcal{D}_1\left(\mathcal{D}_0^{-1} f(\mathbf{y})\right) \tag{2.79}$$

$$f''(\mathbf{y}) = \mathcal{D}_2\left(\mathcal{D}_0^{-1} f(\mathbf{y})\right) \tag{2.80}$$

2.4.4. Structure of the equations

The structure of $\hat{v} - \hat{\eta}$ equations for a given p assumes the following block form:

$$\frac{\partial}{\partial t}\underbrace{\begin{bmatrix}[B_{11}] & 0\\ 0 & [B_{22}]\end{bmatrix}}_{B^{(p)}}\begin{Bmatrix}v\\ \eta\end{Bmatrix}_p = \tag{2.81}$$
$$\underbrace{\begin{bmatrix}[L_{m,11}] & [L_{m,12}]\\ [L_{m,21}] & [L_{m,22}]\end{bmatrix}}_{L_m^{(p)}}\begin{Bmatrix}v\\ \eta\end{Bmatrix}_{p-1} + \underbrace{\begin{bmatrix}[L_{11}] & [0]\\ [L_{21}] & [L_{22}]\end{bmatrix}}_{L^{(p)}}\begin{Bmatrix}v\\ \eta\end{Bmatrix}_p + \underbrace{\begin{bmatrix}[L_{p,11}] & [L_{p,12}]\\ [L_{p,21}] & [L_{p,22}]\end{bmatrix}}_{L_p^{(p)}}\begin{Bmatrix}v\\ \eta\end{Bmatrix}_{p+1}$$

where $L^{(p)}$ represents the interaction of $\hat{v}-\hat{\eta}$ for a given wavenumber $\tilde{\alpha}=(p+m)\kappa$ with itself and $L_m^{(p)}$, $L_p^{(p)}$ represent the interactions with the previous and the subsequent streamwise wavenumbers. $L_m^{(p)}$ and $L_p^{(p)}$ elements are about the spanwise base flow. Neglecting $L_m^{(p)}$ and $L_p^{(p)}$ the problem is reduced to the Orr-Sommerfeld case for a given wavenumber $\tilde{\alpha}=(p+m)\kappa$.

$$\frac{\partial}{\partial t}\underbrace{\begin{bmatrix}[B_{11}] & 0\\ 0 & [B_{22}]\end{bmatrix}}_{B^{(p)}}\begin{Bmatrix}v\\ \eta\end{Bmatrix}_p = \underbrace{\begin{bmatrix}[L_{11}] & [0]\\ [L_{21}] & [L_{22}]\end{bmatrix}}_{L^{(p)}}\begin{Bmatrix}v\\ \eta\end{Bmatrix}_p \tag{2.82}$$

where one may notice the one-way coupling of η equation with v.

Eq. (2.81) must be solved for all v,η in the modal expansion chosen $[-M,..,+M]$. Therefore one obtains the following block form

$$\frac{\partial}{\partial t}\underbrace{\begin{bmatrix} B^{(-M)} & & & & & & & \\ & \ddots & & & & & & \\ & & \ddots & & & & & \\ & & & \ddots & & & & \\ & & & & B^{(p)} & & & \\ & & & & & \ddots & & \\ & & & & & & \ddots & \\ & & & & & & & B^{(+M)} \end{bmatrix}}_{B_s} \begin{Bmatrix} \begin{Bmatrix} v \\ \eta \end{Bmatrix}_{-M} \\ \vdots \\ \vdots \\ \vdots \\ \begin{Bmatrix} v \\ \eta \end{Bmatrix}_{p} \\ \vdots \\ \vdots \\ \vdots \\ \begin{Bmatrix} v \\ \eta \end{Bmatrix}_{+M} \end{Bmatrix} = \tag{2.83}$$

$$\underbrace{\begin{bmatrix} L^{(-M)} & L_p^{(-M)} & & & \\ \ddots & \ddots & \ddots & & \\ & L_m^{(p)} & L^{(p)} & L_p^{(p)} & \\ & & \ddots & \ddots & \ddots \\ & & & L_m^{(+M)} & L^{(+M)} \end{bmatrix}}_{L_s} \underbrace{\begin{Bmatrix} \begin{Bmatrix} v \\ \eta \end{Bmatrix}_{-M} \\ \vdots \\ \vdots \\ \vdots \\ \begin{Bmatrix} v \\ \eta \end{Bmatrix}_{p} \\ \vdots \\ \vdots \\ \vdots \\ \begin{Bmatrix} v \\ \eta \end{Bmatrix}_{+M} \end{Bmatrix}}_{\mathbf{q}}$$

where B_s and L_s are respectively diagonal and block-tridiagonal matrices and subscript s is used to denote the sparcity of the matrices. Matrix dimensions for both B_s and L_s are $(2M+1) \times 2(N+1)$.

The standard state-space form can be obtained by inverting B_s

$$\dot{\mathbf{q}} = B_s^{-1} L_s \mathbf{q} = A_s \mathbf{q} \tag{2.84}$$

The problem is characterized by a block-tridiagonal matrix, and each block is like a standard Orr-Sommerfeld-Squire problem; therefore the size of full problem is $(2M +$

1))$^2\times$ a single Orr-Sommerfeld-Squire problem discretized with the same number off Gauss-Lobatto nodes.

2.4.5. Matrix analysis

For a given integer p one has to compute $B^{(p)}, L^{(p)}, L_m^{(p)}, L_p^{(p)}$. These matrices have been implemented with a specific Matlab® function named `ssl_3D_crossflow_block.m`. We present the mathematical formulation with Chebyshev polynomials of Eq. (2.81).

Matrix $B^{(p)}$

Considering Eq. (2.48,2.50) and Chebyshev polynomials discretization matrix $B^{(p)}$ has the subsequent block-structure:

$$B^{(p)} = \begin{bmatrix} [B_{11}] & 0 \\ 0 & [B_{22}] \end{bmatrix} \tag{2.85}$$

where

$$\begin{aligned} [B_{11}] &= \tilde{\Delta} \\ [B_{22}] &= \mathcal{D}_0 \\ [B_{12}] &= [B_{21}] = [0] \end{aligned} \tag{2.86}$$

Matrix $L^{(p)}$

Matrix $L^{(p)}$ has the subsequent block-structure:

$$L^{(p)} = \begin{bmatrix} [L_{11}] & [0] \\ [L_{21}] & [L_{22}] \end{bmatrix} \tag{2.87}$$

where

$$\begin{aligned} [L_{11}] &= -j\left((p+m)\kappa\right) U\tilde{\Delta} + j(p+m)\kappa\overline{U}''\mathcal{D}_0 + \frac{1}{Re}\tilde{\Delta}\tilde{\Delta} \\ [L_{22}] &= -j\left((p+m)\kappa\right)\overline{U}\mathcal{D}_0 + \frac{1}{Re}\tilde{\Delta} \\ [L_{21}] &= -j\beta\overline{U}'\mathcal{D}_0 \end{aligned} \tag{2.88}$$

Matrix $L_m^{(p)}$

Matrix $L_m^{(p)}$ has the subsequent block-structure:

$$L_m^{(p)} = \begin{bmatrix} [L_{m,11}] & [L_{m,12}] \\ [L_{m,21}] & [L_{m,22}] \end{bmatrix} \tag{2.89}$$

where

$$[L_{m,11}] = -\frac{j\beta}{2}\left[f\tilde{\Delta_-} - f''\mathcal{D}_0 - \kappa f\left(2\left((p+m)\kappa\right) - \kappa\right)\mathcal{D}_0 + 2k\frac{\left((p+m-1)\kappa\right)}{\left((p+m-1)\kappa\right)^2+\beta^2}\left(f'\mathcal{D}_1 + f\mathcal{D}_2\right)\right] \tag{2.90}$$

$$[L_{m,12}] = j\beta^2\frac{\kappa}{\left(\left((p+m-1)\kappa\right)^2+\beta^2\right)}\left[f'\mathcal{D}_0 f + \mathcal{D}_1\right]$$

$$[L_{m,21}] = -\frac{j}{2}\left[\kappa f\left(1+\kappa\frac{\left((p+m-1)\kappa\right)}{\left(\left((p+m-1)\kappa\right)^2+\beta^2\right)}\right)\mathcal{D}_1 - f'\left((p+m)\kappa\right)\mathcal{D}_0\right]$$

$$[L_{m,22}] = -j\frac{\beta}{2}f\left[1-\frac{\kappa^2}{\left(\left((p+m-1)\kappa\right)^2+\beta^2\right)}\right]\mathcal{D}_0$$

Matrix $L_p^{(p)}$

Matrix $L_p^{(p)}$ has the subsequent block-structure:

$$L_p^{(p)} = \begin{bmatrix}[L_{p,11}] & [L_{p,12}]\\ [L_{p,21}] & [L_{p,22}]\end{bmatrix} \tag{2.91}$$

where

$$[L_{p,11}] = -\frac{j\beta}{2}\left[f^*\tilde{\Delta_-} - f^{*''}\mathcal{D}_0 + kf^*\left(2\left((p+m)\kappa\right)+k\right)\mathcal{D}_0 - 2k\frac{\left((p+m+1)\kappa\right)}{\left((p+m+1)\kappa\right)^2+\beta^2}\left(f^{*'}\mathcal{D}_1 + f^*\mathcal{D}_2\right)\right] \tag{2.92}$$

$$[L_{p,12}] = j\beta^2\frac{k}{\left(\left((p+m+1)\kappa\right)^2+\beta^2\right)}\left[f^{*'}\mathcal{D}_0 f^* + \mathcal{D}_1\right]$$

$$[L_{p,21}] = -\frac{j}{2}\left[kf^*\left(1-k\frac{\left((p+m+1)\kappa\right)}{\left(\left((p+m+1)\kappa\right)^2+\beta^2\right)}\right)\mathcal{D}_1 + f^{*'}\left((p+m)\kappa\right)\mathcal{D}_0\right]$$

$$[L_{p,22}] = -j\frac{\beta}{2}f^*\left[1-\frac{k^2}{\left(\left((p+m+1)\kappa\right)^2+\beta^2\right)}\right]\mathcal{D}_0$$

2.4.6. Boundary conditions

The boundary conditions for a given p are

$$\hat{\eta}_p(\pm 1) = 0 \tag{2.93}$$

$$\hat{v}_p(\pm 1) = 0 \tag{2.94}$$

$$\frac{\partial \hat{v}_p}{\partial y}(\pm 1) = 0 \tag{2.95}$$

Boundary conditions are simply imposed modifying properly matrices $B^{(p)}, L^{(p)}, L_m^{(p)}, L_p^{(p)}$ and sets the appropriate values. However boundary conditions for $\hat{v}_p$ and η_p are not set to zero but to negative high values, i.e. $\exp^{-5}$. This is equal to impose two porous walls whose dynamic is extremely fast against than the perturbation dynamic.Therefore, the walls dynamic does not influence the perturbation dynamic. This choice has been done to prevent getting spurious eigenvalues for the eigenvalue problem. Indeed solving a linear eigenvalue problem with a spectral method composed by $N + 1$ expansion function and reordering the eigenvalues in ascending order, generally, only the first $N/2$ eigenvalues will be accurate within a small error percentage. Moreover if the linear (linearized) eigenvalue problem presents singularities in the complex plane may happens to get few accurate eigenvalues, less than $N/2$. Setting boundary conditions different from zero we prevent to obtain singularities, and the eigenvalues computation is more accurate. The imposition of boundary conditions is presented in the following Matlab® script

Listing 2.1: *Boundary conditions*

```
% Setting boundary conditions for the velocity
muv = 1e6;
B(1,:) = zeros(1,2*(N+1));      B(2,:) = zeros(1,2*(N+1));      B(N,:) = zeros
    (1,2*(N+1));      B(N+1,:) = zeros(1,2*(N+1));
Lm(1,:) = zeros(1,2*(N+1));     Lm(2,:) = zeros(1,2*(N+1));     Lm(N,:) = zeros
    (1,2*(N+1));     Lm(N+1,:) = zeros(1,2*(N+1));
L(1,:) = zeros(1,2*(N+1));      L(2,:) = zeros(1,2*(N+1));      L(N,:) = zeros
    (1,2*(N+1));      L(N+1,:) = zeros(1,2*(N+1));
Lp(1,:) = zeros(1,2*(N+1));     Lp(2,:) = zeros(1,2*(N+1));     Lp(N,:) = zeros
    (1,2*(N+1));     Lp(N+1,:) = zeros(1,2*(N+1));

B(1,1:N+1) = op.D0(1,:);
B(2,1:N+1) = op.D1(1,:);
B(N,1:N+1) = op.D1(N+1,:);
B(N+1,1:N+1) = op.D0(N+1,:);

L(1,1:N+1) = muv*op.D0(1,:);
L(2,1:N+1) = muv*op.D1(1,:);
L(N,1:N+1) = muv*op.D1(N+1,:);
L(N+1,1:N+1) = muv*op.D0(N+1,:);

% Setting boundary conditions for the vorticity
mueta = 1e5;
B(N+2,:) = zeros(1,2*(N+1));    B(2*(N+1),:) = zeros(1,2*(N+1));
Lm(N+2,:) = zeros(1,2*(N+1));   Lm(2*(N+1),:) = zeros(1,2*(N+1));
L(N+2,:) = zeros(1,2*(N+1));    L(2*(N+1),:) = zeros(1,2*(N+1));
Lp(N+2,:) = zeros(1,2*(N+1));   Lp(2*(N+1),:) = zeros(1,2*(N+1));

B(N+2,N+2:2*(N+1)) = op.D0(1,:);
B(2*(N+1),N+2:2*(N+1)) = op.D0(N+1,:);

L(N+2,N+2:2*(N+1)) = mueta*op.D0(1,:);
L(2*(N+1),N+2:2*(N+1)) = mueta*op.D0(N+1,:);
```

2.5. Modal Stability: Eigenvalues computation

Eigenvalues of matrix A_s of Eq. (2.84) are computed using Arnoldi method.

In numerical Algebra, Arnoldi iteration [2] [22] [7], [28] is an eigenvalue algorithm and an important example of iterative methods that finds the eigenvalues of general (possibly non-Hermitian) matrices. Arnoldi belongs to a class of linear algebra algorithms, called Krylov methods which are based on the idea of projection on Krylov subspaces and let to compute only a part of the eigenvalues of the problem.

A_s is a large sparse matrix and the computation of all its eigenvalues is quite onerous in terms of computational resources. Moreover we are not interested in all eigenvalues but only to those with the higher real part. Hence we compute only a subset, defined by parameter n_{eig} of all eigenvalues $N_{tot} = 2(N+1) \times 2M + 1$ of A_s

$$[T, \Lambda] = \mathsf{Arnoldi}(A_s, neig) \tag{2.96}$$

where Λ is a diagonal matrix containing the $neig$ eigenvalues computed, and T contains the relative eigenvectors. Rewriting Eq. (2.84)

$$\dot{\mathbf{q}} = A_s \mathbf{q} \tag{2.97}$$

and considering the modal expansion of $\dot{\mathbf{q}}$

$$\mathbf{q} = T\mathbf{x} \tag{2.98}$$

one can write the modal reduced problem (modal truncated)

$$T\dot{\mathbf{x}} = A_s T\mathbf{x} \tag{2.99}$$

$$\dot{\mathbf{x}} = T^{-1} A_s T\mathbf{x} = \Lambda\mathbf{x} \tag{2.100}$$

whose dimensions are quite smaller ($n_{eig} \times n_{eig}$) compared to the initial one $N_{tot} \times N_{tot}$. Hence T is also called truncation operator.

2.6. Nonmodal stability

The nonmodal stability analysis for the plane Poiseuille flow [27] [6],is now developed for the Poiseuille flow over a steady Stokes layer, expressing each operator used in the implementation of the equations.

2.6.1. Energy norm

The kinetic energy density of an infinitesimal perturbation [24], [27], [26] may be written for a given p, or for a streamwise wavenumber $\tilde{\alpha} = (p+m)\kappa$

$$e(p,\beta,t) = \frac{1}{2}\left(\frac{1}{2k^2}\int_{-1}^{+1}\begin{Bmatrix}\{\hat{v}_p\}\\ \{\hat{\eta}_p\}\end{Bmatrix}^H\begin{bmatrix}k^2+\mathcal{D}^2 & 0\\ 0 & 1\end{bmatrix}\begin{Bmatrix}\{\hat{v}_p\}\\ \{\hat{\eta}_p\}\end{Bmatrix}\right)dy \tag{2.101}$$
$$= \frac{1}{2}\left(\frac{1}{2k^2}\int_{-1}^{+1}(\hat{\mathbf{q}}_p)^H\begin{bmatrix}k^2+\mathcal{D}^2 & 0\\ 0 & 1\end{bmatrix}(\hat{\mathbf{q}}_p)\right)dy$$

Expanding $\begin{Bmatrix}\{\hat{v}_p\}\\ \{\hat{\eta}_p\}\end{Bmatrix}$ with Chebyshev polynomials and integrating Eq. (2.101) over Gauss-Lobatto nodes with a Gaussian quadrature, called Clenshaw-Curtis quadrature based on Chebyshev polynomials [22],[23] [21],[13], [9], [5], [10] one obtains

$$e(p,\beta,t) = \begin{Bmatrix}\{v_p\}\\ \{\eta_p\}\end{Bmatrix}^H \underbrace{\left(\frac{1}{4k^2}\begin{bmatrix}k^2\mathcal{D}_0^H[W]\mathcal{D}_0+\mathcal{D}_1[W]\mathcal{D}_1 & [0]\\ [0] & \mathcal{D}_0^H[W]\mathcal{D}_0\end{bmatrix}\right)}_{Q^{(p)}}\begin{Bmatrix}\{v_p\}\\ \{\eta_p\}\end{Bmatrix} \tag{2.102}$$

where W is a diagonal matrix containing the integral weights and $Q^{(p)}$ is the energy weight matrix for a given p. The integral weights are computed through a Clenshaws-Curtis quadrature, which uses Hence For a given p the energy norm can be written as

$$\|\mathbf{q}_p\|_E^2 = \mathbf{q}_p^H Q^{(p)}\mathbf{q}_p \tag{2.103}$$

.

The energy norm for all $p \in [-M,+M]$ has the following diagonal block form

$$\|\mathbf{q}\|_E^2 = \begin{Bmatrix}\begin{Bmatrix}v\\ \eta\end{Bmatrix}_{-M}\\ \vdots\\ \begin{Bmatrix}v\\ \eta\end{Bmatrix}_{p}\\ \vdots\\ \begin{Bmatrix}v\\ \eta\end{Bmatrix}_{+M}\end{Bmatrix}^H \underbrace{\begin{bmatrix}Q^{(p_{-M})} & & & & \\ & \ddots & & & \\ & & Q^{(p)} & & \\ & & & \ddots & \\ & & & & Q^{(p_{+M})}\end{bmatrix}}_{Q_s}\begin{Bmatrix}\begin{Bmatrix}v\\ \eta\end{Bmatrix}_{p_{-M}}\\ \vdots\\ \begin{Bmatrix}v\\ \eta\end{Bmatrix}_{p}\\ \vdots\\ \begin{Bmatrix}v\\ \eta\end{Bmatrix}_{p_{+M}}\end{Bmatrix} \tag{2.104}$$

$$\|\mathbf{q}\|_E^2 = \mathbf{q}^H Q_s \mathbf{q} \tag{2.105}$$

where $(Q_s)_{[2(N+1)\times(2M+1)]}$ is the energy weight matrix for all p considered in the modal expansion and is positive definite.

Let $Q_s = C^H C$ be the Cholesky decomposition of Q_s then

$$\|\mathbf{q}\|_E^2 = \|C\mathbf{q}\|_2^2 \tag{2.106}$$

Matrix C is not computed through Cholesky decomposition, in our implementation, but using singular value decomposition of Q_s considering that $Q_s = Q_s^H$

$$\begin{aligned} Q_s &= U_{Q_s}\Sigma_{Q_s}V_{Q_s}^H \\ Q_s &= V_{Q_s}\Sigma_{Q_s}U_{Q_s}^H \\ Q_s &= Q_s^H \\ &\Downarrow \\ Q_s &= \underbrace{U_{Q_s}\Sigma_{Q_s}^{\frac{1}{2}}}_{C^H}\underbrace{\Sigma_{Q_s}^{\frac{1}{2}}U_{Q_s}^H}_{C} \end{aligned} \tag{2.107}$$

2.6.2. Nonmodal analysis

We report the most important steps needed for a complete nonmodal stability analysis for the problem studied

Expressing the unknowns $\hat{v}, \hat{\eta}$ with an expansion of Chebyshev polynomials leads to a state-space form

$$\dot{\mathbf{q}} = B_s^{-1}L_s\mathbf{q} = A_s\mathbf{q} \tag{2.108}$$

The computation of the higher n_{eig} eigenvalues and their relative eigenvectors, with Arnoldi iterative method, give us a diagonal matrix Λ of eigenvalues and a matrix T of eigenvectors. Then we may express $\mathbf{q}$ using the reduced modal base T.

$$\mathbf{q} = T\mathbf{x} \tag{2.109}$$

The integration of energy density leads to obtain a energy weights operator Q_s:

$$\|\mathbf{q}\|_E^2 = \mathbf{q}^H Q_s \mathbf{q} \tag{2.110}$$

The transient energy growth function is then:

$$G(t) = \max_{\mathbf{q_0}\neq 0} \frac{\|\mathbf{q}(t)\|_E^2}{\|\mathbf{q}_0\|_E^2} = \left\|\mathrm{e}^{At}\mathbf{q}_0\right\|_E^2 \tag{2.111}$$

The numerator of Eq. (2.111) can be written with a modal expansion as

$$\|\mathbf{q}(t)\|_E^2 = \mathbf{q}^H Q_s \mathbf{q} = \mathbf{x}^H \underbrace{T^H Q_s T}_{\overline{Q}}\mathbf{x} = \mathbf{x}^H \overline{Q}\mathbf{x} \tag{2.112}$$

where $\overline{Q} = \overline{Q}^H$ is the condensed (truncated) energy weight matrix for the modal base T. Taking the Cholesky decomposition of $\overline{Q}$ (or using appropriately the singular value decomposition) leads to

$$\overline{Q} = \overline{C}^H \overline{C} \tag{2.113}$$

$$\|\mathbf{q}(t)\|_E^2 = \mathbf{x}^H \overline{C}^H \overline{C}\mathbf{x} = \left\|\overline{C}\mathbf{x}(t)\right\|_2^2 \tag{2.114}$$

The energy growth function, taking into account exponential behaviour of the initial perturbation, can be rewritten as

$$G(t) = \max_{\mathbf{x_0}\neq 0} \frac{\left\|\overline{C}\mathbf{x}(t)\right\|_2^2}{\left\|\overline{C}\mathbf{x}_0\right\|_2^2} = \max_{\mathbf{x_0}\neq 0} \frac{\left\|\overline{C}\mathrm{e}^{\Lambda t}\overline{C}^{-1}\overline{C}\mathbf{x}_0\right\|_2^2}{\left\|\overline{C}\mathbf{x}_0\right\|_2^2} = \left\|\overline{C}\mathrm{e}^{\Lambda t}\overline{C}^{-1}\right\|_2^2 \tag{2.115}$$

The computation of growth function with $norm-2$ operator is quite onerous in terms of computational resources. In order to improve the computation, remembering that $\|*\|_2 = \sigma_{max}$ where σ_{max} is the higher singular value we have taken a singular value decomposition of matrix $\overline{C}\mathrm{e}^{\Lambda t}\overline{C}^{-1}$ for only the first singular value and its relatives singular vectors (using Matlab® funcion $\mathsf{svds}(\overline{C}\mathrm{e}^{\Lambda t}\overline{C}^{-1})$).

Let $\mathbf{v_1}$ be the first right singular vector and $\mathbf{u_1}$ the first left singular vector of matrix $\overline{C}\mathrm{e}^{\Lambda t}\overline{C}^{-1}$ then

- Optimal input condition is $\hat{\mathbf{q}}_{in} = \mathcal{D}_0 T \overline{C}^{-1} v_1$
- Optimal output condition is $\hat{\mathbf{q}}_{out} = \mathcal{D}_0 T \overline{C}^{-1} u_1$

2.7. Spanwise invariance subcase

This Section exposes the stability analysis of a steady Stokes layer when spanwise invariance is imposed ($\frac{\partial}{\partial z} = 0$). Physically, this assumption leads to consider constant perturbations in z direction or in Fourier-space, perturbations whose spanwise wavenumber $\beta = 0$.

Indeed if spanwise invariance is enforced, continuity equation in Fourier space may not be employed for the streamwise wavenumber $\tilde{\alpha} = 0$, i.e. for $p = 0$ with $m = 0$, to obtain the $v - \eta\, formulation$ as before. Therefore we present a different formulation of the equations to take into account conditions, in Fourier space, where the continuity and the wall-normal vorticity equations can not be employed to relate $v, \geq 1eta$ to u, w

We also present the main important changes that have to be considered for a linear stability analysis if spanwise invariance is enforced.

Although the case for $\beta = 0$ requires a different formulation of the equations, we may observe *a posteriori* that it is not characterised by any difference with respect to the case with $\beta \neq 0$. The same reasoning and the same steps employed for $\beta \neq 0$ hold.

Equations for linear stability

The steady solutions of Navier-Stokes equations considered are the plane Poiseuille base flow $\overline{U}(y)$ Eq. (2.3) and a steady spanwise base flow, or SSL, $\overline{W}(x,y)$ Eq. (2.7) as for $\beta \neq 0$.

The linearized Navier-Stokes equation against a plane Poiseuille base flow $\overline{U}(y)$ over a spanwise base flow $\overline{W}(x,y)$ subject to three-dimensional small disturbances when spanwise invariance is enforced ($\frac{\partial}{\partial z} = o\, or\, \beta = 0$) can be obtained from Eq. (1.9) considering the velocity field

$$U = \overline{U} + u \tag{2.116}$$
$$V = v \tag{2.117}$$
$$W = \overline{W} + w \tag{2.118}$$

and through a linearization via dropping the quadratic terms of the perturbation field (u,v,w). Therefore the linearized equations in cartesian coordinates enforcing spanwise invariance are equal to Eq. (2.15) with the only difference of terms containing z-partial derivatives. Then the final form in cartesian coordinate is

$$\begin{cases} u_x + v_y = 0 \\ u_t + \overline{U}u_x + v\overline{U}' = -p_x + \dfrac{1}{Re}\nabla^2 u \\ v_t + \overline{U}v_x = -p_y + \dfrac{1}{Re}\nabla^2 v \\ w_t + \overline{U}w_x + u\overline{W}_x + v\overline{W}_y = +\dfrac{1}{Re}\nabla^2 w \end{cases} \tag{2.119}$$

where $\nabla^2 = \left[\frac{\partial^2}{\partial x^2}; \frac{\partial^2}{\partial y^2}\right]$

Wall-normal velocity-vorticity formulation

The wall-normal velocity-vorticity formulation can be obtained from Eq. (2.119) with the usual procedure or more simply by neglecting terms containing z-partial derivatives in Eqs. (2.25, 2.19). Then it reads:

$$\frac{\partial}{\partial t}\nabla^2 v + \left(\overline{U}\frac{\partial}{\partial x}\right)\nabla^2 v - \left(\overline{U}''\frac{\partial}{\partial x}\right)v = \frac{1}{Re}\nabla^2\nabla^2 v \tag{2.120}$$

$$\eta_t + \left(\overline{U}\frac{\partial}{\partial x}\right)\eta + \left(\overline{W}_x\frac{\partial}{\partial y} - \overline{W}_{xy} - \overline{W}_y\frac{\partial}{\partial x}\right)v - u\overline{W}_{xx} = \frac{1}{Re}\nabla^2\eta \tag{2.121}$$

The equations unlike the Orr Sommerfeld-Squire counterparts are characterized by terms containing spanwise baseflow $\overline{W}$ and also a term containing perturbation u but still be one-way coupled.

The coefficients of equations depend on x and y directions so the simple Fourier transform in streamwise direction can not be taken, the problem is not homogeneous

in x direction. Therefore we must consider a complete modal expansion in streamwise direction and then a Fourier transform of the equations.

Fourier transform in streamwise direction

Expressing the spanwise base flow as in Eq. (2.7) and its derivatives as in Sec. (2.2.3), we assume that a generic perturbation field $q(x, y, t)$ can be expanded as

$$q(x, y, t) = \sum_{i=-M}^{+M} \hat{q}_i(y, t) \mathrm{e}^{j(i+m)\kappa x} \tag{2.122}$$

where i is a positive integer from $-M$ to M with the truncation defined by M expressing the degree of spectral expansion of the flow variables. $m \in [0, 1)$ is the well-known detuning parameter and $\hat{q}_i$ contains the $i - th$ Fourier coefficients of the modal expansion. $\alpha = (m + i)\kappa$ is the streamwise wavenumber and it is defined by the integer index i and by the detuning parameter m.

The continuity equation is a differential system that relates $\hat{v}$ to $\hat{u}$

$$\hat{u} = -\frac{1}{j\,(i+m)\,\kappa}\frac{\partial \hat{v}}{\partial y} \tag{2.123}$$

and wall-normal vorticity definition relates $\hat{\eta}$ to $\hat{w}$

$$\hat{w} = -\frac{1}{j\,(i+m)\,\kappa}\hat{\eta} \tag{2.124}$$

Analysing vorticity and continuity equations one may notice that if $i = 0$ and if the detuning parameter $m = 0$, hence $\alpha = 0$, the equations become respectively

$$\frac{\partial \hat{v}_0}{\partial y} = 0 \tag{2.125}$$

$$\hat{\eta}_0 = 0 \tag{2.126}$$

and can not be used to recover $\hat{u}_0$ and $\hat{w}_0$. Moreover one may observe that, considering homogeneous boundary conditions for the perturbation

$$\hat{v}(\pm 1) = 0, \quad , \frac{\partial \hat{v}}{\partial y} = 0, \quad and \quad \hat{\eta} = 0 \tag{2.127}$$

leads to

$$\hat{v}_0 = 0 \tag{2.128}$$

$$\hat{\eta}_0 = 0 \tag{2.129}$$

so using Eq. (2.123,2.124) $\hat{u}_0$ and $\hat{w}_0$ are indeterminate. This aspect must be taken into account for the subsequent simplifications, indeed for a null streamwise wavenumber

$\alpha = (i+m)\kappa = 0$ continuity equation and wall-normal vorticity definition can not be used to obtain a complete $\hat{v} - \hat{\eta}$ formulation. Therefore, we will define a new partial $\hat{v} - \hat{\eta}$ formulation that considers supplementary equations to take into account the evolution of $\hat{u}_0$ and $\hat{w}_0$.

General case

First of all we consider the case with $\alpha \neq 0$ in which continuity equation can always be employed. Expanding term by term in Eqs.(2.120,2.121) and using continuity one obtains

$$\begin{aligned}\sum_{i=-M}^{+M}\left\{\frac{\partial\hat{\eta}_i}{\partial t}+\overline{U}j(i+m)\kappa\hat{\eta}_i\right\}\mathrm{e}^{j(i+m)\kappa x} = \sum_{i=-M}^{+M}\Big\{&-\frac{j\kappa}{2}\left[f(y)\mathrm{e}^{j\kappa x}-f^*(y)\mathrm{e}^{-j\kappa x}\right]\frac{\partial\hat{v}_i}{\partial y}\\ &+\frac{j\kappa}{2}\left[f'(y)\mathrm{e}^{j\kappa x}-f^{*'}(y)\mathrm{e}^{-j\kappa x}\right]\hat{v}_i\\ &+\frac{j(p+m)\kappa}{2}\left[f'(y)\mathrm{e}^{j\kappa x}+f^{*'}(y)\mathrm{e}^{-j\kappa x}\right]\hat{v}_i\\ &+\frac{j\kappa}{2}\left[f(y)\mathrm{e}^{j\kappa x}+f^*(y)\mathrm{e}^{-j\kappa x}\right]\frac{1}{(i+m)}\frac{\partial\hat{v}_i}{\partial y}\\ &\frac{1}{Re}\hat{\Delta}\hat{\eta}_i\Big\}\mathrm{e}^{j(i+m)\kappa x}\end{aligned} \tag{2.130}$$

$$\sum_{i=-M}^{+M}\left\{\frac{\partial\hat{\Delta}\hat{v}_i}{\partial t}+\overline{U}j(i+m)\kappa\hat{\Delta}\hat{v}_i-\overline{U}''j(i+m)\kappa\hat{v}_i\right\}\mathrm{e}^{j(i+m)\kappa x} = \sum_{i=-M}^{+M}\left\{\frac{1}{Re}\hat{\Delta}\hat{\Delta}\hat{\eta}_i\right\}\mathrm{e}^{j(i+m)\kappa x} \tag{2.131}$$

where $\hat{\Delta} = \frac{\partial^2}{\partial y^2} - (i+m)^2\kappa^2$.

Taking a Fourier transform of previous equations, testing with a function of the form $\exp -j(p+m)\kappa x$ one obtains for a given p:

$$\frac{\partial\tilde{\Delta}\hat{v}_p}{\partial t}+j(p+m)\kappa\overline{U}\tilde{\Delta}\hat{v}_p-j(p+m)\kappa\overline{U}''\hat{v}_p = \frac{1}{Re}\tilde{\Delta}\tilde{\Delta}\hat{v}_p \tag{2.132}$$

$$\begin{aligned}\frac{\partial\hat{\eta}_p}{\partial t}+j(p+m)\kappa\overline{U}\hat{\eta}_p = &\frac{1}{Re}\tilde{\Delta}\hat{\eta}_p\\ &+\frac{j\kappa(p+m)}{2}\Big(f'-\frac{f}{p+m-1}\frac{\partial}{\partial y}\Big)\hat{v}_{p-1}\\ &+\frac{j\kappa(p+m)}{2}\Big(f'^*+\frac{f^*}{p+m+1}\frac{\partial}{\partial y}\Big)\hat{v}_{p+1}\end{aligned} \tag{2.133}$$

where for the p-th index one has:

$$\tilde{\Delta} = \frac{\partial^2}{\partial y^2}-(p+m)^2\kappa^2 \qquad \text{and} \qquad \tilde{\Delta}\tilde{\Delta} = \frac{\partial^4}{\partial y^4}-2(p+m)^2\kappa^2\frac{\partial^2}{\partial y^2}+(p+m)^4\kappa^4 \tag{2.134}$$

Hence if $\tilde{\alpha} \neq 0$, these equations can be employed for $m = 0, |p| > 1$ or $m \neq 0, \forall p$.

Case $m = 0, p \pm 1$

Each streamwise wavenumber $\tilde{\alpha}$ interacts with the previous wavenumber $\tilde{\alpha} - \kappa$ and the subsequent wavenumber $\tilde{\alpha} + \kappa$. Therefore the wavenumbers of index $p = \pm 1$ ($\alpha = (\pm 1 + m)\kappa$) interact with wavenumber of index $p = \pm 0$. If $m = 0$, $p = 0$ the continuity equation can not be used to obtain a well-defined $\hat{v} - \hat{\eta}$ formulation.

Taking a Fourier transform of Eq. (2.131) and Eq. (2.130) considering only $p \pm 1$ ($m = 0$) and remembering that $\hat{v}_0 = 0$ one obtains:

for $m = 0$, $p = 1$:

$$\begin{aligned} \frac{\partial \tilde{\Delta}\hat{v}_1}{\partial t} + j\kappa\overline{U}\tilde{\Delta}\hat{v}_1 - j\kappa\overline{U}''\hat{v}_1 &= \frac{1}{Re}\tilde{\Delta}\tilde{\Delta}\hat{v}_1 \\ \frac{\partial \hat{\eta}_1}{\partial t} + j\kappa\overline{U}\hat{\eta}_1 &= \frac{1}{Re}\tilde{\Delta}\hat{\eta}_1 - \frac{\kappa^2}{2} f\hat{u}_0 + \frac{j\kappa}{2}\Big(f^{*'} + \frac{f^*}{2}\frac{\partial}{\partial y}\Big)\hat{v}_2 \end{aligned} \tag{2.135}$$

for $m = 0$, $p = -1$:

$$\begin{aligned} \frac{\partial \tilde{\Delta}\hat{v}_{-1}}{\partial t} - j\kappa\overline{U}\tilde{\Delta}\hat{v}_{-1} + j\kappa\overline{U}''\hat{v}_{-1} &= \frac{1}{Re}\tilde{\Delta}\tilde{\Delta}\hat{v}_{-1} \\ \frac{\partial \hat{\eta}_{-1}}{\partial t} - j\kappa\overline{U}\hat{\eta}_{-1} &= \frac{1}{Re}\tilde{\Delta}\hat{\eta}_{-1} - \frac{\kappa^2}{2} f^*\hat{u}_0 - \frac{j\kappa}{2}\Big(f' + \frac{f}{2}\frac{\partial}{\partial y}\Big)\hat{v}_{-2} \end{aligned} \tag{2.136}$$

Case $m = 0, p = 0$

If $m = 0$ and $p = 0$ one has to consider directly the linearized x and z momentum equations of Eq. (2.119) equations for x-component and z-component of momentum equation and to proceed as before expanding term by term with Fourier expansions:

$$\begin{aligned} \sum_{i=-M}^{+M} \left\{ \frac{\partial \hat{u}_i}{\partial t} + \overline{U} j(i+m)\kappa\hat{u}_i + \overline{U}'\hat{v}_i \right\} \mathrm{e}^{j(i+m)\kappa x} = \sum_{i=-M}^{+M} \{ & j(i+m)\kappa\hat{p}_i + \\ & + \frac{1}{Re}\left(-(i+m)\kappa^2\hat{u}_i + \frac{\partial^2 \hat{u}_i}{\partial y^2} \right) \Big\} \mathrm{e}^{j(i+m)\kappa x} \end{aligned} \tag{2.137}$$

$$\begin{aligned} \sum_{i=-M}^{+M} \left\{ \frac{\partial \hat{w}_i}{\partial t} + \overline{U} j(i+m)\kappa\hat{\eta}_i \right\} \mathrm{e}^{j(i+m)\kappa x} = \sum_{i=-M}^{+M} \Big\{ & - \left[\frac{j\kappa}{2} \left(f\mathrm{e}^{j\kappa x} - f^*\mathrm{e}^{-j\kappa x} \right) \right] \hat{u}_i \\ & - \frac{1}{2}\left[f'\mathrm{e}^{j\kappa x} + f^{*'}\mathrm{e}^{-j\kappa x} \right] \hat{v}_i \\ & + \frac{1}{Re}\left(-(i+m)\kappa^2\hat{w}_i + \frac{\partial^2 \hat{w}_i}{\partial y^2} \right) \Big\} \end{aligned} \tag{2.138}$$

Taking a Fourier transform of the previous equations considering only $p = 0$ with $m = 0$ and applying continuity one obtains

$$\begin{aligned}\frac{\partial \hat{u}_0}{\partial t} &= \frac{1}{Re}\frac{\partial^2 \hat{u}_0}{\partial y^2} \\ \frac{\partial \hat{w}_0}{\partial t} &= \frac{1}{Re}\frac{\partial^2 \hat{w}_0}{\partial y^2} - \frac{1}{2}\Big(f' + f\frac{\partial}{\partial y}\Big)\hat{v}_{-1} - \frac{1}{2}\Big(f^{*'} + f^*\frac{\partial}{\partial y}\Big)\hat{v}_1\end{aligned} \tag{2.139}$$

Stability analysis

The asymptotic stability analysis for $m \neq 0$ and $m = 0$ for $\beta = 0$ is identical to that of the case $\beta \neq 0$. Asymptotic stability is verified if each eigenvalue of A_s in Eq. (2.84) has negative real part. The only trouble concerns the dimensions of the matrix, so the computation of eigenvalues and relatives eigenvectors is truncated to the first *neig* higher eigenvalues.

The nonmodal stability analysis steps are the same as for the plane Poiseuille flow over a steady Stokes layer case, reported in Sec. (2.6.2). The only difference is due to the definition of the energy per unit volume of the flow and consequently to the definition of the energy norm.

Using the notation above, one obtains the following expressions for energy per unit volume:

For $m \neq 0$:

$$E = \sum_{i=-M}^{M} \frac{1}{4(i+m)^2\kappa^2} \int_{-1}^{1} (i+m)^2\kappa^2|\hat{v}_i|^2 + |\frac{\partial \hat{v}_i}{\partial y}|^2 + |\hat{\eta}_i|^2 \, dy \tag{2.140}$$

For $m = 0$:

$$E = \frac{1}{4}\int_{-1}^{1} |\hat{u}_0|^2 + |\hat{w}_0|^2 \, dy + \sum_{i=-M; i\neq 0}^{M} \frac{1}{4i^2\kappa^2} \int_{-1}^{1} i^2\kappa^2|\hat{v}_i|^2 + |\frac{\partial \hat{v}_i}{\partial y}|^2 + |\hat{\eta}_i|^2 \, dy \tag{2.141}$$

For a given integer p for $m \neq 0$ or for a given integer p with $p \neq 0$ and $m = 0$ using inner-product representation

$$e(p,t) = \frac{1}{2}\left(\frac{1}{2(p+m)^2\kappa^2}\int_{-1}^{+1} \begin{Bmatrix}\{\hat{v}_p\} \\ \{\hat{\eta}_p\}\end{Bmatrix}^H \begin{bmatrix}(p+m)^2\kappa^2 + \mathcal{D}^2 & 0 \\ 0 & 1\end{bmatrix} \begin{Bmatrix}\{\hat{v}_p\} \\ \{\hat{\eta}_p\}\end{Bmatrix}\right) dy \tag{2.142}$$

For $m = 0$ and for $p = 0$

$$e(0,t) = \frac{1}{4}\left(\int_{-1}^{+1} \begin{Bmatrix}\{\hat{u}_0\} \\ \{\hat{w}_0\}\end{Bmatrix}^H \begin{bmatrix}1 & 0 \\ 0 & 1\end{bmatrix} \begin{Bmatrix}\{\hat{u}_0\} \\ \{\hat{w}_0\}\end{Bmatrix}\right) dy \tag{2.143}$$

Expanding unknowns with Chebyshev polynomials and integrating Eqs. (2.142,2.143) over Gauss-Lobatto nodes with a Clenshaw-Curtis quadrature, one obtains:

$$e(p,\beta,t) = \begin{Bmatrix} \{v_p\} \\ \{\eta_p\} \end{Bmatrix}^H \underbrace{\left(\frac{1}{4(p+m)^2\kappa^2} \begin{bmatrix} (p+m)^2\kappa^2 \mathcal{D}_0^H[W]\mathcal{D}_0 + \mathcal{D}_1[W]\mathcal{D}_1 & [0] \\ [0] & \mathcal{D}_0^H[W]\mathcal{D}_0 \end{bmatrix} \right)}_{Q^{(p)}} \begin{Bmatrix} \{v_p\} \\ \{\eta_p\} \end{Bmatrix} \tag{2.144}$$

and if $m = 0$ and $p = 0$

$$e(p,\beta,t) = \begin{Bmatrix} \{u_0\} \\ \{w_0\} \end{Bmatrix}^H \underbrace{\left(\frac{1}{4} \begin{bmatrix} \mathcal{D}_0^H[W]\mathcal{D}_0 & \\ [0] & \mathcal{D}_0^H[W]\mathcal{D}_0 \end{bmatrix} \right)}_{Q^{(0)}} \begin{Bmatrix} \{u_0\} \\ \{w_0\} \end{Bmatrix} \tag{2.145}$$

where W is a diagonal matrix containing the integral weights and $Q^{(p)}$ is the energy weight matrix for a given $p-th$ streamwise wavenumber .

The energy weight matrix Q_s for all $p \in [-M, M]$ has the following diagonal block form

$$Q_s = \begin{bmatrix} Q^{(-M)} & & & & \\ & \ddots & & & \\ & & Q^{(0)} & & \\ & & & \ddots & \\ & & & & Q^{(+M)} \end{bmatrix} \tag{2.146}$$

where $Q^{(0)}$ is computed with Eq. (2.144) if $m \neq 0$ whereas if $m = 0$ with Eq. (2.145).

After the definition of the energy norm through energy weight matrix one may proceed with the standard procedure to compute the transient growth function and the optimal input for the maximum amplification of the perturbations.

CHAPTER 3

Results

The present work is essentially a parametric study that requires exploring a huge parameter space, where the following physical parameters are at play: Re, A, κ, β. Re is the Reynolds number, A and κ are respectively the non-dimensional wave amplitude and the wavenumber of the wall forcing and β is the spanwise wavenumber. The parameter space has been discretized employing the following discretization:

$$Re = [500, 1000, 2000] \tag{3.1}$$
$$A = [0.0 : 0.1 : 1.0] \tag{3.2}$$
$$\kappa = [0.5 : 0.25 : 5] \tag{3.3}$$
$$\beta = [0.0, 0.1, 0.2, 0.3, 0.5, 0.7, 0.9, 1.0, 1.1, 1.25, 1.5, 2.0, 2.5, 3.0, 3.5, 4.0, 4.5, 5.0] \tag{3.4}$$

Uniform discretization is employed for the wavenumber κ and for the amplitude A whereas the spanwise wavenumber β has been discretized, after some preliminary studies on the least stable eigenvalues, introducing a denser discretization for $\beta \simeq 1$.

The discretization of the parameter space is then shown in Fig. (3.1).

In addition to physical parameters there are two main discretization parameters: the number of Chebyshev polynomials N and the truncation factor of the modal expansion M. These are crucial parameters that have great influence on the reliability of the results and have to be setted properly to carry out correct modal and nonmodal stability analysis within a small error percentage.
Finally, the number of eigenvalue n_{eig} computed through Arnoldi iteration and the time discretization employed to compute the transient energy growth need to be defined properly.

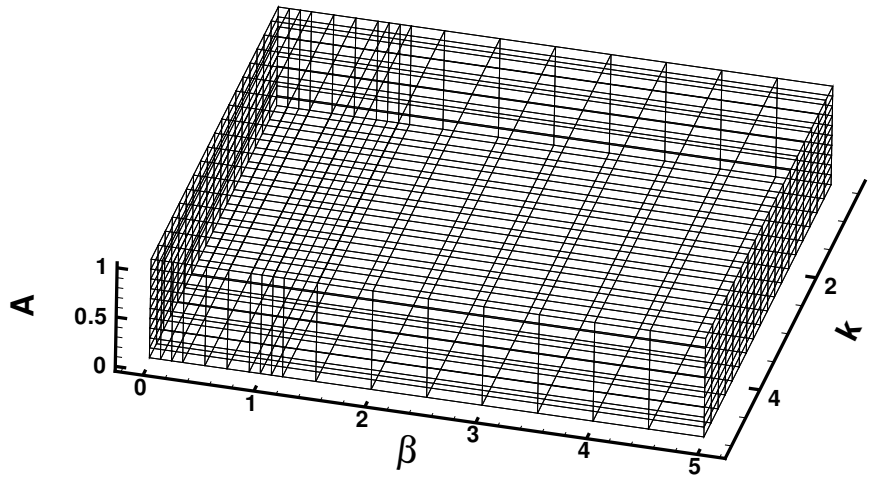

Figure 3.1.: *Mesh grid discretization of parameters for each Reynolds number*

This chapter presents the main implementation settings employed for the linear computation, its validations against a DNS code and some preliminary results carried out for different Reynolds numbers considered with the detuning parameter $m = 0$ and $m = 0.5$

Further results are reported in Apx. (A)

3.1. Implementation Settings

In this section we show how the discretization parameters $M, N, time$ and the number of eigenvalues n_{eig} have been defined.

3.1.1. Choice of modal truncation parameter

The modal truncation parameter M has been defined to ensure reliability of the results of both modal and nonmodal stability analysis.

The asymptotic stability of a given base flow depends on the real part of the least stable eigenvalue. Hence the truncation parameter M of the modal expansion must be

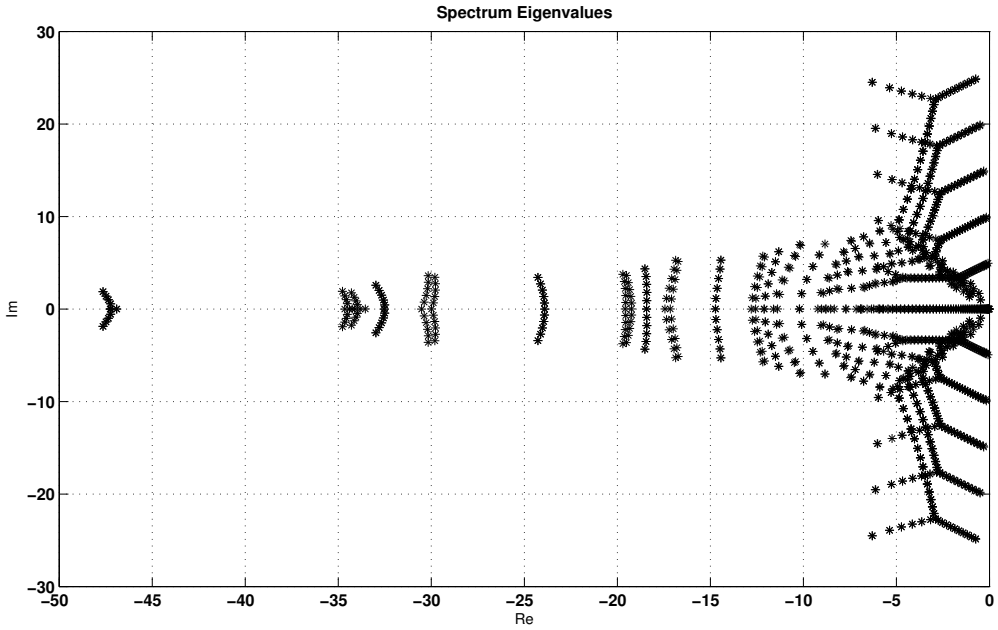

Figure 3.2.: *Eigenvalue spectrum for* $Re = 1000, k = 5, A = 1, \beta = 1. The discretization parameters are : N = 80, M = 5$

defined so that the least stable eigenvalue λ_1 is made independent from M itself. The eigenvalue spectrum is reported in Fig. (3.2).

The eigenvalue spectrum of the plane Poiseuille flow over a SSL can be related to the Orr-Sommerfeld case. Hence, it can be considered as the Orr-Sommerfeld-Squire spectrum repeated and translated on the imaginary axis for each streamwise wavenumber considered in the modal expansion. The imaginary part of the eigenvalues of the spectrum increases with the streamwise wavenumber $\tilde{\alpha} = (p + m)\kappa$ with $p \in [-M, M]$. Moreover, as the modulus of the streamwise wavenumber $|\tilde{\alpha}|$ increases the real part of the eigenvalues decreases.

The reliability of results of modal stability analysis is ensured implementing a loop on the truncation factor M so that the relative error between the least stable eigenvalue computed for M and for $M - 1$ is less then a specific value ($O(-6)$) defined, in our code with the parameter *ratio*.

However the analysis on the eigenvalue with the largest real part does not give us information about the accuracy of the nonmodal stability and its transient growth. It is necessary to define a criterion to choose M high enough to compute the transient energy growth with adequate accuracy.

For a given set of physical parameters Re, κ, A, β, the transient energy growth function is the envelope of all possible energy amplifications for each initial perturbations. The

maximum of the transient energy growth is reached when the optimal initial condition is imposed on the base flow. Hence an useful criterion to establish a proper value of the modal truncation factor M is to analyse the distribution of the modulus of the optimal initial conditions and the optimal output conditions on the modal expansion. We must ensure compact support for the modulus of the optimal initial conditions and the optimal output conditions on the modal expansion to ensure reliability of results of the nonmodal stability analysis.

Computing the singular values and the singular vectors of matrix

$$A = CT\mathrm{e}^{\Lambda t_{G_{max}}}T^{-1}C^{-1}$$

with the detuning parameter $m = 0$, two possible distributions of the optimal initial condition on the modal expansion have been found.

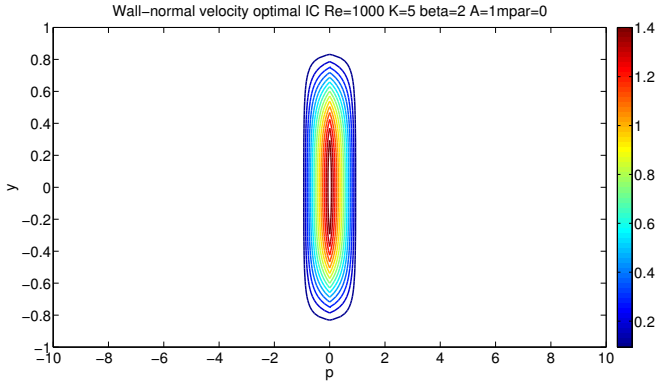

(a) *Wall-normal velocity*

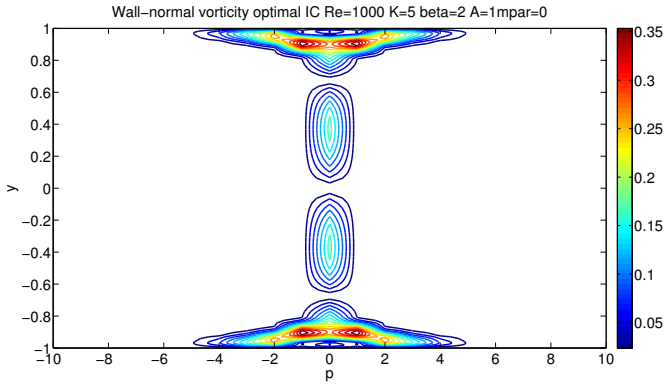

(b) *Wall-normal vorticity*

Figure 3.3.: *Optimal initial condition for the wall-normal velocity and wall-normal vorticity as a function of the wall-normal position y and $p-th$ wavenumber of the modal expansions. The contours describe the modulus of the optimal initial condition for $Re = 1000, \kappa = 5, A = 1, \beta = 2$ with detuning parameter $m = 0$. The discretization parameters are: $N = 100$, $M = 10$, $n_{eig} = 1415$*

Fig. (3.3) plots the modulus of the first type of the optimal initial condition in terms of wall-normal velocity and wall-normal vorticity as a function of the wall-distance, and of the $p-th$ wavenumber of the modal expansion. The first distribution is characterized by an optimal initial condition for the wall-normal velocity which has its maximum components on the streamwise wavenumber $\tilde{\alpha} = 0$, i.e. at index $p = 0$ of the modal expansion. The optimal initial condition for the wall-normal vorticity reaches its maximum values, near the walls, for the streamwise wavenumbers $\tilde{\alpha}$ proportional to the ratio between the non-dimensional wave amplitude A of the wall forcing and its relative wavenumber κ. As A/κ increases, the maximum values of the optimal initial condition for the wall-normal vorticity are found at streamwise wavenumbers of higher modulus of index p. Hence increasing A/κ ratio, the maximum values of the optimal initial condition for the wall-normal vorticity are located at higher streamwise wavenumbers. Therefore M_{init} has to be defined high enough to ensure compact support for the wall-normal vorticity on the modal expansion.

The second distribution of the optimal initial condition for the wall-normal velocity and wall-normal vorticity on the modal expansion is shown in Fig. (3.4). This case is characterized by maximum values for both wall-normal velocity and wall-normal vorticity whose position p on the modal expansion depends on A/κ as seen for the wall-normal vorticity of the first distribution. Finally these optimal initial conditions cover a set of streamwise wavenumbers on the modal expansion inversely proportional to κ. A criterion that let us to relate the two possible frameworks of the optimal initial condition on the modal expansion with the physical parameters has not been understood yet.

Therefore in order to ensure compact support for the optimal initial conditions, considering the assumptions exposed before, we take:

$$M_{init} \propto \frac{CA}{\kappa} + \frac{1}{\kappa} \tag{3.5}$$

where C is a security factor, usually $C = 2$ or $C = 3$ are good choices.

Hence the reliability of results of both modal and nonmodal stability analysis is achieved defining: M_{init} to ensure compact support of the optimal initial conditions and then iterating on M till the relative error between the least stable eigenvalues computed for M and for $M-1$ is less then $ratio$. The optimal output conditions modulus in terms of wall-normal velocity and wall-normal vorticity as a function of the wall-distance, and of the $p-th$ wavenumber of the modal expansion are characterized by the same distribution of maximum values of the corresponding optimal initial conditions and are reported in Apx. (A).

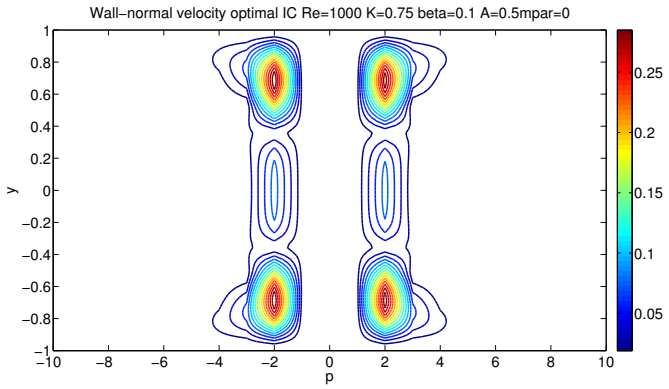

(a) *Wall-normal velocity*

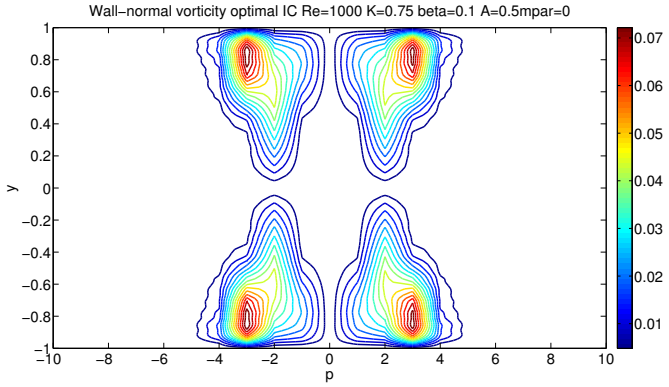

(b) *Wall-normal vorticity*

Figure 3.4.: *Optimal initial condition for the wall-normal velocity and wall-normal vorticity as a function of the wall-normal position y and $p-th$ wavenumber of the modal expansions. The contours describe the modulus of the optimal initial condition for $Re = 1000, \kappa = 0.75, A = 0.5, \beta = 0.1$ with detuning parameter $m = 0$. The discretization parameters are: $N = 130$, $M = 10$, $n_{eig} = 917$*

3.1.2. Choice of N parameter

The number of Chebyshev polynomials N employed must ensure a regular compact support for the optimal initial conditions and the optimal output conditions. The components of the singular vectors must define a regular pattern both on y direction and on the modal expansion. Moreover N must be defined so that the maximum value of the transient energy growth does not depend on N itself. The number of Chebyshev polynomials chosen in this work is $N = 80$ for wavenumbers $\kappa \geq 1$ and $N = 100$ for wavenumbers $\kappa < 1$. We found, after some preliminary analysis that, for lower values of κ the number of Chebyshev polynomials required to obtain accurate results is higher.

3.1.3. Choice of n_{eig} parameter

The eigenvalues are computed using Arnoldi iteration with the ARPACK option "smallest magnitude". Then the computed eigenvalues are the n_{eig} eigenvalues whose modules are nearest to zero The choice of n_{eig} is done considering both the optimal initial condition, as a function of wall-distance and of the modal expansion, and the spectrum of the eigenvalues. One has to define n_{eig} in order to ensure a good approximation of the dynamics of the maximum components of the optimal initial condition. Hence the needed n_{eig} increases if the locations of the maximum values of the optimal initial condition lie at higher values of modulus of p. The number of eigenvalues n_{eig} employed is $N_{tot}/6$ for $\kappa \geq 1$ whereas is $N_{tot}/3$ for $\kappa < 1$ with $N_{tot} = 2(N+1) \times (2M+1)$.

Arnoldi option "largest real" which computes the eigenvalues with the largest real parts is not used, because does not always converge and the time of convergence is 10 or 100 times higher than "smallest magnitude" option.

3.1.4. Time discretization

The transient energy growth function $G(t)$, for the problem analysed is not characterized by only a global maximum as in Orr-Sommerfeld-Squire case. The stability of the plane Poiseuille flow indeed is characterized by a monotonic growth till the maximum and beyond it, a monotonic decrease as represented in Fig. (3.5). Moreover the maximum value is reached with a smooth trend of growth function, then an uniform time discretization is considered as an appropriate choice for a good computation of the energy growth function.

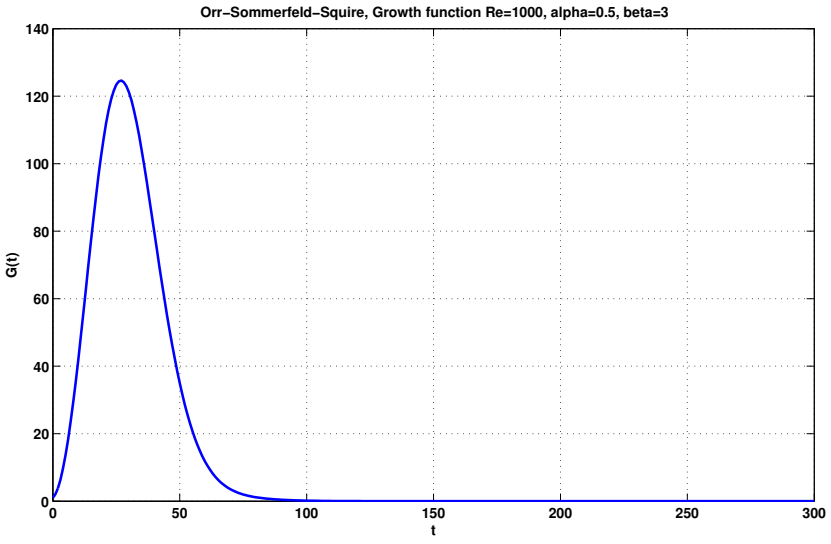

Figure 3.5.: *Orr-Sommerfeld-Squire growth function for* $Re = 1000, \alpha = 0.5, \beta = 3$

On the other hand, for the plane Poiseuille flow over a steady Stokes layer the energy

growth function is characterized by at least two local maximum. The actual global maximum of the energy growth depends, as for the optimal initial conditions, by the singular values of the matrix:

$$A = CT\mathrm{e}^{\Lambda t_{G_{max}}}T^{-1}C^{-1}.$$

Two possible maximum conditions are observed and are strictly related with the distribution of the modulus of the optimal initial conditions on the modal expansion.

If the distribution of the modulus of the optimal initial condition on the modal expansion is that represented in Fig. (3.3) then the transient growth function is shown in Fig. (3.6).Hence the transient growth function at the global maximum is sufficiently smooth that a loose discretization is allowed.

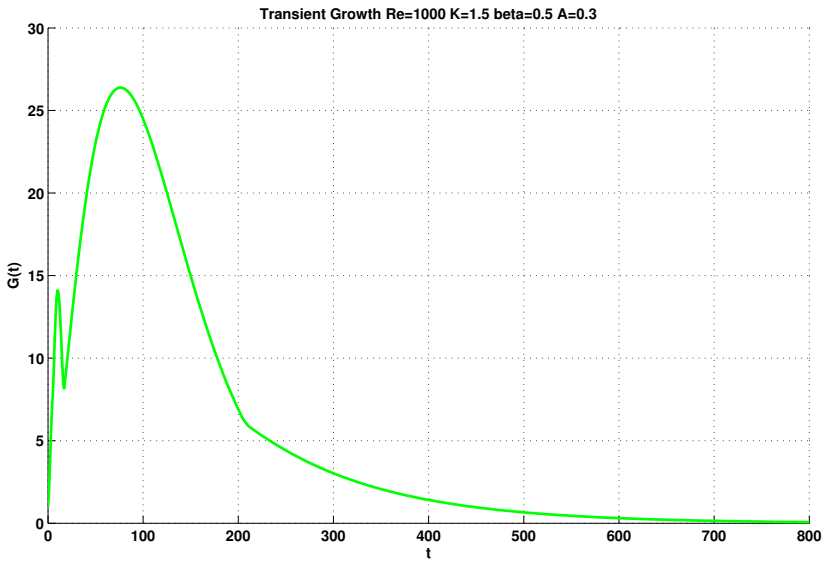

Figure 3.6.: *Plane Poiseuille over a SSL growth function for* $Re = 1000, \kappa = 1.5, \beta = 0.5, A = 0.3$. *The discretization parameters are:* $N = 80$, $M = 10$, $n_{eig} = 567$

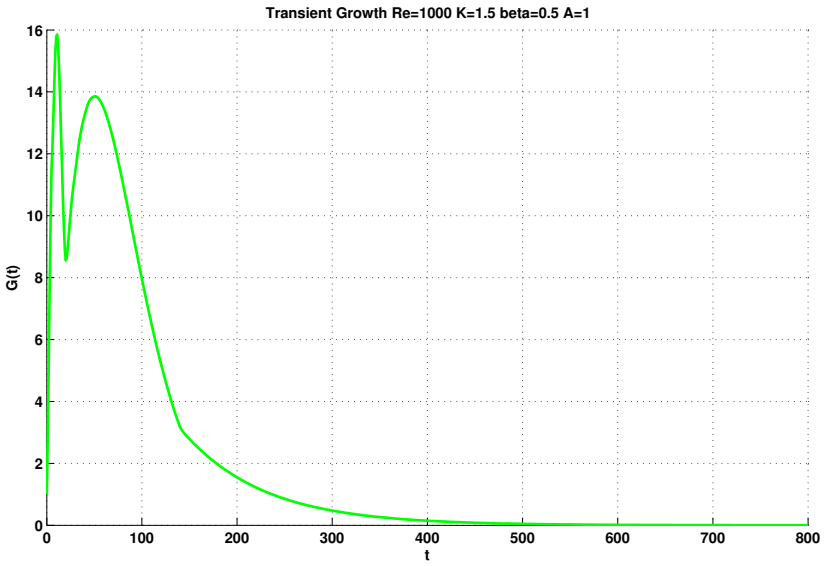

Figure 3.7.: *Plane Poiseuille over a SSL growth function for* $Re = 1000, \kappa = 1.5, \beta = 0.5, A = 1$. *The discretization parameters are:* $N = 80$, $M = 10$, $n_{eig} = 567$

Otherwise if the distribution of the modulus of the optimal initial condition on the modal expansions is represented in Fig. (3.4) then the corresponding transient energy growth function is represented in Fig. (3.7). Hence the transient growth is characterized by a peak trend at the maximum, therefore a denser discretization is needed to ensure sufficiently accurate results.

The two possible maximum conditions occur at two different distinct time steps and the maximum of the second condition occurs always before the first one. This separation on time steps is shown in Fig. (3.8) where is represented the time step in which the transient growth function reaches its maximum for $\kappa = 1.50$ as a function of the spanwise wavenumber β and of the amplitude A. One may observe that the two conditions occur at two different time levels, i.e. for $A = 0.2, \beta = 0.1$ the first one is found at $time \simeq 15$ and the second one, $\beta = 0.3$ at $time \simeq 85$. Further studies may evince a possible dependence of the maximum values of the transient energy growth function on Reynolds number and on β

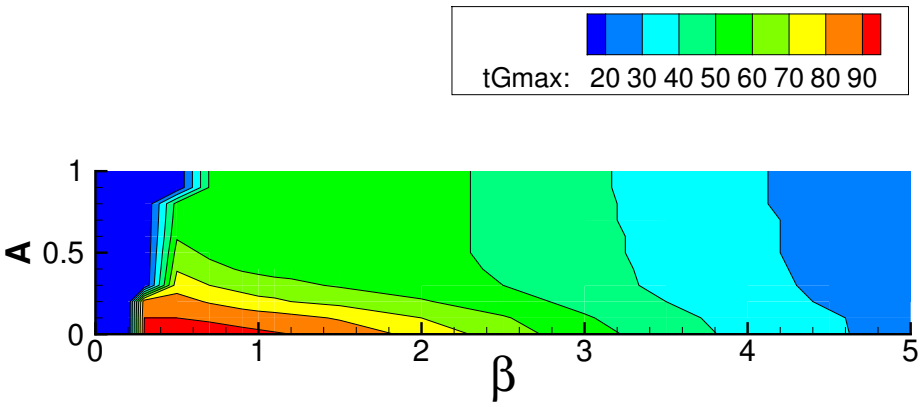

Figure 3.8.: *Plane Poiseuille over a SSL time for G_{max} for $Re = 1000, \kappa = 1.5$ as a function of A and β*

The second maximum condition, occurs always before $time_1 = 100$, for each combination of physical parameters analysed in this work; then the following time discretization is employed:

$$\begin{aligned} \text{time}_1 &= \{0 : 1 : 99\} \\ \text{time}_2 &= \{100 : 10 : 800\} \\ \text{time} &= \{\text{time}_1, \text{time}_2\} \end{aligned}$$

3.1.5. Effect of the detuning parameter

The main important effect introduced by the detuning parameter $m \neq 0$ can be considered as a shift on the modal expansion. This is clearly reported in Fig. (3.9), where is shown the modulus of the optimal initial condition in terms of wall-normal velocity and wall-normal vorticity as a function of wall-distance, and of the $p - th$ streamwise wavenumber of the modal expansion for $m = 0.5$. The corresponding optimal output condition is reported in Apx. (A).

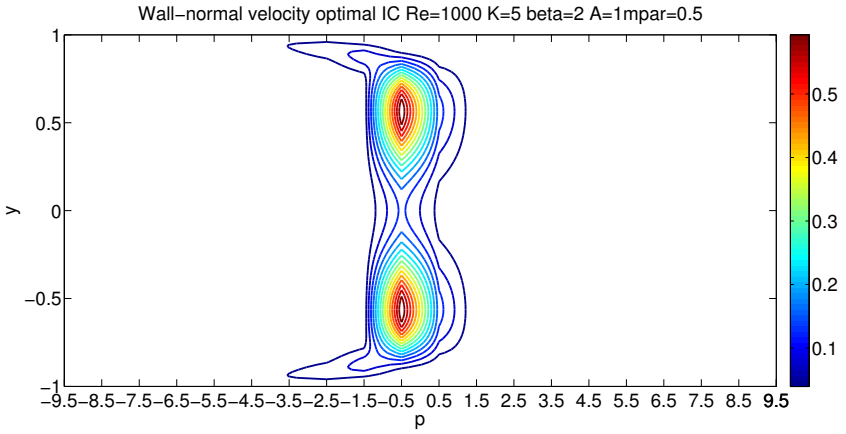

(a) *Wall-normal velocity*

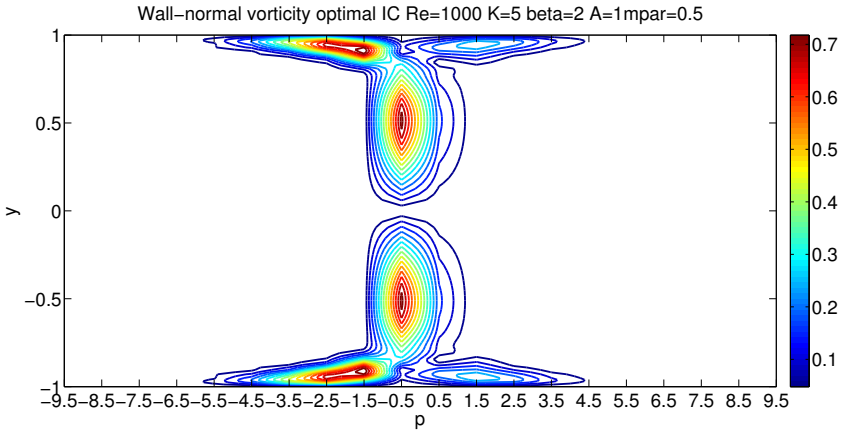

(b) *Wall-normal vorticity*

Figure 3.9.: *Optimal initial condition for the wall-normal velocity and wall-normal vorticity as a function of the wall-normal position y and $p-th$ wavenumber of the modal expansions. The contours describe the modulus of the optimal initial condition for $Re = 1000, \kappa = 5, A = 1, \beta = 2$ with detuning parameter $m = 0.5$. The discretization parameters are: $N = 100$, $M = 10$, $n_{eig} = 1415$*

Comparing Fig. (3.9) with Fig. (3.3) it may be observed that the parameter m shifts the maximum values from $p = 0$ to $p = -0.5$. Moreover assuming $m = 0.5$ we are implicitly excluding $\tilde{\alpha} = (p+m)\kappa = 0$ and then the lower streamwise wavenumbers considered are $\tilde{\alpha}_p = m\kappa$ and $\tilde{\alpha}_m = (m-1)\kappa$. This aspect in not relevant for implementation purposes but has important effects on modal and nonmodal stability characteristics of the plane Poiseuille flow over a SSL; as will be shown later. See also Apx. (A)

3.2. Validations

In order to verifying the correctness of the linear code implemented, validations against a DNS code are required. We aim at verify the results of both modal and nonmodal stability analysis considering respectively the correctness of the least stable or unstable eigenvalue and the reliability of the transient growth function computed.

The DNS has been carried out with the same DNS code employed by [19]

A validation of modal stability analysis against a DNS code is carried out for the following condition: $Re = 9000, A = 1, \kappa = 1, \beta = 1$. For the calculation of the most unstable eigenvalue in the linear code, we employ $N = 80$ Chebyshev polynomials and a truncation parameter $M = 10$. The DNS is initialized with the optimal initial condition obtained from the nonmodal stability analysis. The predicted growth rate from the stability code is 0.0090382 for the dominant mode, and twice that for the growth of its energy. The temporal evolution of energy of an initial perturbation computed with the DNS code represented in Fig. (3.10) is a nice validation of the linear code. It may be notice that after a transient period the emergence of a dominant mode whose energy grows at exactly the expected rate.

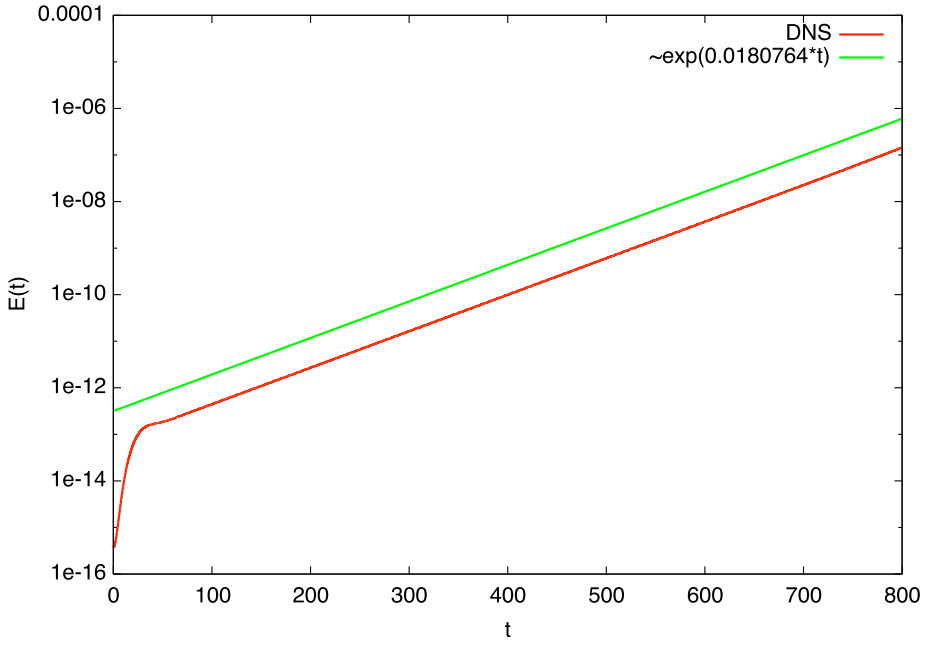

Figure 3.10.: *Validation of the calculation of the most unstable eigenvalue. Green straight line is the energy growth prediction from the linear stability code, whereas red line is the DNS-computed temporal evolution of energy. The discretization parameters are:* $N = 80$, $M = 10$, $n_{eig} = 567$

Validations of nonmodal stability analysis against a DNS code are carried out for the following conditions: $Re = 1000, A = 0, \kappa = 1, \beta = 2$ and for $Re = 1000, A = 0.1, \kappa =$

$1, \beta = 2$. The first one is simply the plane Poiseuille flow for which we employ $N = 80$ Chebyshev polynomials and $M = 10$. The second one is the Poiseuille flow subject to a wall forcing whose non-dimensional amplitude is $A = 0.1$, for which we employ the same discretization used for the Poiseuille unforced flow. The DNS-computed temporal evolutions of energy are initialized with the optimal initial conditions obtained by the nonmodal stability analysis. DNS and linear analysis comparison are represented in Fig. (3.11) for the plane Poiseuille flow and in Fig. (3.12) for the case with wall forcing. One may observe that the optimal initial condition computed with the linear code produce the expected energy growth at the expected time. Indeed the red curve and the green curve coincide at time $t = 0$ where the energy of the initial perturbation is $E(t) = 1$ and at time t_max where the temporal evolution of energy reaches its maximum value. The transient energy growth function computed with the linear code is characterized by a local maximum at time step $t \simeq 20$ which is due to the non-homogeneity of the streamwise direction.

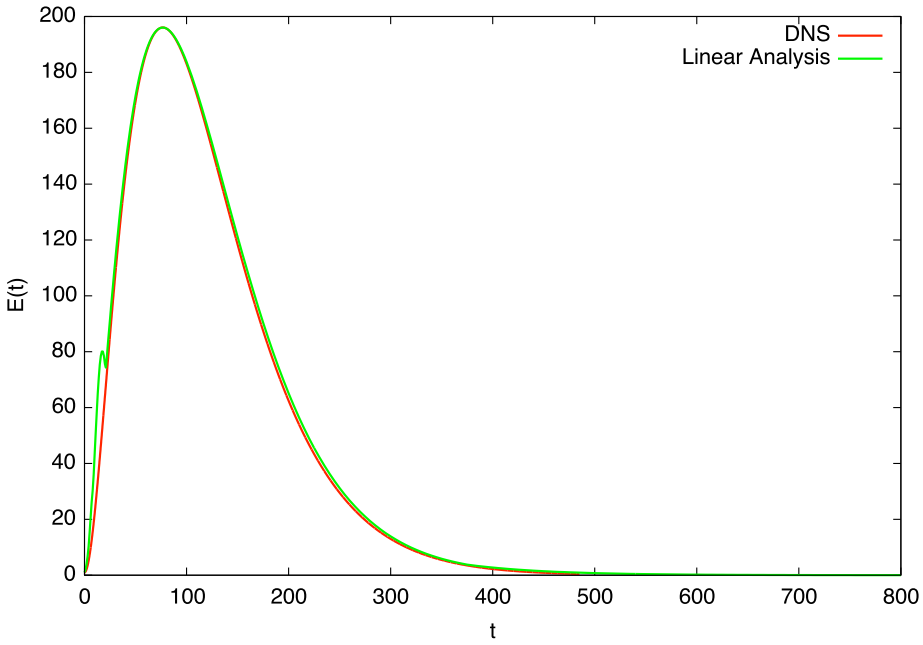

Figure 3.11.: *Transient energy growth validation against DNS code for* $Re = 1000, A = 0, \kappa = 1, \beta = 2$. *Green line is the energy growth prediction from the linear stability code, whereas red line is the DNS-computed temporal evolution of energy. The discretization parameters are:* $N = 80$, $M = 10$, $n_{eig} = 567$

The forced case is characterized by a small discrepancy between the maximum values of the temporal evolution of energy computed with the linear code and with DNS. However this discrepancy has not been completely understood, hence further analysis are required. A good approximation of the transient energy growth is still observed. Finally, as first consideration, comparing Fig. (3.11) and Fig. (3.12) one may notice

that the effect of the wall forcing causes a reduction of the maximum of the transient energy growth verified both through DNS code and linear analysis.

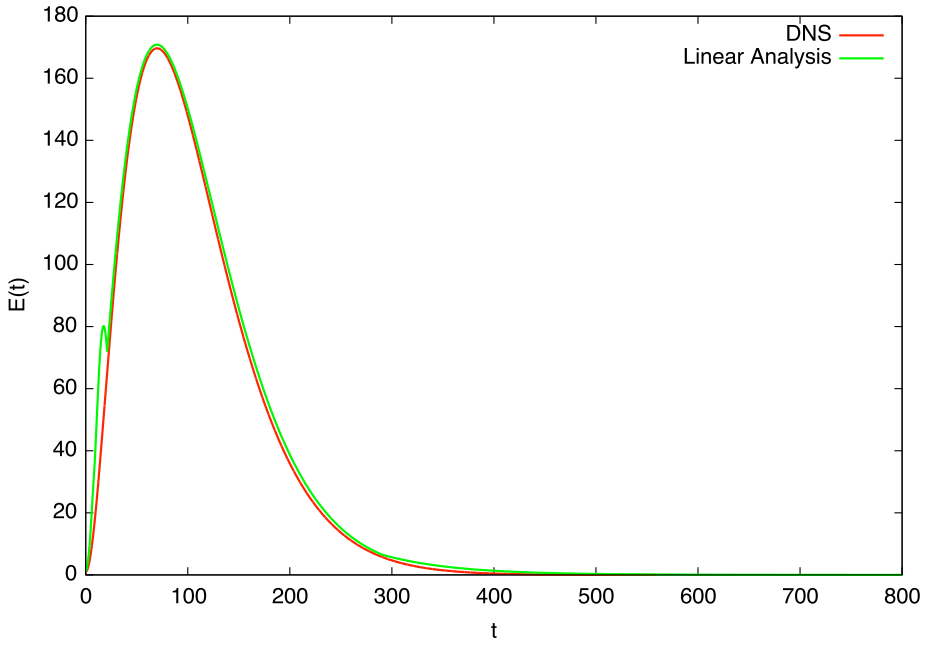

Figure 3.12.: *Transient energy growth validation against DNS code for* $Re = 1000, A = 0.1, \kappa = 1, \beta = 2$. *Green line is the energy growth prediction from the linear stability code, whereas red line is the DNS-computed temporal evolution of energy. The discretization parameters are:* $N = 80$, $M = 10$, $n_{eig} = 567$

3.3. Modal Stability

Modal stability of plane Poiseuille flow over a steady Stokes layer has been studied considering the least stable eigenvalue λ_1 as function of parameters κ, A, β at different Re. Results are exposed comparing the effect of the wall forcing on the plane Poiseuille flow with respect to the reference unforced problem.

Tab. (3.1) reports the combinations of wavenumber κ, wave amplitude A, and spanwise wavenumber β that maximize the ratio $Re(\lambda_1)/Re(\lambda_{1,ref})$, at different Re numbers considered, where $Re(\lambda_{1,ref})$ is the real part of the least stable eigenvalue for the plane Poiseuille flow and $Re(\lambda_1)$ is the real part of the least stable eigenvalue when the wall forcing is imposed. Therefore, the wall forcing increases the modulus of the real part of the least stable eigenvalue leading to a more asymptotic stable condition. Indeed the modulus of the real part of the least stable eigenvalue at $Re = 2000$ is more than two times the modulus of the least stable eigenvalue for the unforced flow.

Re	κ	β	A	$Re(\lambda_1)/Re(\lambda_{1,ref})$
500	2.25	0.7	1	1.9380
1000	2	0.5	1	2.1725
2000	3	0.5	1	2.3636

Table 3.1.: *Physical parameter combinations for maximum* $Re(\lambda_1)/Re(\lambda_{1,ref})$ *at* $Re = 500$,$Re = 1000$ *and* $Re = 2000$

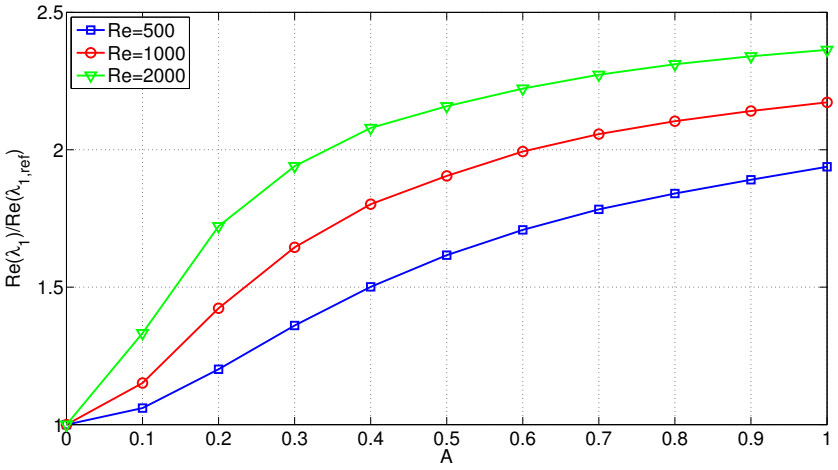

Figure 3.13.: *Maximum* $Re(\lambda_1)/Re(\lambda_{1,ref})$ *,for all* κ *and for all* β *as a function of* A*. The curves represent the different Reynolds numbers analysed.*

We report in Fig. (3.13) the maximum $Re(\lambda_1)/Re(\lambda_{1,ref})$ ratio, for all wavenumbers κ and for all spanwise wavenumbers β considered, as a function of amplitude A at different Reynolds numbers analysed. Fig. (3.13) clearly shows that the maximum $Re(\lambda_1)/Re(\lambda_{1,ref})$ ratio increases with A for each Reynolds number considered. The reference Poiseuille flow is asymptotically stable, then the wall forcing has a stabilization effect in terms of modal stability. Indeed the absolute value of the real part of the least stable eigenvalue increases monotonically with A.

The maximum values of $Re(\lambda_1)/Re(\lambda_{1,ref})$ are found for $A = 1$ and are the same reported in Tab. (3.1).

Moreover the maximum $Re(\lambda_1)/Re(\lambda_{1,ref})$ ratio for all wavenumbers κ and for all spanwise wavenumbers β considered increases with Re.

We report in Fig. (3.14) the maximum $Re(\lambda_1)/Re(\lambda_{1,ref})$ ratio, for all wave amplitudes A and for all spanwise wavenumbers β, as a function of wavenumber κ of the wall forcing at different Reynolds numbers considered. The asymptotic stabilizing effect also depends on κ. As κ increases, the maximum $Re(\lambda_1)/Re(\lambda_{1,ref})$ ratio increases till $\kappa = 2.25$ for $Re = 500$, $\kappa = 2$ for $Re = 1000$ and till $\kappa = 3$ for $Re = 2000$. At higher values of κ the maximum $Re(\lambda_1)/Re(\lambda_{1,ref})$ (for all A and for all β) mildly

decreases as κ increases but the wall forcing still has an asymptotic stabilization effect with respect to the Poiseuille flow.

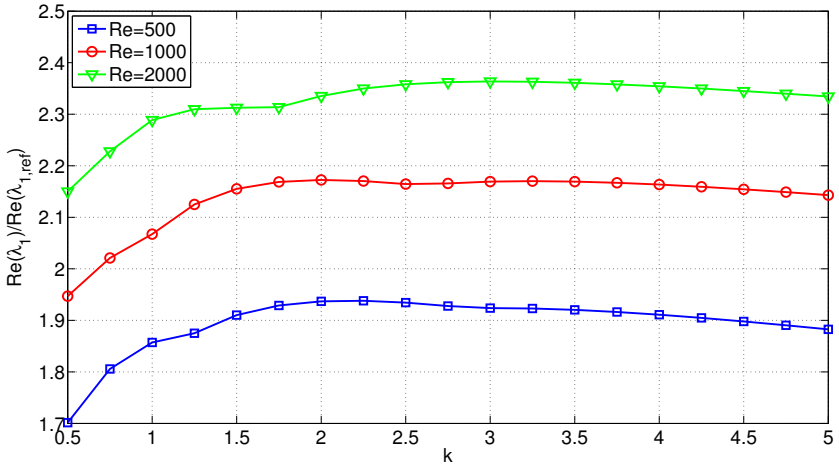

Figure 3.14.: *Maximum $Re(\lambda_1)/Re(\lambda_{1,ref})$ for all A and for all β as a function of κ. The curves represent the Reynolds numbers analysed*

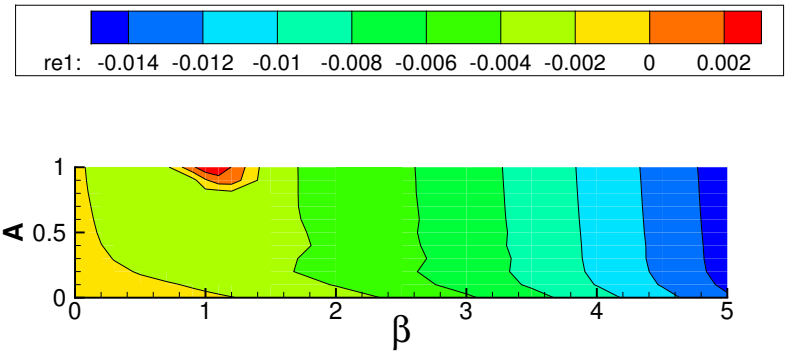

Figure 3.15.: *Least stable eigenvalue as a function A and β with $Re = 2000$, $\kappa = 0.5$*

Modal unstable conditions have been obtained at $Re = 2000$ for $\kappa = 0.5$ as reported in Fig. (3.15), where one may observe a crucial decrease of the stabilization properties due to the wall forcing. Indeed for $A \simeq 1$ and $\beta \simeq 1$ one may observe a region of the least stable eigenvalues whose real parts are positive.

We do not know if the flow is physically unstable for these conditions or if instabilities may be due to possible poor discretizations for $\kappa < 1$. Hence a DNS analysis is required

to confirm these unstable regions of the parameter space.

3.3.1. Dependence on detuning parameter

The effect of a detuning parameter $m = 0.5$ on the real part of the least stable eigenvalue is considered. Tab. (3.2) reports the combinations of wavenumber κ, wave amplitude A, and spanwise wavenumber β that maximize the ratio $Re(\lambda_1)/Re(\lambda_{1,ref})$ with a detuning parameter $m = 0.5$

Re	κ	β	A	$Re(\lambda_1)/Re(\lambda_{1,ref})$
1000	1.5	0.5	0.8	1.0142

Table 3.2.: *Physical parameter combination for maximum* $Re(\lambda_1)/Re(\lambda_{1,ref})$ *at* $Re = 1000$ *with* $m = 0.5$

Fig. (3.16) shows the maximum $Re(\lambda_1)/Re(\lambda_{1,ref})$ ratio, for all κ and for all β, as a function of A at $Re = 1000$ with $m = 0$ and $m = 0.5$. One may observe that the wall forcing with $m = 0.5$ affects weakly $Re(\lambda_1)/Re(\lambda_{1,ref})$ as A increases. Even if small growths of $Re(\lambda_1)/Re(\lambda_{1,ref})$ are observed, they are not significant, and also may depend on possible discretization effect.

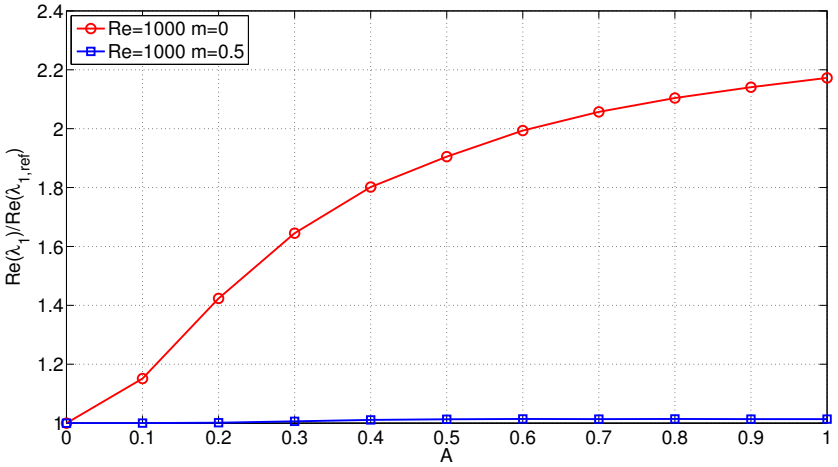

Figure 3.16.: *Maximum* $Re(\lambda_1)/Re(\lambda_{1,ref})$ *for all* κ *and for all* β *as a function of* A *at* $Re = 1000$ *with* $m = 0$ *and* $m = 0.5$

Fig. (3.16) shows the maximum $Re(\lambda_1)/Re(\lambda_{1,ref})$ ratio for all A and for all β as a function of κ at $Re = 1000$ with $m = 0$ and $m = 0.5$. Even wavenumber κ of the wall forcing does not influence the real part of the least stable eigenvalue if perturbations with $m = 0.5$ are considered.

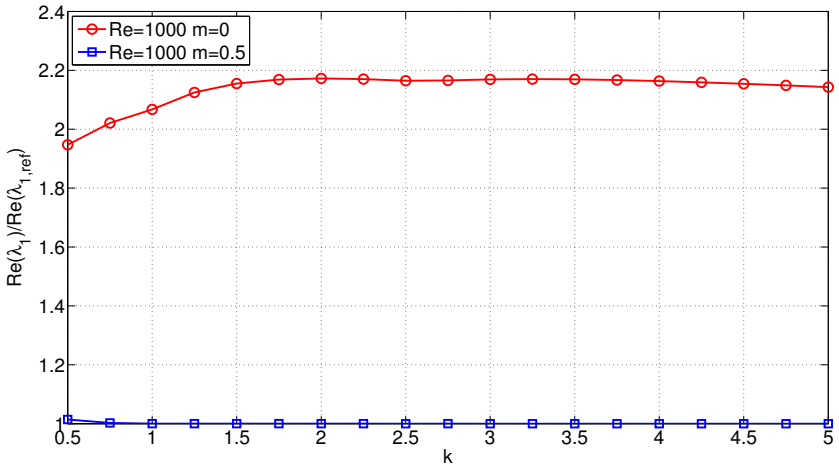

Figure 3.17.: *Maximum* $Re(\lambda_1)/Re(\lambda_{1,ref})$ *for all* A *and for all* β *as a function of* κ *at* $Re = 1000$ *with* $m = 0$ *and* $m = 0.5$

Therefore modal stability characteristics of the flow are not affected by the wall forcing if $m = 0.5$

The modal analysis leads us to infer that for $m = 0$ the SSL has a stabilization effect on the plane Poiseuille flow especially for $A \simeq 1$. This asymptotic stabilization is not observed for $m = 0.5$ but we do not know what happens for other values of m. The highest value of $Re(\lambda_1)/Re(\lambda_{1,ref})$ is found for $Re = 2000$ and is equal to 2.3636. However for the same Re has been observed a strong downgrading of these asymptotic characteristics for small values of κ.

Hence in order to ensure an improvement of the asymptotic stability characteristics of a plane Poiseuille flow one could think to impose a wall forcing with $2 \leq \kappa \leq 3$ and possibly $A \simeq 1$

3.4. Nonmodal Stability

Nonmodal stability analysis is carried out computing the transient energy growth function and taking its maximum as a function of physical parameters A, κ, β. Tab.(3.3) reports the combinations of wavenumber κ, wave amplitude A, and spanwise wavenumber β that minimize the ratio $G_{max}/G_{max,ref}$ at different Re numbers considered, where $G_{max,ref}$ is the maximum of the transient energy growth function for the plane Poiseuille flow and G_{max} is the maximum of the transient energy growth when the wall forcing is imposed. Therefore, for $Re = 2000$ the wall forcing may reduce the G_{max} up to 72%

Re	κ	β	A	$G_{max}/G_{max,ref}$
500	1.25	1.5	1	0.3463
1000	0.75	2.5	1	0.2970
2000	0.75	1.5	1	0.2767

Table 3.3.: *Physical parameter conditions for minimum $G_{max}/G_{max,ref}$ ratio at $Re = 500$,$Re = 1000$ and $Re = 2000$*

We report in Fig. (3.18) the minimum $G_{max}/G_{max,ref}$ ratio, for all wavenumbers κ and for all spanwise wavenumber β considered, as a function of amplitude A for different Reynolds numbers analysed. As A increases the minimum $G_{max}/G_{max,ref}$ ratio decreases and reaches its minimum values for $A = 1$, in our study. Possible further reductions may be obtained for higher values of A. Moreover one may observe that the effect of wall forcing on $G_{max}/G_{max,ref}$ increases with Re even if this is less remarkable for high values of A ($A \geq 0.7$)

We report in Fig. (3.19) the minimum $G_{max}/G_{max,ref}$ ratio, for all wave amplitudes A and for all spanwise wavenumbers β considered, as a function of wavenumber κ at different Reynolds numbers. Considering Fig. (3.19) one may observe that $G_{max}/G_{max,ref}$ reaches its minimum values for $\kappa = 0.75$ at $Re = 1000$ or $Re = 2000$ and for $\kappa = 1.25$ at $Re = 500$.

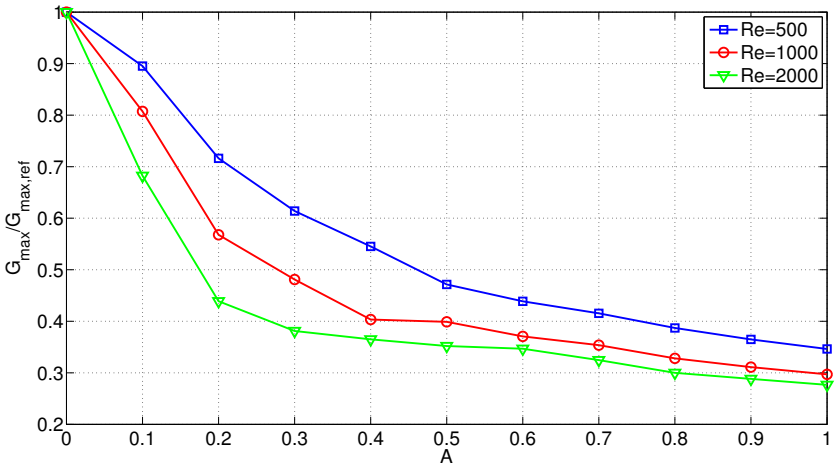

Figure 3.18.: *Minimum $G_{max}/G_{max,ref}$ ratio for all κ and for all β as a function of A. The curves represent the Reynolds numbers analysed with $m = 0$*

Beyond the minimum conditions, the minimum $G_{max}/G_{max,ref}$ ratio mildly depends on κ for each Re number considered. For $\kappa < 1$ at $Re = 500$ and for $\kappa < 0.75$ at $Re = 1000$ the ratio $G_{max}/G_{max,ref}$ increases significantly. This increment is not observed for $Re = 2000$ but a further study considering lower κ values may be useful to understand if we have similar behaviour as for $Re = 500$ and $Re = 1000$.

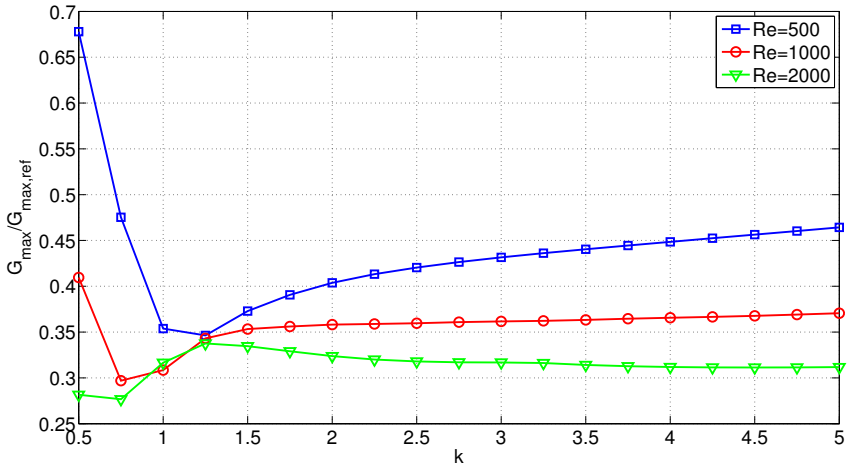

Figure 3.19.: *Minimum $G_{max}/G_{max,ref}$ ratio for all A and for all β as a function of κ. The curves represent the Reynolds numbers analysed with $m = 0$*

Unstable conditions for $Re = 2000$ and $\kappa = 0.5$ are also confirmed by nonmodal analysis. Moreover for $\beta \simeq 1$ an increment of $G_{max}/G_{max,ref}$ is observed at small values of wavenumber κ as reported in Fig. (3.20) for $\kappa = 0.5$ where is reported G_{max} as a function of A and β at $Re = 1000$

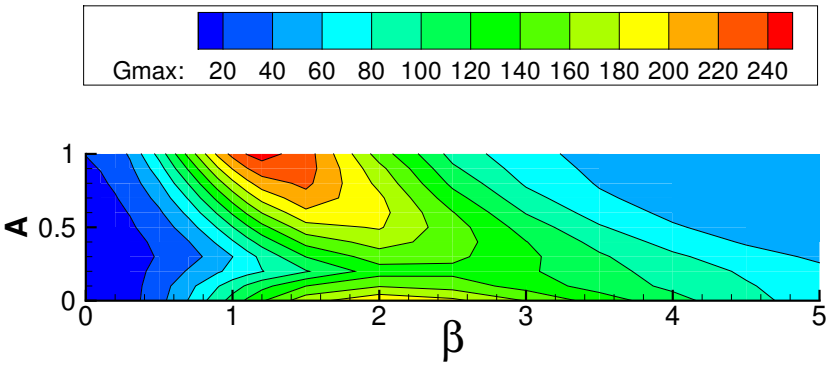

Figure 3.20.: *G_{max} as a function A and β with $Re = 2000$, $\kappa = 0.5$*

One may observe a region located at $A = 1$, $\beta \simeq 1$ of strong growth of G_{max} with respect to the plane Poiseuille flow ($A = 0$). Hence the positive stabilization effects observed, in terms of nonmodal stability, are vanished. These regions where G_{max} grows

with respect to $G_{max,ref}$ of the plane Poiseuille flow, must be verified with DNS in order to exclude possible discretization problems. Therefore we aim at verify if these conditions are physically observed.

3.4.1. Dependence on detuning parameter

The dependence of nonmodal stability of the flow is analysed for a detuning parameter $m = 0.5$. Results are reported comparing the conditions: $Re = 1000$ with $m = 0$ and $Re = 1000$ with $m = 0.5$. Tab.(3.4) the combination of wavenumber κ, wave amplitude A, and spanwise wavenumber β that minimize the ratio $G_{max}/G_{max,ref}$ with $m = 0.5$ at $Re = 1000$. Therefore, the wall forcing may reduce the maximum energy growth up to 65%, less than the case with $m = 0$ but it is still quite remarkable.

Re	κ	β	A	$G_{max}/G_{max,ref}$
1000	0.75	2.5	1	0.3575

Table 3.4.: *Physical parameter condition for minimum* $G_{max}/G_{max,ref}$ *at* $Re = 1000$ *and* $m = 0.5$

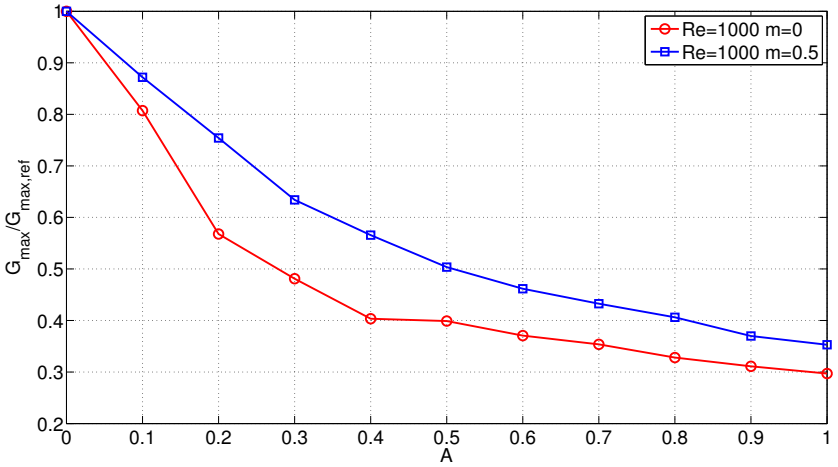

Figure 3.21.: *Minimum* $G_{max}/G_{max,ref}$ *ratio for all* κ *and for all* β *as a function of* A *at* $Re = 1000$ *with* $m = 0$ *and* $m = 0.5$

We report in Fig. (3.19) the minimum $G_{max}/G_{max,ref}$ ratio, for all κ and for all β considered, as a function of A at $Re = 1000$ for $m = 0$ and $m = 0.5$ As A increases $G_{max}/G_{max,ref}$ ratio monotonically decreases for $m = 0.5$ and reaches its minimum value for $A = 1$ even if the effect on energy growth ratio is smaller than for $m = 0$ for all wave amplitudes considered.

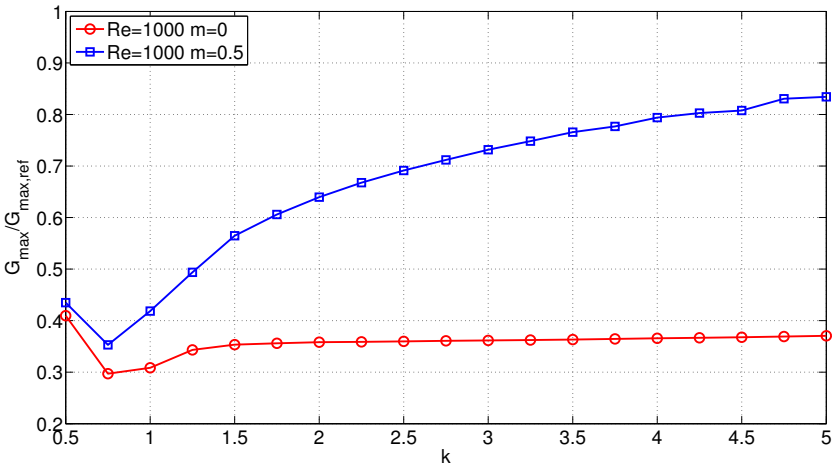

Figure 3.22.: *Minimum* $G_{max}/G_{max,ref}$ *ratio for all* A *and for all* β *as a function of* κ *at* $Re = 1000$ *with* $m = 0$ *and* $m = 0.5$

We report in Fig. (3.19) the minimum $G_{max}/G_{max,ref}$ ratio for all A and for all β as a function of κ at $Re = 1000$ for $m = 0$ and $m = 0.5$ Considering Fig. (3.22) one may observe that the $G_{max}/G_{max,ref}$ ratio for $\kappa \geq 0.75$ increases with κ both for $m = 0$ and $m = 0.5$ but this growth is more significant for $m = 0.5$. Indeed for $\kappa = 5$ the minimum ratio $G_{max}/G_{max,ref} \simeq 0.83$ and the positive effects of the SSL on the nonmodal stability characteristics of the flow are significantly reduced.

The steady Stokes layer allows us to obtain important improvements on both modal and nonmodal stability properties of the plane Poiseuille flow. The most important results are observed for $A \simeq 1$ and $\kappa \simeq 1$ where the module of the least stable eigenvalue is approximately doubled and the maximum of the energy growth function may be reduced up to 72% with respect to the maximum observed for the plane Poiseuille flow.

The main wall forcing parameter that affects both modal and nonmodal stability properties of the plane Poiseuille flow is the wave amplitude A. Indeed as A increases the module of the real part of least stable eigenvalue increases for a detuning parameter $m = 0$, and the maximum of the transient energy growth decreases for both $m = 0$ and $m = 0.5$.

Modal and nonmodal stability characteristics of the plane Poiseuille flow over a SSL also depend on κ, but this dependence for $\kappa \geq 1.25$ is less remarkable incrementing Re number. However these improvements may downgrade considering $\kappa < 1$ where amplifications of the transient energy growth function with respect to the plane Poiseuille flow are observed.

3.4.2. Optimal initial conditions

A nonmodal analysis also provides us with the spatial shape of the optimal input, or optimal initial condition, i.e. the spatial shape of the pertubation at time $t = 0$ that is capable of maximum energy growth amplification before long-term decay. For the present problem, the optimal initial condition is not constrained to be described by a single streamwise wavenumber but covers a set of streamwise wavenumbers considered in the modal expansion.

The optimal initial and optimal output conditions in physical domain are reported comparing the unforced plane Poiseuille flow $A = 0$ and the Poiseulle flow subject to a wavelike wall forcing with non-dimensional wave amplitude $A = 1$. Only the detuning parameter $m = 0$ is considered: no subharmonics are allowed.

We report the optimal initial and the optimal output conditions space appearance for $Re = 1000$, $\kappa = 1, \beta = 2.0$, in Figs. (3.23, 3.24), a further case, for $Re = 1000$, $\kappa = 2, \beta = 0.5$, is reported in Apx. (A).

The wall forcing affects the shape of both optimal initial and optimal output conditions. For $A = 0$ with $m = 0$ no modulations in streamwise direction are observed, for all velocity components u, v, w of the perturbation for both optimal input and optimal output. These perturbation appearances in Fourier space are represented by only the mode $p = 0$ of the modal expansion. Indeed considering a modal expansion on streamwise wavenumbers, the optimal initial condition for the plane Poiseuille flow that leads to the maximum of the transient energy growth for a spanwise wavenumber $\beta = 2$ occurs for a streamwise wavenumber $\alpha = 0$. Hence the spatial shape of the optimal initial condition does not modulate in streamwise direction.

For $A = 1$, optimal initial condition is characterized by an overlap of perturbations of different wavenumbers in streamwise direction; i.e. the optimal initial condition u component is characterized by one-time periodic fundamental harmonics overlapped with higher harmonics components. The wall forcing also modulates w component of the optimal input in streamwise direction introducing higher harmonics of lower magnitude to the fundamental mode with $p = 0$.

Similar effects are also noticeable in the spatial shape of the output condition. Indeed the wall forcing modulates w component of the optimal output in streamwise direction introducing higher harmonics of lower magnitude to the fundamental mode with $p = 0$

Similar modulation effects of the spatial shape of the optimal initial condition and of the optimal output condition due to the steady Stokes layer may be observed for the case $Re = 1000$, $\kappa = 2, \beta = 0.5$ reported in Apx. (A).

The Orr mechanism [12] [14] leads to a shear inversion between the spatial shapes of the optimal input and of the optimal output . The initial perturbation pattern is simply advected by the flow. Indeed the effect of Orr-mechanism is to rotate the initial vorticity pattern in the direction of the shear; this may be observed considering u, w components.

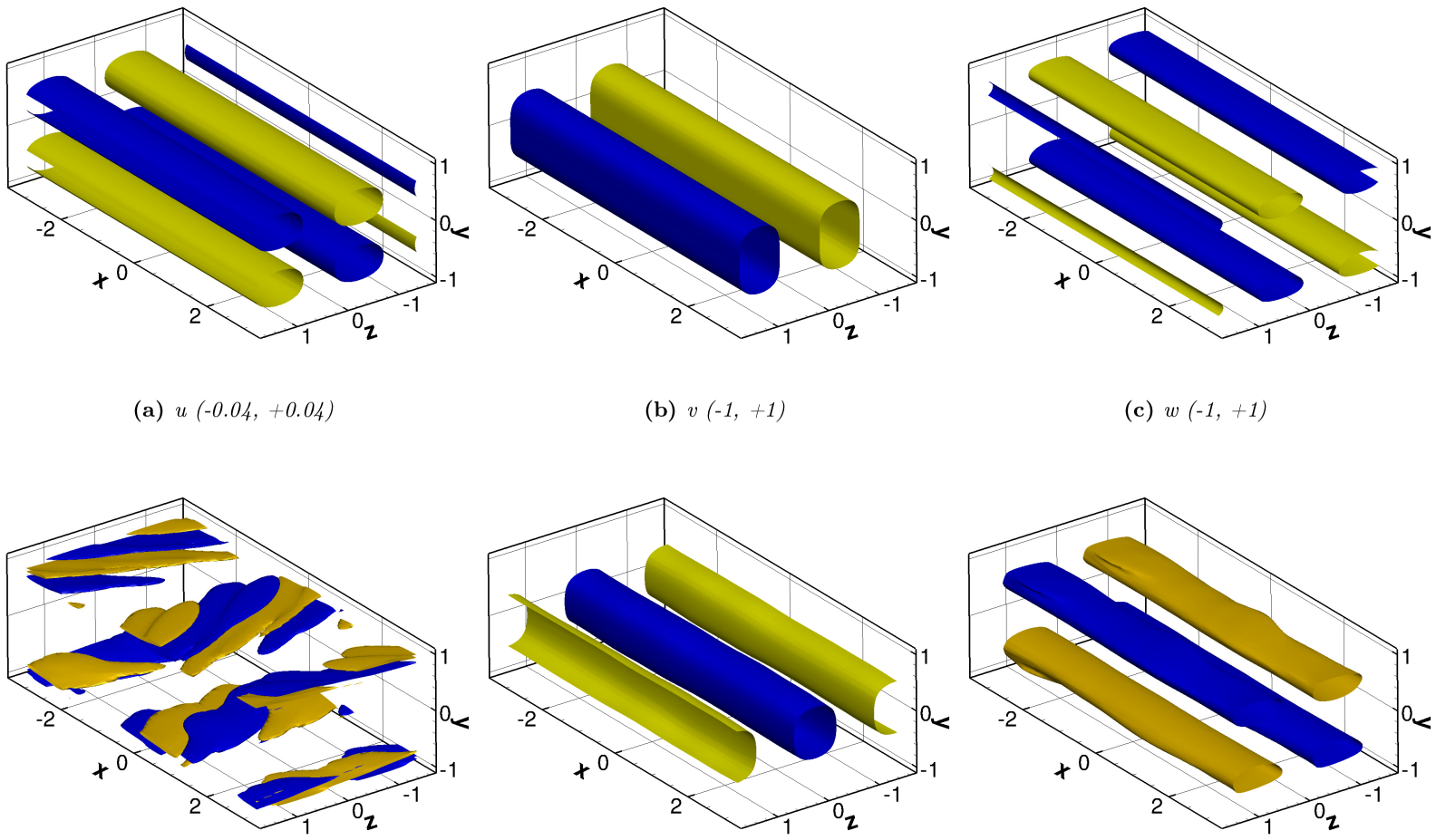

(a) *u (-0.04, +0.04)* **(b)** *v (-1, +1)* **(c)** *w (-1, +1)*

(d) *u (-0.2, +0.2)* **(e)** *v (-1, +1)* **(f)** *w (-1, +1)*

Figure 3.23.: *Optimal initial conditions isosurfaces at* $Re = 1000$, $\kappa = 1, \beta = 2$ *and* $A = 0$ *(TOP)* $A = 1$ *(BOTTOM). Discretization parameters employed:* $N = 80$, $M = 10$, $n_{eig} = 567$

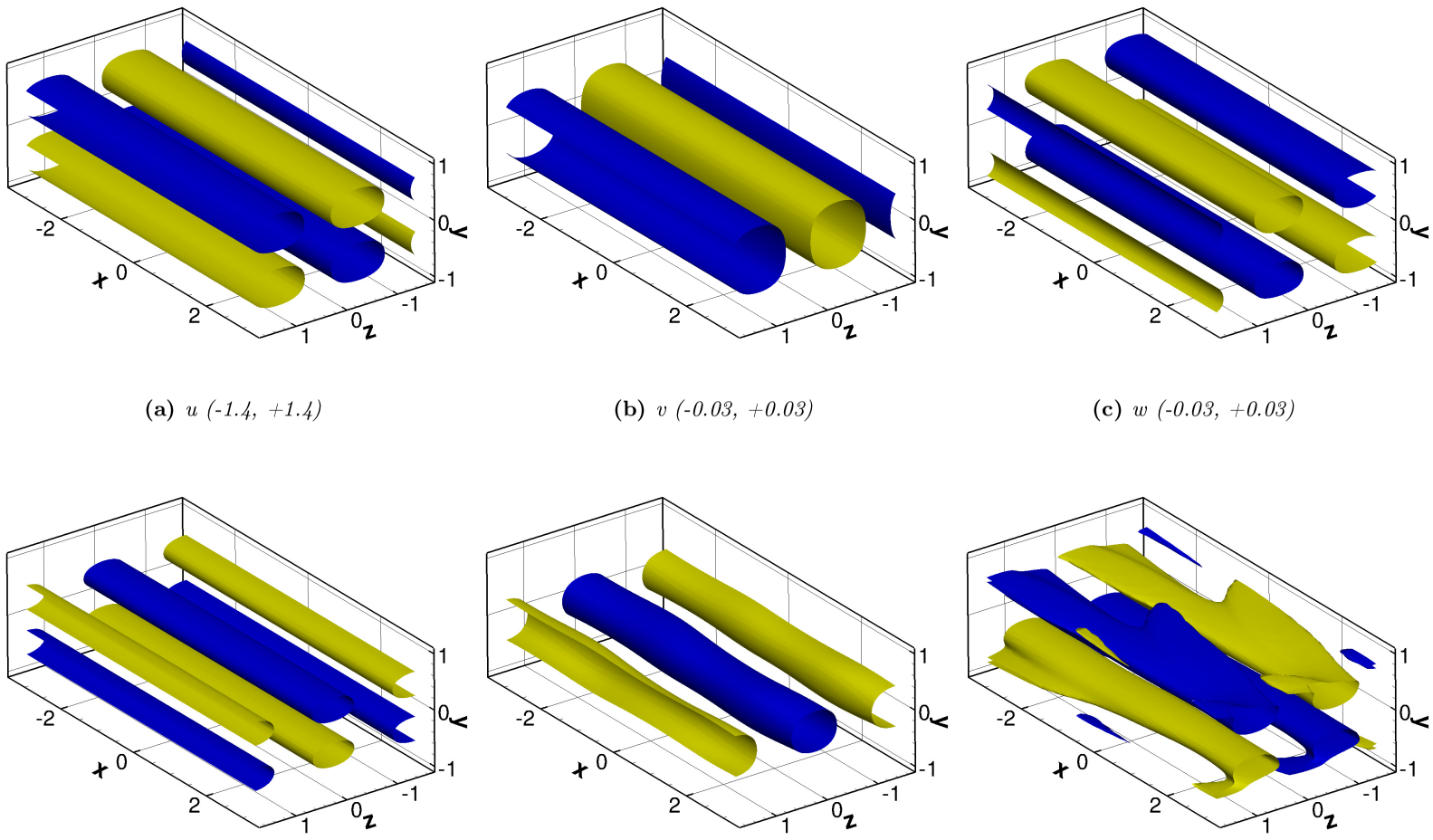

(a) *u (-1.4, +1.4)* **(b)** *v (-0.03, +0.03)* **(c)** *w (-0.03, +0.03)*

(d) *u (-1.5, +1.5)* **(e)** *v (-0.06, +0.06)* **(f)** *w (-0.06, +0.06)*

Figure 3.24.: *Optimal output conditions isosurfaces at* $Re = 1000$, $\kappa = 1, \beta = 2$ *and* $A = 0$ *(TOP)* $A = 1$ *(BOTTOM). Discretization parameters employed:* $N = 80$, $M = 10$, $n_{eig} = 567$

Conclusions

The linear stability of plane Poiseuille flow modified by a wall velocity forcing in the form of streamwise stationary waves of spanwise velocity has been analized. Both modal and nonmodal stability characteristics have been studied analysing respectively the real part of the least stable eigenvalue and the maximum of the transient energy growth function.

The mathematical formulation and its implementation of linearized wall-normal velocity and vorticity equations are not straightforward due to the fact that the wall forcing introduces inhomogeneity in streamwise direction.

The simple transform in Fourier space to decouple wavenumbers and to transform the problem to a one-dimensional eigenvalue study can not be taken any more. Hence we have to consider a sufficient large set of wavenumbers in streamwise direction to describe correctly its spatial non-homogeneity.

The linearized equations have been implemented using Chebyshev polynomials and their integration with a Gaussian quadrature over Gauss-Lobatto nodes. Reliability of results has been verified against DNS code employed by [19].

Modal stability analysis shows:

- The presence of a SSL with $m = 0$ leads to asymptotic more stable conditions: as A increases, the real part of the least stable eigenvalues decreases; even if it is not always observed for values of $\kappa < 1$.
- The modal stability for $m = 0.5$ is not influenced by the wall forcing.
- The modal stabilization effect due to the SSL increases with Re.
- Unstable conditions are found for $\beta = 1, \kappa < 1, Re = 2000, A \simeq 1$.

Nonmodal stability analysis shows:

- The maximum of the transient energy growth decreases as wave amplitude A increases, and for $A = 1$ reductions up to $\sim 72\%$ with respect to the plane Poiseuille flow are observed.
- Transient energy growth amplifications with respect to the reference plane Poiseuille flow are observed for $\kappa < 1$.
- Nonmodal maximum energy growth reduction increases with Re number.
- The maximum reduction of G_{max} for $m = 0.5$ is lower than for $m = 0$, even if an important $G_{max}/G_{max,ref}$ decrease with A is also observed.

Therefore a steady Stokes layer allows us to obtain important improvements on both modal and nonmodal stability properties of the plane Poiseuille flow. These improvements reach their maximum values imposing a wall forcing with $\kappa \simeq 1$ and $A = 1$ (where κ is the non-dimensional streamwise wavenumber and A the non dimensional amplitude). Wall forcing with $\kappa << 1$ may lead to $G_{max}/G_{max,ref}$ amplifications and if $m = 0.5$ for $\kappa \geq 1$ the positive stabilization effects may vanish. However these strange amplifications of the maximum of the transient energy growth have to be verified against a DNS analysis.

Future studies

This work is essentially a preliminary study that spans the entire parameter space, to comprehend how the SSL affects the stability characteristics of a plane Poiseuille flow. Some other relevant studies may be done:

- Repeat the analysis for higher Re numbers to confirm the reduction of the maximum of the transient energy growth observed increasing Re for $k \geq 1$.
- Carry out a complete study on Re for $m \neq 0$.
- DNS analysis to understand energy amplification against the plane Poiseuille reference case for values of κ lower than 1.
- DNS analysis to verify the unstable conditions found at $Re = 2000$ for $\kappa < 1$
- Analyse the stability of plane Poiseuille flow over a generalized Stokes layer, when the wall forcing is time dependent.

APPENDIX A

Further results

In this Appendix we present further results analysed. We aim at showing the main modal and nonmodal stability properties of plane Poiseuille flow over a SSL as functions of physical parameters $Re\kappa, \beta, A$ that we have not considered in the preliminary results exposed in Chap. (3). We provide visualizations of the least stable eigenvalue and the maximum of the energy growth function in the physical parameter space, that let us to observe the global effect of the SSL on the main streamwise base flow.

A.1. Modal Stability

Modal stability has been studied considering the least stable eigenvalue as a function of parameters κ, A, β. We show in Figs. (A.1, A.2, A.3) how the main parameters affect the asymptotic stability of the least stable eigenvalue.

In these figures is shown the condition for $A = 0$, which corresponds to the plane Poiseuille flow. One may notice that the presence of spanwise base flow gives us eigenvalues with lower real parts and then more stable asymptotic conditions.

As A increases for $\beta > 3$ the real part of the largest eigenvalue approximately decreases monotonically . For $\beta < 3$ the least stable eigenvalue also decreases with respect to the Poiseuille flow but at $\beta = 1$ we observe an increment of its real part for $A > 0.5$. Indeed comparing Figs. (A.1, A.2, A.3) one may observe a region for $\beta < 2$ where as A increases the real part of the least stable eigenvalue decreases, i.e. the asymptotic stabilization effect, in terms of modal stability, of the spanwise wall forcing diminishes. This reduction of asymptotic stability margin increase with Re number, in particular for $Re = 2000$ for $\kappa < 1, \beta = 1$ and $A = 1$ an asymptotic unstable region is observed Fig.(A.3). A further DNS analysis could be useful to understand if the instability, could be related to some discretization problems, or if the asymptotic stability properties of the baseflow are actually unstable for that wall forcing condition. DNS of small κ conditions are not presented in this work, which is only a preliminary study that may introduce further complete studies on the main important difficulties or problems evinced.

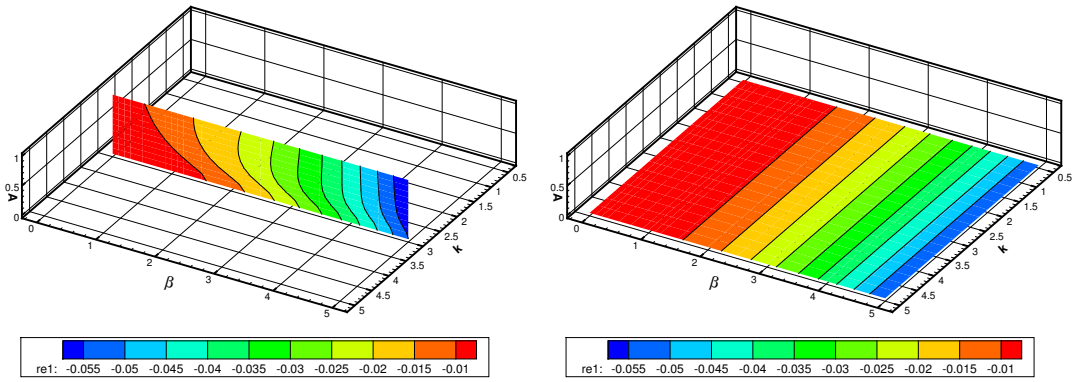

(a) $\kappa = 3$ **(b)** $A = 0.0$

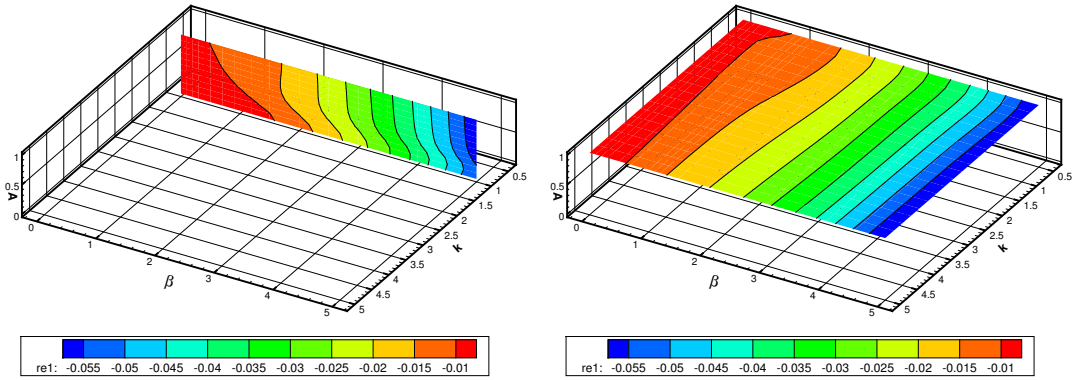

(c) $\kappa = 1$ **(d)** $A = 1$

Figure A.1.: *Least stable eigenvalue at* $Re = 500$ *as a function of parameters* κ, A *and* β

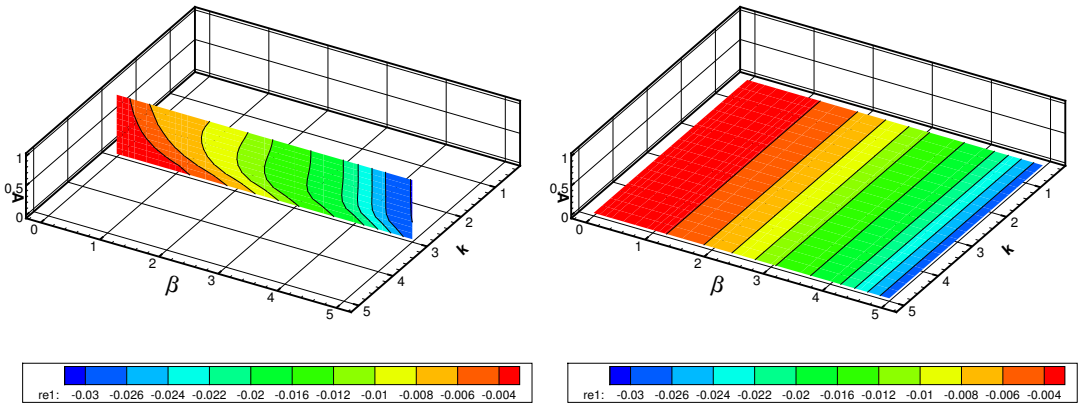

(a) $\kappa = 3$ **(b)** $A = 0.0$

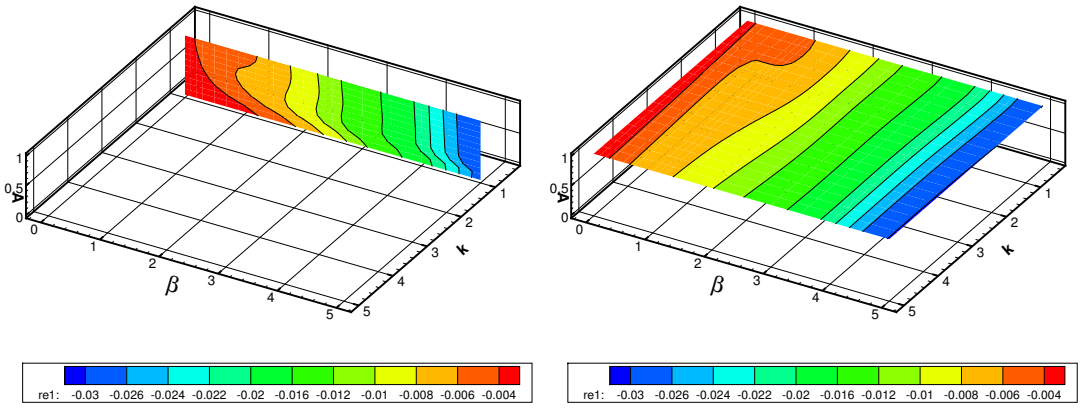

(c) $\kappa = 1$ **(d)** $A = 1$

Figure A.2.: *Least stable eigenvalue at* $Re = 1000$ *as a function of parameters* κ, A *and* β

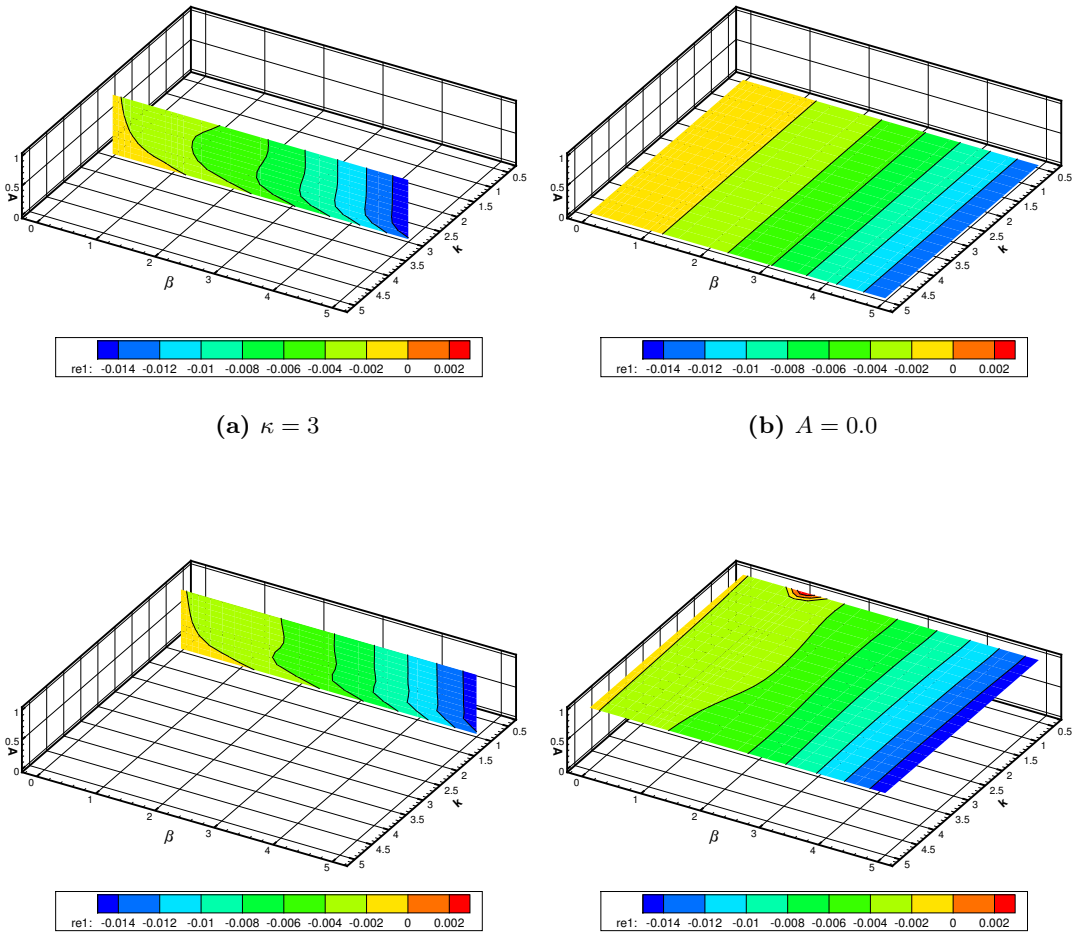

(a) $\kappa = 3$ **(b)** $A = 0.0$

(c) $\kappa = 1$ **(d)** $A = 1$

Figure A.3.: *Least stable eigenvalue at* $Re = 2000$ *as a function of parameters* κ, A *and* β

We report in Fig. (3.13) the maximum $Re(\lambda_1)/Re(\lambda_{1,ref})$ ratio for all wavenumbers κ and for all wave amplitudes A as a function of β at different Reynolds numbers considered. The maximum $Re(\lambda_1)/Re(\lambda_{1,ref})$ ratio is achieved for low values of β, i.e. for $\beta = 0.5$ at $Re = 1000$ or $Re = 2000$ and for $\beta = 0.7$ at $Re = 500$. For $\beta > 1$ as β increases the maximum $Re(\lambda_1)/Re(\lambda_{1,ref})$ ratio, for all κ and for all A, monotonically decreases. Moreover the maximum $Re(\lambda_1)/Re(\lambda_{1,ref})$ ratio increases with Re. Therefore the maximum asymptotic stabilization effects due to the SSL are observed for perturbations whose spanwise wavenumbers are sufficiently small, i.e. $\beta \leq 1$.

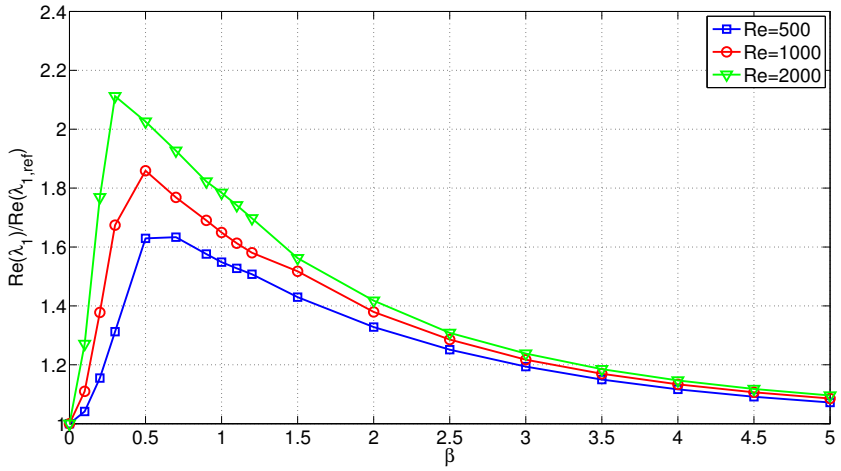

Figure A.4.: *maximum $Re(\lambda_1)/Re(\lambda_{1,ref})$ ratio for all κ and for all A as a function of β. The curves represent the Reynolds numbers analysed*

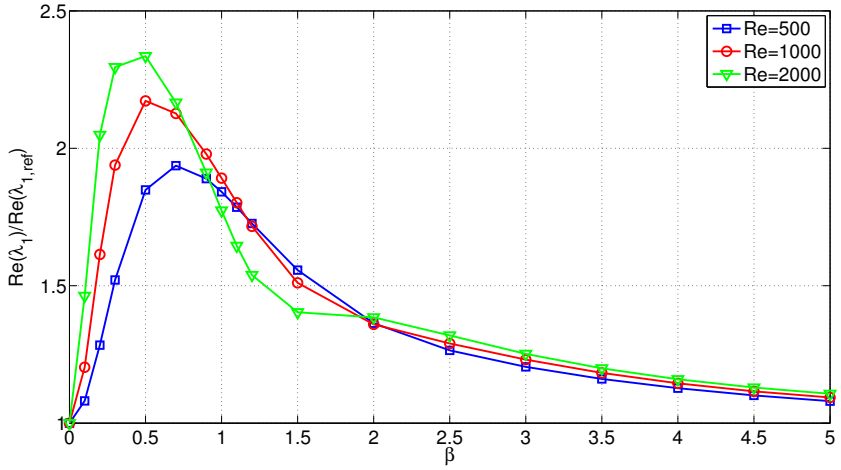

Figure A.5.: *$Re(\lambda_1)/Re(\lambda_{1,ref})$ ratio for, $A = 1$, $\kappa = 3$ as a function of β. The curves represent the Reynolds numbers analysed*

However considering Fig(A.2), possible regions in which $Re(\lambda_1)$ increases with A may exist. We report in Fig. (A.5) the $Re(\lambda_1)/Re(\lambda_{1,ref})$ ratio for, $A = 1$, $\kappa = 3$ as a function of β. Therefore for $0.7 \leq \beta \leq 2$ the $Re(\lambda_1)/Re(\lambda_{1,ref})$ decreases as Re increases. It looks as if for $0.7 \leq \beta \leq 2$ the asymptotic stabilization effect of the wall forcing is reduced and this reduction, may lead to unstable conditions for $Re = 2000$ as observed in Fig. (A.3). However further analysis against DNS may be useful to understand if these unstable conditions may be related with possible discretization problems.

A.1.1. Dependence on detuning parameter

The least stable eigenvalues may be affected by the detuning parameter. We report in Fig. (A.6) the least stable eigenvalue as a function of parameters κ, A, β for a detuning parameter $m = 0.5$. We report in Fig. (3.13) the maximum $Re(\lambda_1)/Re(\lambda_{1,ref})$ ratio for all κ and for all A as a function of β at $Re = 1000$ with $m = 0$ and $m = 0.5$.

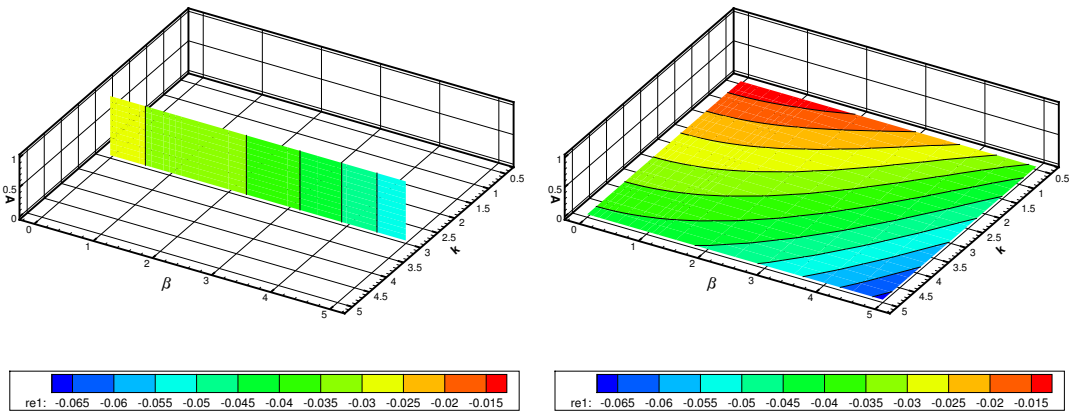

(a) $\kappa = 3$ **(b)** $A = 0.0$

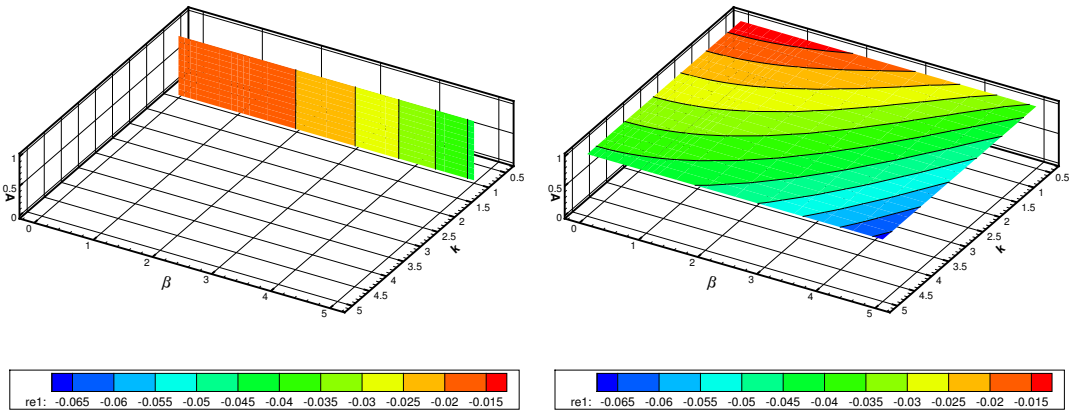

(c) $\kappa = 1$ **(d)** $A = 1$

Figure A.6.: *Least stable eigenvalue at* $Re = 1000$ *as a function of parameters* κ, A *and* β *with* $m = 0.5$

One may observe that the asymptotic stability of the flow is not affected by the wall forcing for any combination of parameters κ, β, A as we observed in Chap. (3). Therefore, the flow, is characterized by the same asymptotic stability characteristics of

the plane Poiseuille flow. Indeed, the maximum $Re(\lambda_1)/Re(\lambda_{1,ref})$ ratio for all κ and for all A, with $m = 0.5$ is unitary for all β values considered.

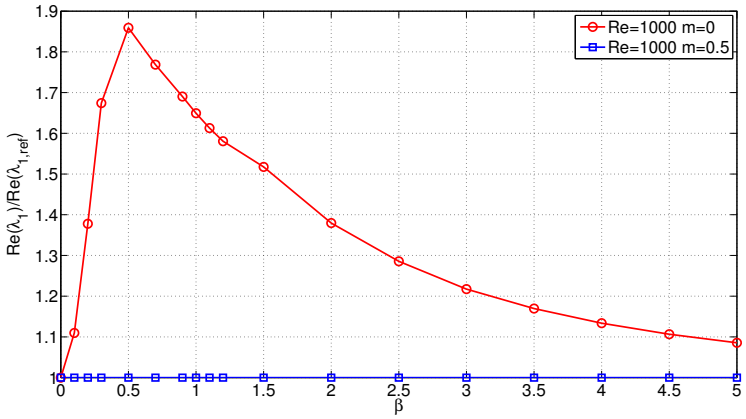

Figure A.7.: *Maximum* $Re(\lambda_1)/Re(\lambda_{1,ref})$ *ratio for all* κ *and for all* A *as a function of* β *at* $Re = 1000$ *with* $m = 0$ *and* $m = 0.5$.

A.2. Nonmodal Stability

Non modal stability analysis is done computing the transient energy growth function and taking its maximum as a function of physical parameters A, κ, β.

Figs. (A.8, A.9, A.10) concern the maximum growth of an initial perturbation at respectively $Re = 500$, $Re = 1000$ and $Re = 2000$.

$A = 0$ is the reference plane Poiseuille flow. As A increases the maximum of energy growth progressively decreases. Hence the presence of the steady Stokes layer has a stabilization effect, in terms of nonmodal stability, on the plane Poiseuille flow.

The amplification of an infinitesimal initial perturbation is less significant than the reference plane Poiseuille flow, in terms of nonmodal stability this implies that the flow may be more stable. Indeed if the energy growth is lower than the plane Poiseuille flow for each given combination of physical parameters then an infinitesimal perturbation may remain small enough to prevent transition, when nonlinearity are considered.

The effect of the nonlinear quadratic terms dropped in the $v - \eta$ formulation is less important than in the Poiseuille flow. Amplifications of the transient energy growth are found for $\kappa < 1$, $\beta \simeq 1$ and $A \simeq 1$. The flow as predicted by modal analysis at $Re = 2000$, for $\kappa = 0.5$, $A = 1$ and $\beta = 1$ is unstable and linearity is lost.

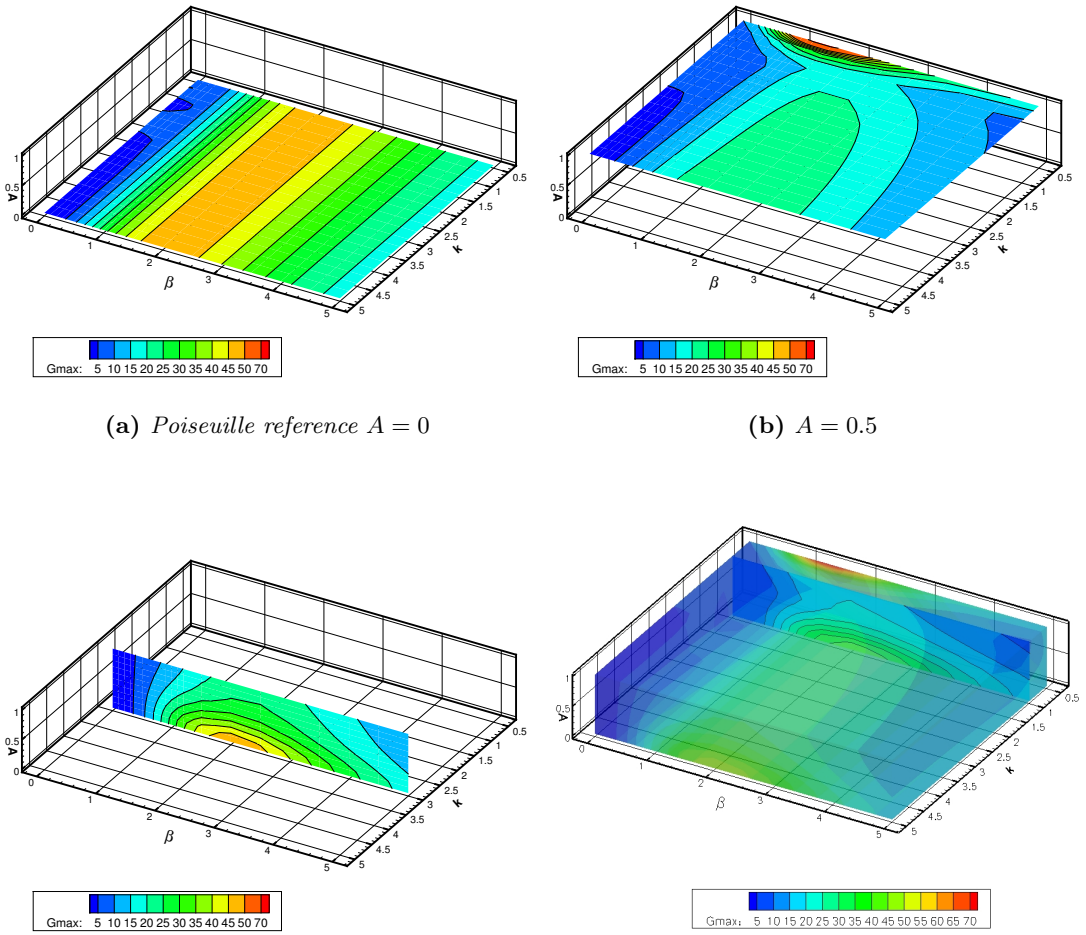

(a) *Poiseuille reference* $A = 0$ **(b)** $A = 0.5$

(c) $\kappa = 3$ **(d)** *Parameters view*

Figure A.8.: *Maximum energy growth at* $Re = 500$ *as a function of parameters* κ, A *and* β

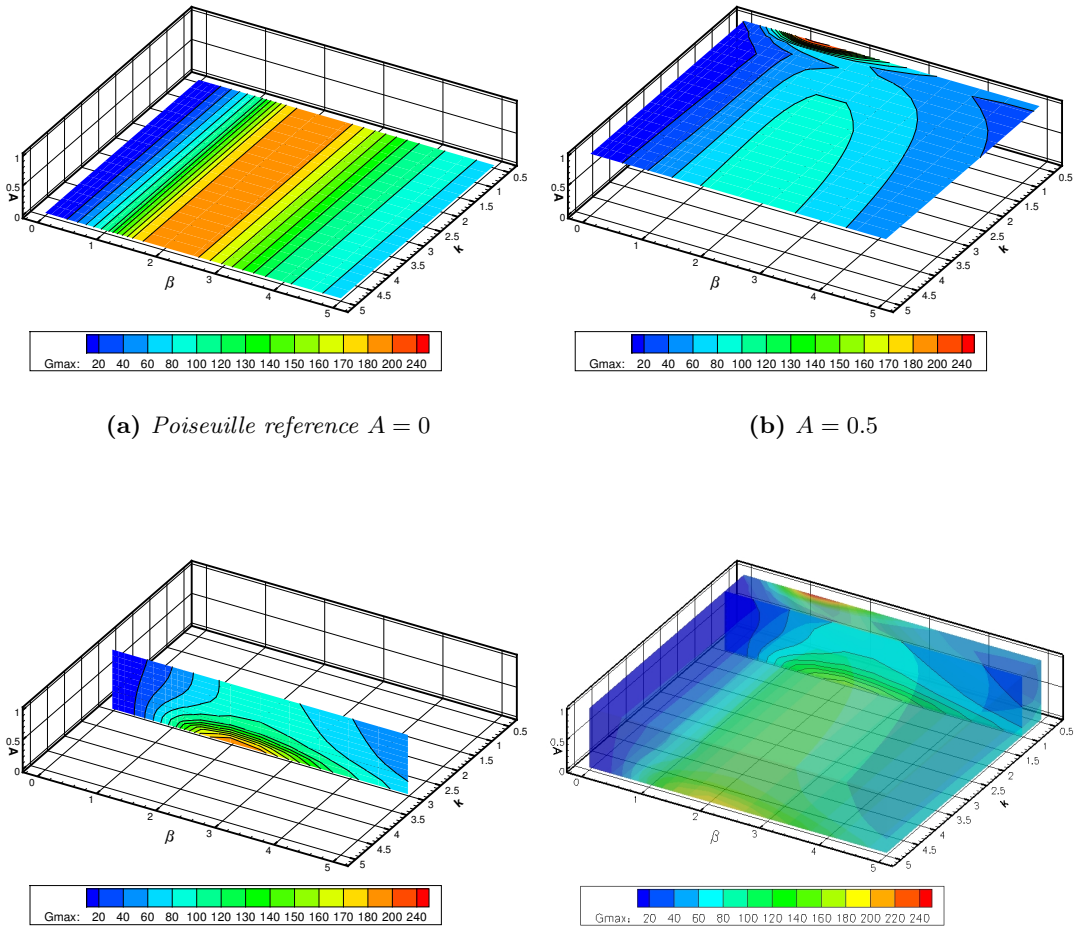

(a) *Poiseuille reference* $A = 0$ **(b)** $A = 0.5$

(c) $\kappa = 3$ **(d)** *Parameters view*

Figure A.9.: *Maximum energy growth at* $Re = 2000$ *as a function of parameters* κ, A *and* β

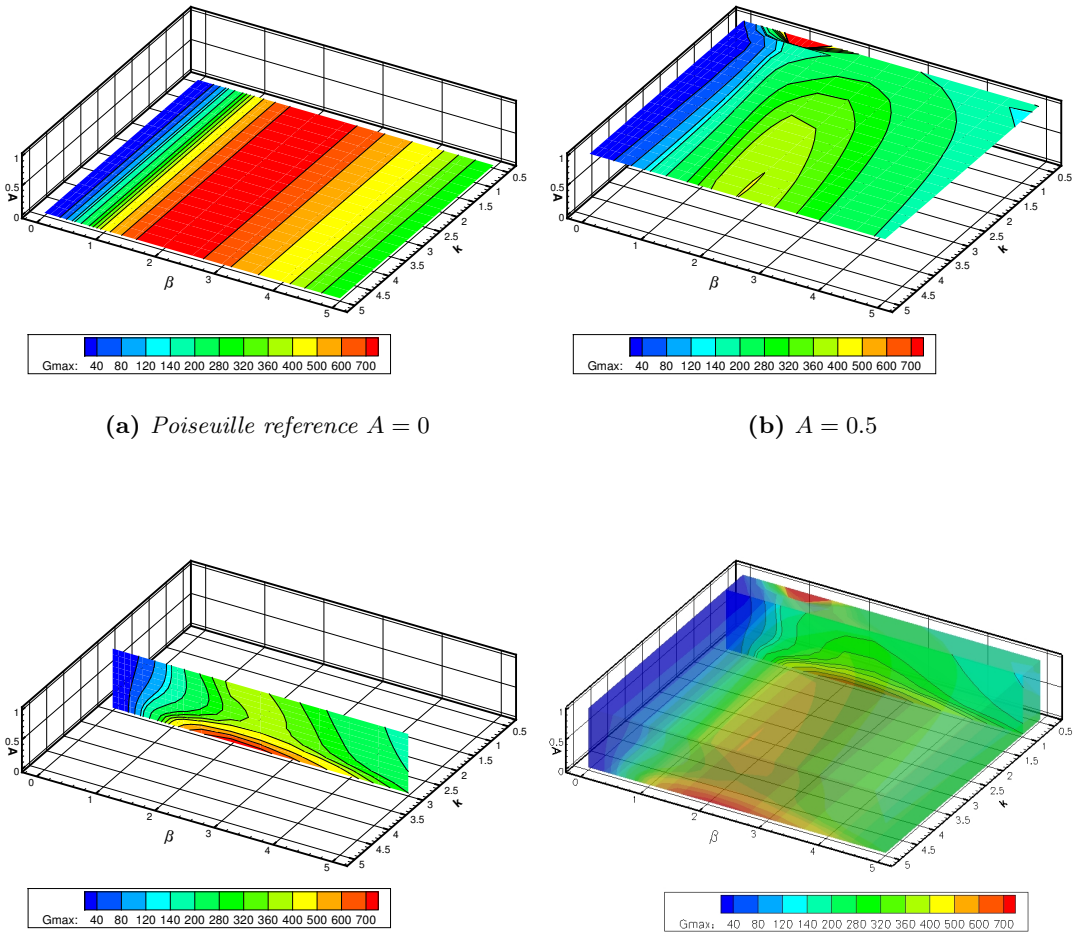

(a) *Poiseuille reference* $A = 0$ **(b)** $A = 0.5$

(c) $\kappa = 3$ **(d)** *Parameters view*

Figure A.10.: *Maximum energy growth at* $Re = 2000$ *as a function of parameters* κ, A *and* β

We report in Fig. (A.11) the minimum $G_{max}/G_{max,ref}$ ratio for all κ and for all A as a function of β at different Reynolds numbers considered. One may observe that the minimum values $G_{max}/G_{max,ref}$ ratio are obtained for $1 \leq \beta \leq 3$. For $\beta < 1$ as β increases, the minimum $G_{max}/G_{max,ref}$ ratio for all κ and for all A, strongly increases and reaches its maximum values $G_{max}/G_{max,ref} = 1$ for $\beta \leq 0.3$ for each Re considered. Therefore, for $\beta \leq 0.3$ the condition that minimizes $G_{max}/G_{max,ref}$ ratio is the plane Poiseuille flow. Indeed considering the $G_{max}/G_{max,ref}$ ratio for $\kappa = 0.75$, $A = 1$ as a function of β, reported in Fig. (A.12), one may observe that the presence of the wall forcing may lead to possible G_{max} amplification against the plane Poiseuille flow for $\beta \leq 1$

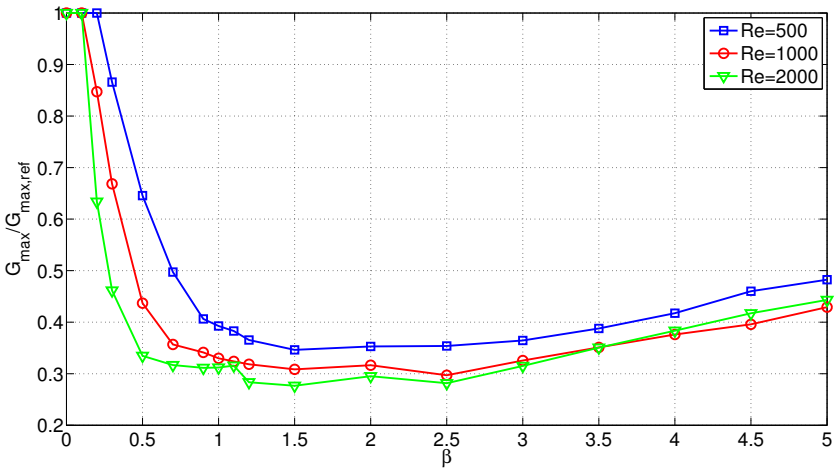

Figure A.11.: *Minimum $G_{max}/G_{max,ref}$ ratio for all κ and for all A as a function of β at different Reynolds numbers considered.*

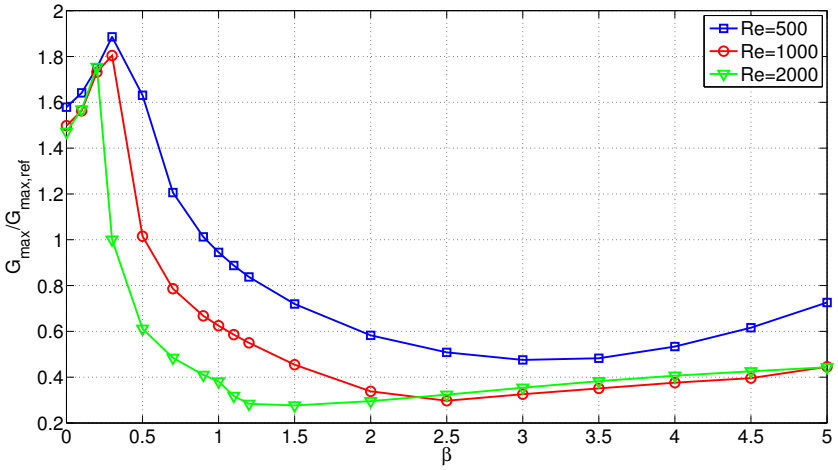

Figure A.12.: *$G_{max}/G_{max,ref}$ ratio for $\kappa = 0.75$, $A = 1$ as a function of β. The curves represent the Reynolds numbers analysed*

A.2.1. Dependence on detuning parameter

The detuning parameter m has also an important role on the maximum of the transient growth function. We have only analysed the case for $m = 0.5$ at $Re = 1000$ and reported the results in Fig. (A.13).

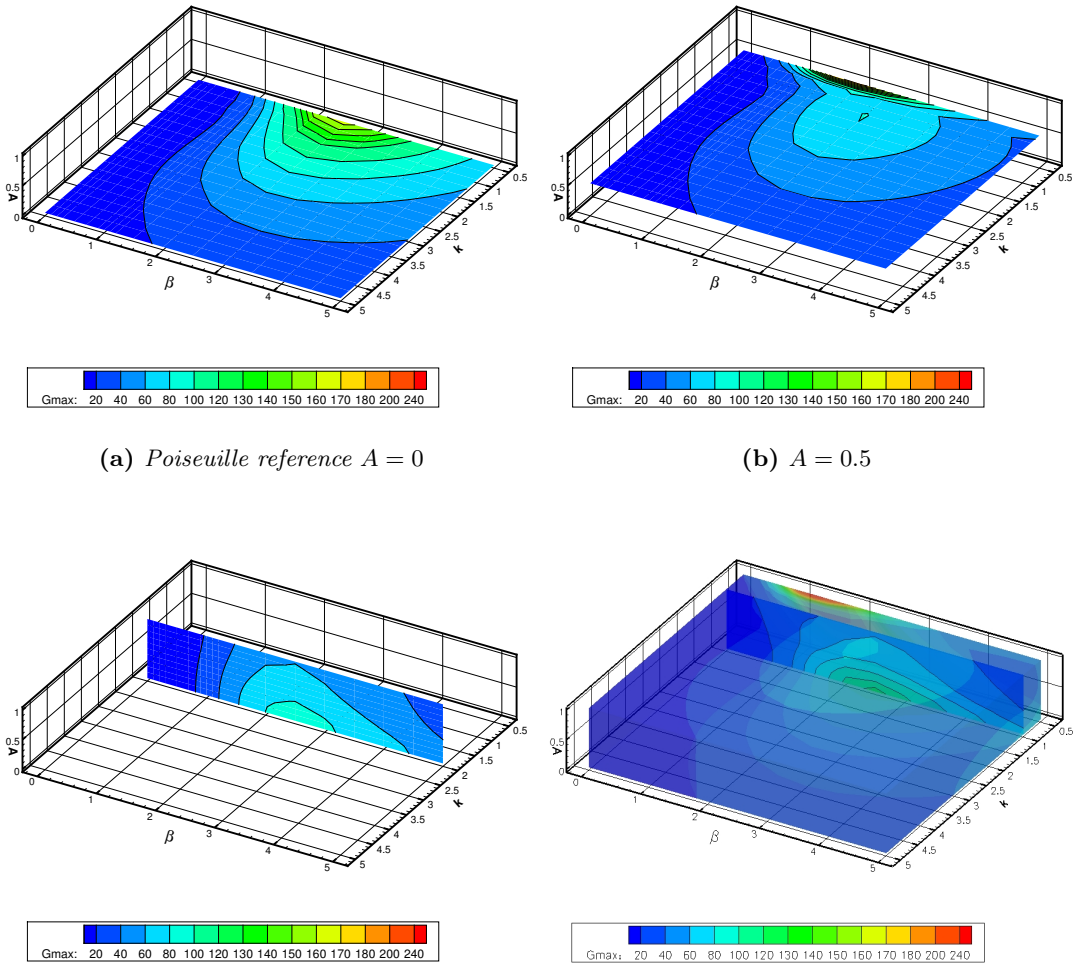

(a) *Poiseuille reference* $A = 0$ **(b)** $A = 0.5$

(c) $\kappa = 3$ **(d)** *Parameters view*

Figure A.13.: *Maximum energy growth at* $Re = 1000$ *as a function of parameters* κ, A *and* β *with detuning parameter* $m = 0.5$

$A = 0$ is the plane Poiseuille model problem. The distribution of G_{max} on parameters κ, β with $A = 0$ is comparable with G_{max} dependence on wavenumbers α, β for an equivalent nonmodal stability analysis with $\alpha \neq 0$ of the Orr-Sommerfeld-Squire equations.

Differently from the case with $m = 0$, G_{max} for $A = 0$ depends also on κ with $\kappa \neq 0$. It looks as if we set the detuning parameter $m \neq 0$ for $A = 0$, (hence we are implicitly excluding $\tilde{\alpha} = \kappa = 0$ streamwise wavenumber) the G_{max} is also dependent by $p - th$ streamwise wavenumber of the modal expansion. The analysis in Fourier space leads us to infer that for a given SSL of wavenumber κ, the G_{max} distribution on parameters (κ, β) is comparable to the Orr-Sommerfeld case distribution for a given couple of wavenumbers (α, β) with $\alpha = m\kappa$.

As A increases the G_{max} decreases, and the flow could be considered more stable in terms of nonmodal stability.

The combination of physical parameters that minimizes the $G_{max}/G_{max,ref}$ is reported in Tab. (3.4), and the main effect of the wall forcing on nonmodal stability are addressed in Chap. (3).

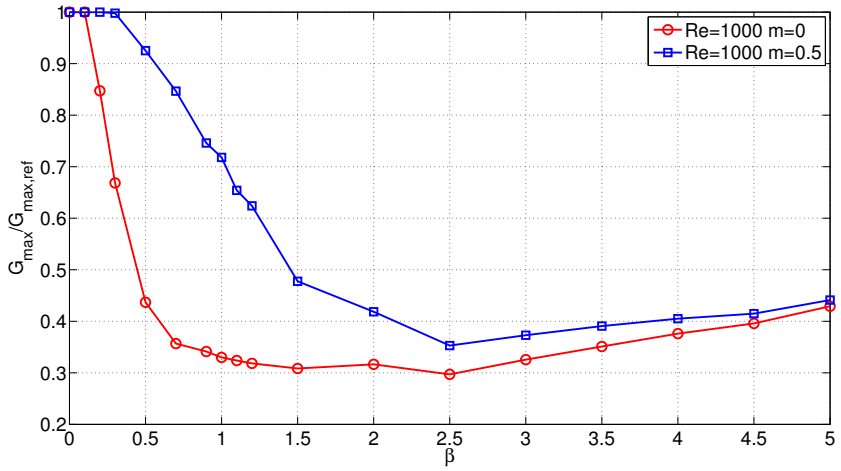

Figure A.14.: *Minimum $G_{max}/G_{max,ref}$ ratio, for all κ and for all A considered, as a function of β at $Re = 1000$ with $m = 0$ and $m = 0.5$*

We show in Fig. (A.14) the minimum $G_{max}/G_{max,ref}$ ratio for all κ and for all A as a function of β at $Re = 1000$ with $m = 0$ and $m = 0.5$. One may observe that if $m = 0.5$ the minimum $G_{max}/G_{max,ref}$ ratio for $\beta < 2.5$ could strongly increase than the case for $m = 0$ and its maximum values are obtained for $\beta \leq 0.3$ where the condition that minimizes G_{max} is the reference plane Poiseuille flow. Indeed considering Fig. (A.15) for $\beta \leq 1.5$ the $G_{max}/G_{max,ref}$ strongly increases for both $m = 0$ and $m = 0.5$, but this growth is greater for $m = 0.5$.

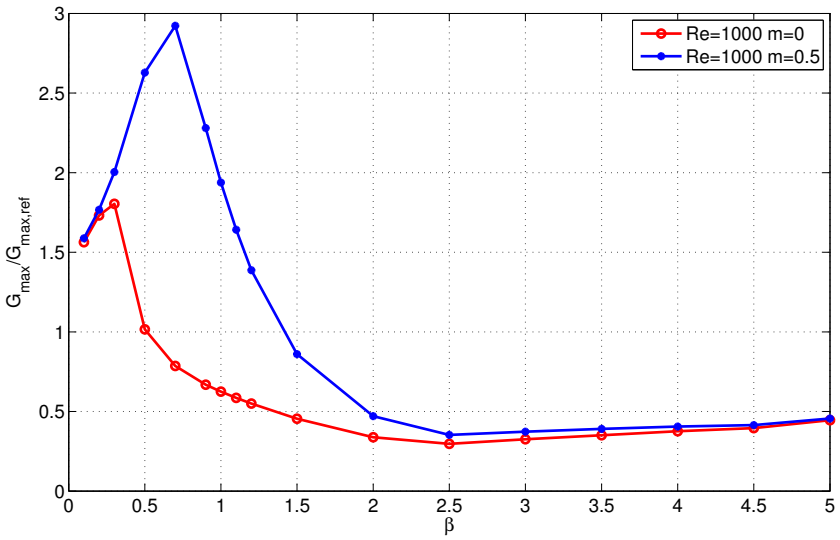

Figure A.15.: $G_{max}/G_{max,ref}$ *ratio for* $\kappa = 0.75$ *and for* $A = 1$ *as a function of* β *at* $Re = 1000$ *with* $m = 0$ *and* $m = 0.5$

A.2.2. Output conditions in Fourier space

We report the optimal output conditions relative to the optimal initial conditions shown in Chap. (3). Figs. (A.16, A.17, A.18) plot the modulus of the optimal output conditions in terms of wall-normal velocity and wall-normal vorticity as a function of wall-distance, and of the $p-th$ wavenumber of the modal expansion.

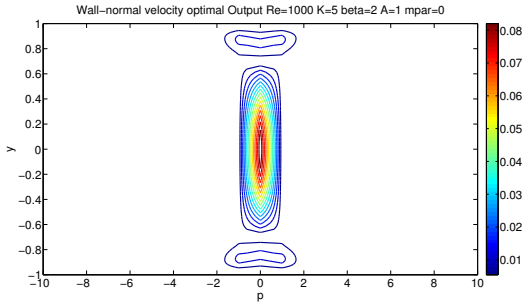

(a) *Wall-normal velocity*

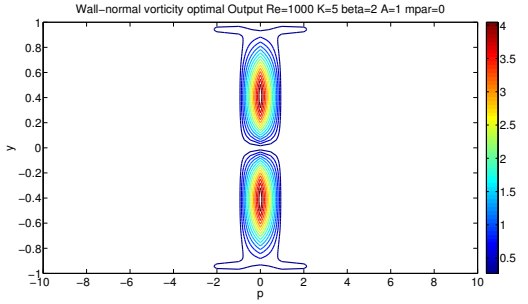

(b) *Wall-normal vorticity*

Figure A.16.: *Optimal output condition for the wall-normal velocity and wall-normal vorticity as a function of the wall-normal position y and $p-th$ wavenumber of the modal expansions. The contours describe the modulus of the optimal output condition for $Re = 1000, \kappa = 5, A = 1, \beta = 2$ with detuning parameter $m = 0$. The discretization parameters are: $N = 100$, $M = 10$, $n_{eig} = 1415$*

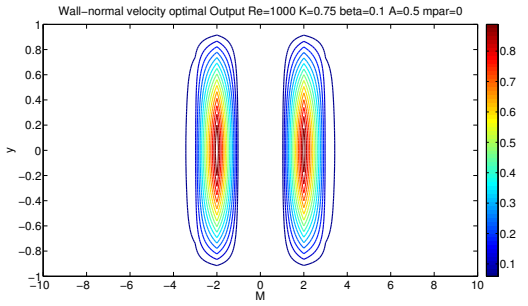

(a) *Wall-normal velocity*

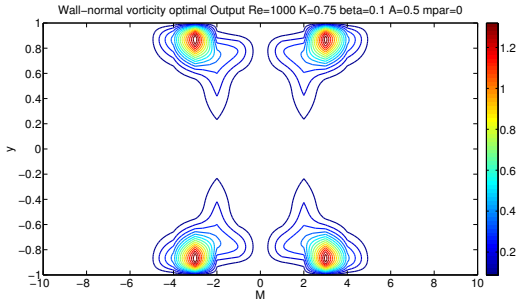

(b) *Wall-normal vorticity*

Figure A.17.: *Optimal output condition for the wall-normal velocity and wall-normal vorticity as a function of the wall-normal position y and $p-th$ wavenumber of the modal expansions. The contours describe the modulus of the optimal output condition for $Re = 1000, \kappa = 0.75, A = 0.5, \beta = 0.1$ with detuning parameter $m = 0$. The discretization parameters are: $N = 130$, $M = 10$, $n_{eig} = 917$*

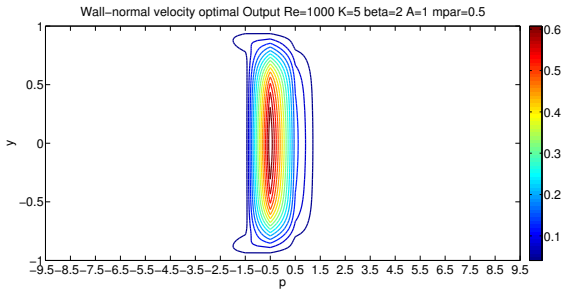

(a) *Wall-normal velocity*

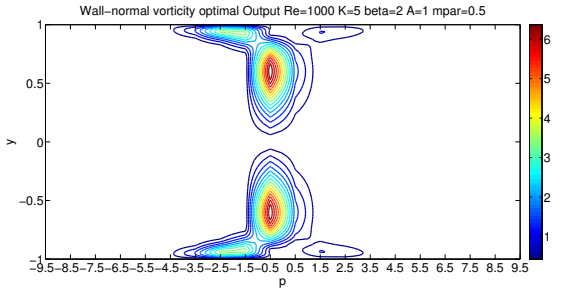

(b) *Wall-normal vorticity*

Figure A.18.: *Optimal output condition for the wall-normal velocity and wall-normal vorticity as a function of the wall-normal position y and $p-th$ wavenumber of the modal expansions. The contours describe the modulus of the optimal output condition for $Re = 1000, \kappa = 5, A = 1, \beta = 2$ with detuning parameter $m = 0.5$. The discretization parameters are: $N = 100$, $M = 10$, $n_{eig} = 1415$*

A.2.3. Spatial shape of optimal initial conditions

We report the optimal initial condition and the optimal output condition in physical domain for $Re = 1000$, $\kappa = 2, \beta = 0.5$, in Figs. (A.19, A.20)

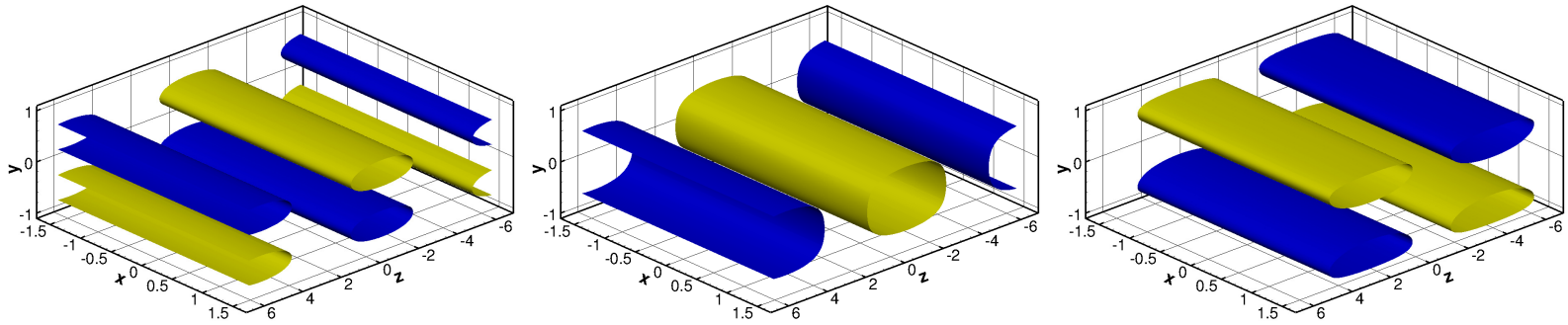

(a) *u (-0.2, +0.2)* **(b)** *v (-0.3, +0.3)* **(c)** *w (-1.0, +1.0)*

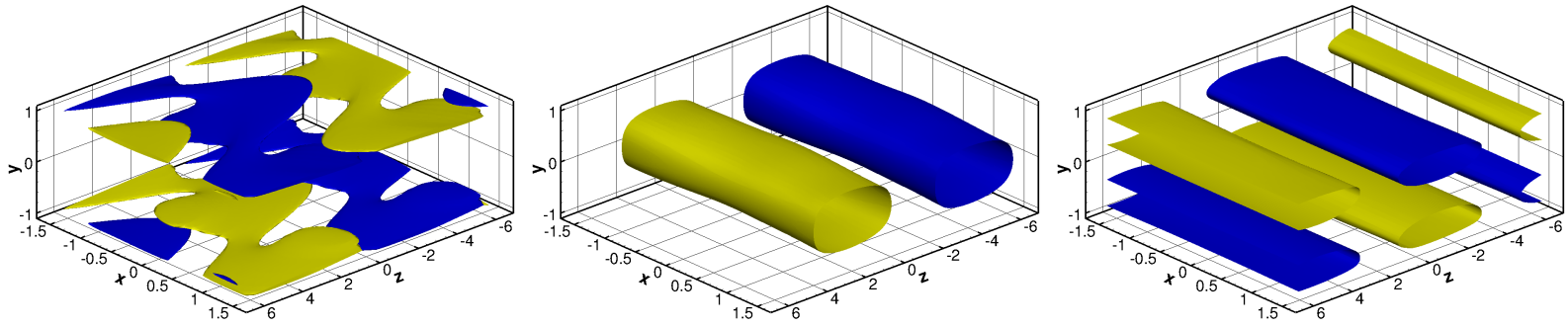

(d) *u (-0.4, +0.4)* **(e)** *v (-0.3, +0.3)* **(f)** *w (-1.0, +1.0)*

Figure A.19.: *Optimal initial conditions isosurfaces at* $Re = 1000$, $\kappa = 2, \beta = 0.1$ *and* $A = 0.5$ *(TOP)* $A = 1$ *(BOTTOM). Discretization parameters employed:* $N = 80$, $M = 10$, $n_{eig} = 567$

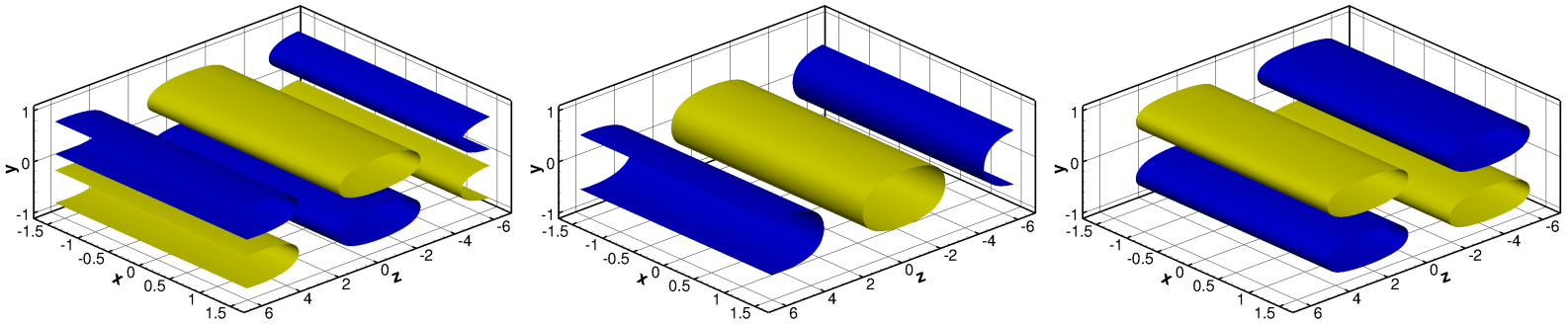

(a) *u (-1.0, +1.0)* **(b)** *v (-0.03, +0.03)* **(c)** *w (-0.1, +0.1)*

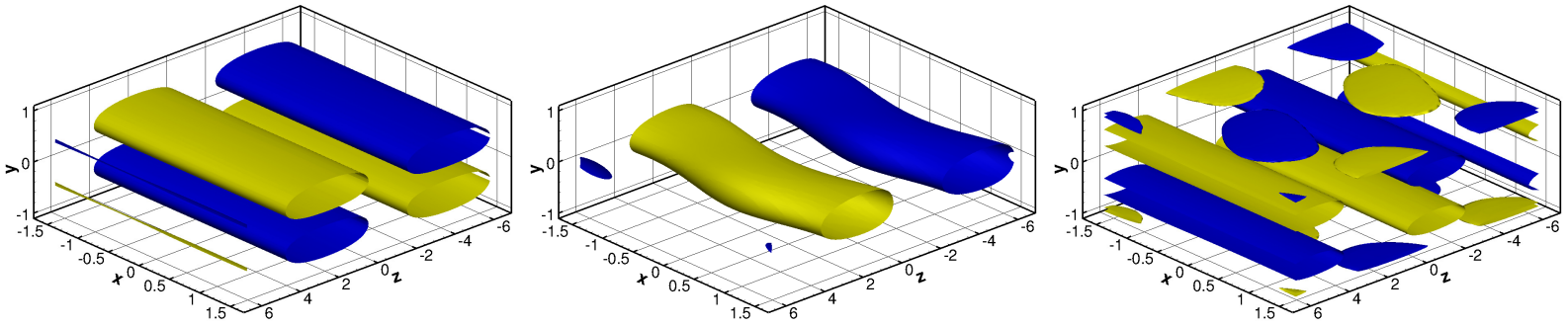

(d) *u (-1.0, +1.0)* **(e)** *v (-0.04, +0.04)* **(f)** *w (-0.2, +0.2)*

Figure A.20.: *Optimal output conditions isosurfaces at* $Re = 1000$, $\kappa = 2, \beta = 0.5$ *and* $A = 0$ *(TOP)* $A = 1$ *(BOTTOM). Discretization parameters employed:* $N = 80$, $M = 10$, $n_{eig} = 567$

Allegato

Estratto in Italiano ai sensi dell'Art. 9 del Regolamento degli esami di Laurea magistrale 2012

Questa Tesi presenta uno studio della stabilità lineare di un flusso di Poiseuille soggetto ad uno strato limite di Stokes Stazionario. Il problema analizzato introduce una forzante sinusoidale a parete stazionaria al comune flusso di Poiseuille piano. Si intende pertanto analizzare in qual modo quest'ultima ne influenzi la stabilità.

L'idea di questo studio nasce da un'analisi su un problema differente ovvero dalle osservazioni di riduzione di resistenza di attrito turbolento in presenza di onde viaggianti rispetto al flusso di canale piano (channel flow) [19]. In questo caso le onde creano uno strato limite trasversale al flusso non stazionario sinusoidale nella direzione del flusso che è stato chiamato strato limite di Stokes generalizzato (o GSL) [18]. Tali onde definite per diminuire la resistenza hanno mostrato riduzioni di attrito a parete anche superiori al 50 %. Inoltre questo elevato beneficio è ottenuto a basso costo energetico e l'energia risparmiata netta è circa il 20 %.
Tuttavia si è notato che zone a forte riduzione di resistenza d'attrito sono state trovate per condizioni di strato limite gereralizzato di Stokes non dipendente dal tempo, che è stato quindi chiamato strato limite di Stokes stazionario.

Questi fenomeni di riduzione della resistenza di attrito turbolento hanno forti implicazioni ingegneristiche in quanto l'attrito costituisce una importante fonte di costi energetici in diversi ambiti e applicazioni quali l'aeronautico, l'automobilistico o il navale. Trovare una metodologia che consenta quindi una riduzione dei fenomeni legati all'attrito è estremamente importante.

Questo lavoro si fonda su questo concetto anche se tratta di un argomento totalmente differente, ovvero di stabilità lineare. L'obbiettivo ultimo è capire come lo strato limite generalizzato di Stokes interagisce con il flusso di Poiseuille nell'ambito della stabilità lineare per capire come questo GSL influenza la resistenza di attrito turbolento.

Lo studio della stabilità lineare di un flusso di Poiseuille soggetto a una forzante a parete comporta svariate difficoltà rispetto al caso indisturbato. Tali difficoltà sono strettamente legate allo strato limite di Stokes che rende il problema non omogeneo nella direzione del flusso.
In caso di flusso piano di Poiseuille, anche noto come channel flow, si può osservare che le direzioni parallela al flusso e trasversale ad esso sono omogenee; ciò permette di definire un sistema di equazioni di Navier Stokes i cui coefficienti dipendono solo dalla

coordinata normale a parete. Il problema pertanto si dice autonomo nelle direzioni parallela e trasversale al flusso piano di Poiseuille. La linearizzazione delle equazioni di Navier-Stokes e la successiva rielaborazione delle stesse rispetto alle variabili di velocità e vorticità normale alla parete, ovvero la famosa formulazione $v-\eta$, consente di ottenere le equazioni di Orr-Sommerfeld-Squire. Tali equazioni sono puramente evolutive e non più equazioni alle derivate parziali, come nel caso delle equazioni di Navier-Stokes. Pertanto, considerando una dipendenza esponenziale rispetto al tempo, costituiscono un problema agli autovalori che può essere risolto nello spazio di Fourier semplicemente considerando una espansione modale delle incognite nelle direzioni parallela e trasversale al flusso di Poiseuille e sfruttando l'ortogonalità dei modi (grazie alla omogeneità di tali direzioni) .

In caso di flusso di Poiseuille soggetto ad una forzante sinusoidale a parete modulata in direzione del flusso, il problema si complica. La direzione parallela al flusso non è più omogenea e l'ortogonalità dei modi lungo essa non può essere sfruttata.
Il problema pertanto si dice essere globale nella direzione parallela al flusso di Poiseuille e spettrale in direzione trasversale ad esso. Pertanto per ottenere equazioni analoghe a quelle di Orr-Sommerfeld-Squire nel caso di un flusso di Poiseuille soggetto a strato limite di Stokes stazionario, sfruttando la sinusoidalità della forzante a parete, si opera una espansione in serie di Fourier delle incognite che consideri tutti i numeri d'onda (o una espansione opportunatamente troncata) nella direzione del flusso e si effettua quindi una trasformata di Fourier nella direzione dello stesso. Un aspetto cruciale di queste equazioni scritte nel dominio di Fourier è che ciascun numero d'onda definito nella direzione del flusso interagisce con se stesso e i numeri d'onda successivo e precedente dell'espansione modale considerata.

Questo lavoro di tesi presenta pertanto un confronto sia matematico sia intermini di analisi di stabilità tra ciò che accade nel caso di flusso piano di Poiseuille e quanto invece riguarda il caso perturbato dalla forzante sinusoidale imposta.

In una prima parte viene analizzata la fisica del problema osservando che se il flusso di Poiseuille è laminare il suo profilo parabolico non interagisce con lo strato limite trasversale a esso. Vengono pertanto ricavati analiticamente i due flussi base considerati: ll flusso di Poiseuille, il flusso trasversale o strato limite stazionario di Stokes. Introducendo quindi un campo di velocità perturbatorio infinitesimo, vengono linearizzate le equazioni di Navier Stokes rispetto ai flussi base in gioco, eliminando i termini quadratici della perturbazione. Effettuando un cambiamento di variabili si può ottenere la formulazione nelle variabili di velocità e vorticità normale a parete. Infine viene effettuata una trasformata di Fourier nelle direzioni parallela e trasversale al flusso di Poiseuille per ottenere la formulazione finale delle equazioni del problema.

Le incognite del problema, fissato il numero d'onda in direzione trasversale al flusso di Poiseuille, sono pertanto le componenti di velocità e di vorticità normale a parete per ogni numero d'onda considerato nella espansione modale adottata.

Successivamente si è passati alla implementazione numerica delle equazioni trasformate nel dominio di Fourier. Per ogni numero d'onda considerato nell'espansione modale, le incognite di velocità e vorticità normale a parete vengono discretizzate mediante una

esapnsione di polinomi di Chebyshev.

La discretizzazione delle equazioni rispetto ad una espansione troncata di numeri d'onda nella direzione del flusso di Poiseuille permette di ottenere un problema di tipo evolutivo nelle variabili di velocità e vorticità normali a parete (per ogni numero d'onda nella direzione del flusso considerato). Si ottiene quindi un problema agli autovalori che, portato agli stati, è caratterizzato da una matrice sparsa tridiagonale a blocchi.

Tale matrice tuttavia è di dimensioni ragguardevoli infatti dato il fattore di troncamento dell'espansione modale M, la sua dimensione è comparabile al problema standard di Orr-Sommerfeld moltiplicato per un fattore pari a $(2M+1)^2$. Volendo calcolare con buona approssimazione la dinamica della perturbazione infinitesima imposta, tuttavia non è necessario considerare tutti i modi del problema, ma solo un sottoinsieme degli stessi. Gli autovalori, necessari sia per l'analisi modale, sia per l'analisi non-modale sono quindi calcolati mediante metodo di Arnoldi, della libreria ARPACK, che calcola i primi n_{eig} autovalori con parte reale più grande.

L'analisi di stabilità modale o stabilità modale considera l'autovalore a parte reale più grande, in quanto definisce il comportamento asintotico di una generica perturbazione. Se l'autovalore a parte reale più grande λ_1 ha parte reale positiva, si ha una condizione di instabilità altrimenti il flusso è asintoticamente stabile per quella data perturbazione infinitesima imposta. Pertanto si effettua uno studio dell'andamento dell'autovalore a parte reale più grande in funzione dei parametri fisici del problema analizzato che risultano essere: il numero di Reynolds Re, il numero d'onda relativo alla direzione trasversale al flusso di Poiseuille β e il numero d'onda κ della forzante sinusoidale in streamwise e la sua relativa ampiezza A adimensionalizzata rispetto velocità di mezzeria del flusso di Poiseuille U_p.

L'analisi di stabilità non-modale è basata sul concetto di crescita transitoria, [24], [27], [26] per il quale è necessario definire l'operatore *norma energia*. Si tratta di un operatore integrale che deve essere ridefinito rispetto al semplice caso di Orr-Sommerfeld per considerare tutti i numeri d'onda della espansione modale nella direzione parallela al flusso di Poiseuille. L'integrazione numerica utilizzata è una particolare quadratura gaussiana che sfrutta i polinomi di Chebyshev per definire gli opportuni pesi di integrazione; tale integrazione è anche chiamata quadratura di Clenshaw-Curtiss. L'analisi di stabilità non-modale è quindi definita analizzando il massimo della crescita transitoria in funzione dei parametri fisici Re, κ, A, β.

Sia per l'analisi di stabilità modale sia per quella non-modale sono state considerate anche possibili perturbazioni infinitesime il cui primo numero d'onda dell'espansione modale possa essere una sub-armonica del numero d'onda della forzante a parete introducendo un opportuno parametro di detuning pari a $m = 0.5$.

A seguito della implementazione del codice si è passati quindi alla calibrazione dei parametri di discretizzatione adottati quali, il numero di polinomi di Chebishev N adottati, il fattore di troncamento dell'espansione modale M per ottenere risultati affidabili. Tale calibrazione è stata effettuata considerando diversi casi test in modo tale che i risultati fossero dipendenti dai parametri di discretizzazione con un piccolo errore percentuale. In tesi vengono mostrati i criteri osservati per ottenere questa accuratezza

nei risultati. A seguito di una indagine preliminare di stabilità modale e non modale è stata definita anche una discretizzazione dei parametri fisici Re, κ, A, β infittendo la griglia di calcolo dove particolari variazioni delle proprietà di stabilità sono state riscontrate.

Si è quindi passati alla validazione del codice lineare mediante DNS. Sono stati verificati il corretto calcolo dell'autovalore a parte reale più grande considerando una condizione instabile e verificando che il rateo di crescita dell'energia cinetica della perturbazione fosse pari al doppio della parte reale dell'autovalore più instabile. Si è verificata anche la completa accordanza tra la funzione di crescita transitoria calcolata mediante ilcalcolo lineare e mediante DNS.

Infine, una volta accertata l'affidabilità dei risultati si è passati alla vera e propria analisi della stabilità modale e non modale per differenti combinazioni dei parametri fisici Re, κ, A, β, considerando come parametro di detuning $m = 0$, $m = 0.5$

I risultati vengono riportati in tesi nei termini di massima diminuzione della parte reale dell'autovalore meno stabile e di massima riduzione della funzione di crescita transitoria per tutti i parametri fisici analizzati.

I risultati ottenuti sono particolarmente significativi sia in termini di stabilità modale, sia in termini di stabilità non modale. La forzante sinusoidale a parete infatti per $m = 0$ determina una diminuzione (un aumento del modulo) della parte reale degli autovalori rispetto al caso di flusso di Poiseuille non forzato. Il flusso risulta quindi essere asintoticamente più stabile, anche se sono state trovate condizioni di asintotica instabilità per $Re = 2000, A \simeq 1, \beta \simeq 1$ e $\kappa = 0.5$. Lo strato limite di Stokes non influenza praticamente la stabilità modale del flusso di Poiseuille in caso di parametro di detuning $m = 0.5$. Il massimo della crescita transitoria viene diminuito rispetto al caso di flusso di Poiseuille piano. In particolare, sono state osservate riduzioni fino al 70 % del massimo valore della funzione di crescita energetica transitoria del flusso di Poiseuille non forzato. Si è notato che il massimo della funzione di crescita transitoria decresce monotonicamente al crescere dell'ampiezza adimensionalizzata della forzante di parete. Si osserva inoltre che le più significative riduzioni del massimo della crescita transitoria rispetto al flusso di Poiseuille piano si ottengono per valori di $\kappa \simeq 1$. Aumentando κ questo effetto diminuisce e risulta particolarmente ridotto in caso si consideri $m = 0.5$. Amplificazioni della funzione di crescita transitoria sono state determinate per $\kappa < 1$

Si può quindi concludere che la forzante sinusoidale imposta a parete determina un incremento delle caratteristiche di stabilità modale e non modale del flusso piano di Poiseuille. I maggiori benefici si ottengono per valori di $A = 1$ e $\kappa \simeq 1$.

Questo lavoro è strutturato come segue:

- **Introduzione**: Viene presentato il problema analizzato, il tipo di analisi che verrà condotta e le motivazioni di questo studio

- **Capitolo 1: Equazioni di governo**: Vengono presentati i concetti alla base della stabilità linerare,ì cercando di evidenziare gli aspetti della linearizzazione delle equazioni di Navier-Stokes rispetto ad un flusso base stazionario imposto, eliminando i termini quadratici perturbatori. Viene presentata la formulazione $v-\eta$, la sua trasformazione nel dominio di Fourier e le equaziondi Orr-Sommerfeld-Squire.

- **Capitolo 2: Flusso piano di Poiseuille soggetto ad uno strato limite stazionario di Stokes**: Viene esposto il problema in analisi della tesi, definitii flussi base, la formulazione matematica delle equazioni, e la loro successiva linearizzazione. Si evidenziano i problemi dovuti alla globalità della direzione parallela al flusso base e si trasformano le equazioni nel dominio di Fourier. Si presenta inoltr la discretizzazione delle equazioni mediante polinomi di Chebyshev e la struttura implementativa del codice. Viene analizzato il sottocaso di una possibile perturbazionie invariante spazialmente nella direzione trasversale al flusso di Poiseuille. Vengono evidenziate le problematiche matematiche connesse e analizzata la struttura delle equazioni. Viene infine riportato un metodo per il calcolo degli autovalori più efficiente ma valido solo nel caso $\beta = 0$

- **Capitolo 3: Risultati**: Si presenta come sono stati definiti i parametri di discretizzazione principali del codice. Si effettua la validazione del calcolo lineare mediante DNS. Vengono riportati i principali risultati di stabilità modale e non-modale. Viene analizzata la dipendenza dell'autovalore a parte reale maggiore dai parametri fisici in analisi Viene analizzato l'andamento del massimo della crescita transitoria in funzione dei parametri Re, κ, A, β

- **Conclusioni**: Vengono riportate le principali conclusioni e i possibili sviluppi futuri per questo lavoro di Tesi

- **Appendice A: Ulteriori risultati** Vengono riportati ulteriori risultati per differenti numeri di Reynolds, sia per la stabilità modale sia per la stabilità non-modale. Si riportano i risultati di stabilità modale e non modale in funzione del numero d'onda in direzione trasversale al flusso di Poiseuile. Si riportano le condizioni di optima initial e optimal output sia nello spazio fisico sia in funzione dell'espansione modale e della coordinata normale a parete.

Bibliography

[1] M. Abramowitz and I. Stegun. *Handbook of Mathematical Functions*. Number 55 in Applied Mathematics Series. National Bureau of Standards, 1964.

[2] W. Arnoldi. The principle of minimized iterations in the solution of the matrix eigenvalue problem. *Quarterly of Applied Mathematics*, 9:17–29, 1951.

[3] F. Auteri, A. Baron, M. Belan, G. Campanardi, and M. Quadrio. Experimental assessment of drag reduction by traveling waves in a turbulent pipe flow. *Phys. Fluids*, 22(11):115103/14, 2010.

[4] M. Bramanti, C. D. Pagani, and S. Salsa. *Matematica: Calcolo infinitesimale e algebra lineare*. Zanichelli, 2006.

[5] C. W. Clenshaw and A. R. Curtis. A method for numerical integration on an automatic computer. *Numerische Mathematik 2*, 2, 1960.

[6] W. O. Criminale, T. L. Jackson, and R. D. Joslin. *Theory and Computation of Hydrodynamic Stability*. Cambridge, 2003.

[7] I. E. and H. Keller. *Analysis of Numerical Methods*. John Wiley, 1966.

[8] F. Gazzola, A. Ferrero, and M. Zanotti. *Elementi di analisi superiore per la fisica e l'ingegneria*. Progetto Leonardo, 2007.

[9] A. Hanifi, P. Schmid, and D. Henningson. Transient growth in compressible boundary laer flow. *Phys. Fluids*, 1996.

[10] J. P. Imhof. On the method for numerical integration of clenshaw and curtis. *Numerische Mathematik*, 5:138–141, 1963.

[11] N. N. Lebedev. *Special Functions and Their Applications*. Dover, 1972.

[12] R. Lindzen. Instability of plane parallel shear flow. *Pageoph*, 1988.

[13] K. Maleknejad and K. Lotfi. Numerical expansion methods for solving integral equations by interpolation and gauss quadrature rules. *Elsevier*, 2004.

[14] W. M. F. Orr. The stability or instability of the steady motions of a perfect liquid and of a viscous liquid. Part II. A viscous liquid. *Proc. R. Irish Acad. Sect. A: Math. Phys. Sci.*, 27:69–138, 1907.

[15] Orszag S. A. Accurate solution of the Orr-Sommerfeld stability equation. *J. Fluid Mech.*, 50(4):689–703, 1971.

[16] S. Pope. *Turbulent Flows*. Cambridge University Press, Cambridge, 2000.

[17] M. Quadrio. Drag reduction in turbulent boundary layers by in-plane wall motion. *Phil. Trans. R. Soc. A*, 369(1940):1428–1442, 2011.

[18] M. Quadrio and P. Ricco. The laminar generalized Stokes layer and turbulent drag reduction. *J. Fluid Mech.*, 667:135–157, 2011.

[19] M. Quadrio, P. Ricco, and C. Viotti. Streamwise-traveling waves of spanwise wall velocity for turbulent drag reduction. *J. Fluid Mech.*, 627:161–178, 2009.

[20] L. Quartapelle and F. Auteri. Fluidodinamica, 2008.

[21] A. Quarteroni. *Modellistica numerica per Problemi Differenziali*. Springer, 4th edition, 2008.

[22] A. Quarteroni, R. Sacco, and F. Saleri. *Matematica Numerica*. Springer-Verlag, 2000.

[23] A. Quarteroni and F. Saleri. *Introduzione al calcolo scientifico*. Springer, 3rd edition, 2006.

[24] S. Reddy and D. Henningson. Energy growth in viscous channel flows. *J. Fluid Mech.*, 252:209–238, 1993.

[25] F. Sabetta. *Gasdinamica*. La Sapienza, 2009.

[26] P. Schmid. Nonmodal stability theory. *Annu. Rev. Fluid Mech.*, 39:129–162, 2007.

[27] P. Schmid and D. Henningson. *Stability and Transition in Shear Flows*. Springer, 2001.

[28] L. B. Trefethen and D. Bau. *Numerical linear algebra*. siam, 1997.

[29] C. Viotti, M. Quadrio, and P. Luchini. Streamwise oscillation of spanwise velocity at the wall of a channel for turbulent drag reduction. *Phys. Fluids*, 21:115109, 2009.